EFFECT OF THE INTERACTIONS OF SURFACTANT/DYE AND SURFACTANT/DRUG ON THE FORMATION OF DIFFERENT TYPES OF LYOTROPIC NEMATIC PHASE

MASTER OF SCIENCE

MERVE TABAK

ACADEMIC SUPERVISOR
Prof. Dr. EROL AKPINAR

BOLU, TEMMUZ - 2023

APPROVAL OF THE THESIS

EFFECT OF THE INTERACTIONS OF SURFACTANT/DYE AND SURFACTANT/DRUG ON THE FORMATION OF DIFFERENT TYPES OF LYOTROPIC NEMATIC PHASE submitted by **Merve TABAK** and defended before the Examining Committe Members listed below in partial fulfillment of the requirements for the degree of **Master of Science** in **Department of Chemistry, Institute of Graduate Studies of Bolu Abant Izzet Baysal University in 14.07.2023** by

Examining Committee Members	**Signature**
Supervisor Prof. Dr. Erol AKPINAR Bolu Abant Izzet Baysal University	.....
Member Prof. Dr. Öznur DEMİR ORDU Bolu Abant Izzet Baysal University	.....
Member Assoc. Prof. Dr. Emre BÜKÜŞOĞLU Middle East Technical University	.....

Prof. Dr. İbrahim KÜRTÜL

Director of Instıtute of Graduate Studies

ETHICAL DECLARATION

In this thesis dissertation that was properly prepared according to the Thesis Writing Rules of Bolu Abant İzzet Baysal University of the Institute of Graduates Studies, I here by declare that;

- All data, information, and documents presented in the thesis were obtained in accordance with the academic and ethical rules,
- All data, documents, assessments, and results were presented in accordance with the scientific ethical and moral rules,
- All works that were benefitted in the thesis were appropriately cited,
- No alteration was made in the data used,
- Study presented in this thesis is original,

Otherwise, I declare that I accept the loss of all my rights in case any contradiction that may arise against me.

Based on the plagiarism report that was generated on the date of 09/08/2023 by using predetermined filtrations set by Directorate of Institute of Graduate Studies of the Turnitin programme, a plagiarism detection sofware, the similarity index detected was 30 %.

_____

Merve TABAK

ABSTRACT

EFFECT OF THE INTERACTIONS OF SURFACTANT/DYE AND SURFACTANT/DRUG ON THE FORMATION OF DIFFERENT TYPES OF LYOTROPIC NEMATIC PHASE
MSC THESIS
MERVE TABAK
BOLU ABANT IZZET BAYSAL UNIVERSITY
INSTITUTE OF GRADUATE STUDIES
DEPARTMENT OF CHEMISTRY
(SUPERVISOR: PROF. DR. EROL AKPINAR)

BOLU, JULY 2023
(xv + 88)

Lyotropic nematic liquid crystal phases, a subclass of lyotropic liquid crystals, have continued to attract the attention of many research groups due to the magnetic field sensitivity of their phase directors or optical axes ($\vec{n}$) compared to other liquid crystal phases. Lyotropic nematic phases are divided into two uniaxial (N_D, N_C) and biaxial (N_B) based on their orientations, micelle symmetries or geometries. Lyotropic nematic phase properties of some novel mixtures of dodecyltrimethylammonium bromide (DTMABr)/1-dodecanol (DDeOH)/water, doping with some anionic azo dyes (Sunset Yellow, amaranth, and tartrazine) and a drug molecule disodium cromoglycate (cromolyn, DSCG), were investigated in the present study. The textural analysis of the uniaxial and biaxial nematic phases was performed by a conventional technique, polarizing optical microscopy (POM). Uniaxial-to-biaxial nematic phase transitions were determined from the temperature dependence of the birefringences of the nematic phases via laser conoscopy. Partial phase diagrams of the mixtures were constructed as a function of dyes/drug "molecules' concentrations" by combining the POM and laser conoscopy results. Small-angle X-ray scattering (SAXS) was performed to evaluate micellar structure parameters. The results indicate that dye and drug molecules have a greater effect on (a) the nematic-nematic phase transitions, (b) the biaxial nematic phase domain range in the partial phase diagrams, and (c) micelle shape anisotropy than the conventional inorganic electrolyte ions. Furthermore, dye/drug molecules may be sequenced in the Hofmeister series of ions, considering the number of ionic groups in their molecular structures and also the chaotropic and/or kosmotropic degrees of the ionic groups. Since the dye/drug molecules may have a resonance structure (e.g. DSCG) as a result of the existence of the aromatic parts in their structure, this resonance structure should be considered to investigate their effects on the formation of the lyotropic nematic phases.

KEYWORDS: Lyotropic nematic phases, biaxial phase, nematic-nematic phase transitions, surfactant-dye/drug interactions, birefringence, partial phase diagram, polarizing optical microscopy, laser conoscopy, micelle structural parameters, Small-angle X-ray scattering

ÖZET

SÜRFAKTAN/BOYAR MADDE VE SÜRFAKTAN/İLAÇ ETKİLEŞİMLERİNİN FARKLI TÜRDE LİYOTROPİK NEMATİK FAZ OLUŞUMLARI ÜZERİNE ETKİLERİ
YÜKSEK LİSANS TEZİ
MERVE TABAK
BOLU ABANT İZZET BAYSAL ÜNİVERSİTESİ
LİSANSÜSTÜ EĞİTİM ENSTİTÜSÜ
KİMYA ANABİLİM DALI

(TEZ DANIŞMANI: PROF. DR. EROL AKPINAR)

BOLU, TEMMUZ - 2023
(xv + 88)

Liyotropik nematik sıvı kristal fazlar, liyotropik sıvı kristallerin bir alt sınıfı olup, diğer sıvı kristal fazlarına göre faz direktörlerinin veya optik eksenlerinin ($\vec{n}$) manyetik alan duyarlılığı nedeniyle birçok araştırma grubunun dikkatini çekmeye devam etmektedir. Liyotropik nematik fazlar yönelimleri, misel simetrilerine veya geometrilerine bağlı olarak tek eksenli (N_D, N_C) ve çift eksenli (N_B) olarak ikiye ayrılmaktadır. Bu çalışmada, dodesiltrimetilamonyum bromür (DTMABr)/1-dodekanol (DDeOH)/su bazı yeni karışımlarının, anyonik azo boyalar (Sunset Yellow, amaranth ve tartrazin) ve bir ilaç molekülü olan disodyum kromoglisat (kromolin, DSCG) ile katkılanmış lyotropik nematik faz özellikleri incelenmiştir. Tek eksenli ve çift eksenli nematik fazların dokusal analizi, geleneksel bir teknik olan polarize optik mikroskopisi (POM) ile gerçekleştirilmiştir. Tek eksenliden çift eksenli nematik faz geçişler, lazer konoskopisi yoluyla nematik fazların çift kırılmasının sıcaklığa bağımlılığından belirlenmiştir. Karışımların kısmi faz diyagramları, POM ve lazer konoskopi sonuçları birleştirilerek boyaların/ilaç moleküllerin konsantrasyonlarının bir fonksiyonu olarak oluşturulmuştur. Misel yapı parametrelerini değerlendirmek için küçük açılı X-ışını saçılımı (SAXS) yapılmıştır. Sonuçlar, boya ve ilaç moleküllerinin (a) nematik-nematik faz geçişleri, (b) kısmi faz diyagramlarındaki çift eksenli nematik faz alanı aralığı ve (c) misel şekil anizotropisi üzerinde geleneksel inorganik elektrolit iyonlarından daha büyük bir etkiye sahip olduğunu göstermektedir. Ayrıca boya/ilaç moleküller moleküler yapılarındaki iyonik grupların sayısı ve ayrıca iyonik grupların kaotropik ve/veya kozmotropik dereceleri dikkate alınarak Hofmeister iyon serisinde sıralanabilir. Boya/ilaç moleküller, yapılarında aromatik kısımların varlığından dolayı rezonans yapısına sahip olabilir (örneğin DSCG); bu rezonans yapı, liyotropik nematik fazların oluşumu üzerindeki etkilerini araştırırken dikkate alınmalıdır.

ANAHTAR KELİMELER: Liyotropik nematik fazlar, çift eksenli faz, nematik-nematik faz geçişleri, sürfaktan-boya/ilaç etkileşimleri, çift kırınım, kısmi faz diyagramı, polarize optik mikroskopisi, lazer konoskopisi, misel yapısal parametreler, Küçük açılı X-ışını saçılması

TABLE OF CONTENTS

LIST OF FIGURES

Page

LIST OF TABLES

Page

LIST OF ABBREVIATIONS AND SYMBOLS

LCs : Liquid Crystals

LLCs : Lyotropic liquid crystals

TLCs : Thermotropic liquid crystals

LCLCs : Lyotropic chromonic liquid crystals

LNPs : Surfactant-based lyotropic nematic phases

N : Nematic phase

N_B : Biaxial nematic phase

N_C : Calamitic nematic phase

N_D : Discotic nematic phase

H : Hexagonal phase

CMC : Critical micelle concentration

DDeOH : 1-Dodecanol

DSCG : Disodium chromoglycate

DTMABr : Dodecyltrimethylammonium bromide

SSY : Sunset Yellow

KL : Potassium Laurate

SDS : Sodium dodecylsulfate

H : Magnetic field direction

X : Mol fraction

χ : Magnetic susceptibility

Δn/δn : Birefringences

ΔT_{NB} : Biaxial nematic phase range

Δχ : Diamagnetic susceptibility anisotropy

°C : Degree Celsius

POM : Polarize optical microscope

ACKNOWLEDGEMENTS

The author wishes to express his deepest gratitude to his supervisor Prof. Dr. Erol AKPINAR for their guidance, advice, criticism, encouragements and insight throughout the research.

The author would also like to thank Prof. Dr. Öznur DEMİR ORDU for her suggestions and comments.

I would like to thank to my mother and my father for their endless support and endless sacrifices.

To Nazlı UYGUR and my friends, I offer sincere thanks for their patience and continuous moral to complete this thesis.

This study was supported by the The Scientific and Technological Research Council of TURKEY (TUBITAK, Grant No: 120Z721) and Bolu Abant Izzet Baysal University Directorate of Research Projects Commission (BAP, Grant no: 2022.03.03.1555).

1. INTRODUCTION

In 1888, Australian botanist Friedrich Reinitzer in a study with cholesterol derivatives (cholesterol and cholesterol benzoate) detected that the cholesterol benzoate had two different melting points (145 ^{o}C-179 ^{o}C) (1). Depending on the increase in temperature, Reinitzer's observation showed that matter (solid) turns to a blurry liquid and then a clear liquid (2). Afterward, the German physicist D. Lehmann examined in more detail the physical properties of crystals for this phase using a polarizing microscope (1,3) and detected that this intermediate phase exhibits birefringence like the property of a crystal. With this discovery of the new phase of the matter, "liquid crystal" phenomenon was, for the first time, used for this thermodynamically stable phase (1).

Liquid crystals (LCs) are defined as the peculiar phase observed between liquid and solid states, Figure 1.1. LCs behave as a liquid with some degree of fluidity, but their molecules have a similar orientation pattern to solids. This orientation pattern causes the light to be refracted because they resemble crystals. LCs are formed by the self-assembly of molecules in an ordered structure.

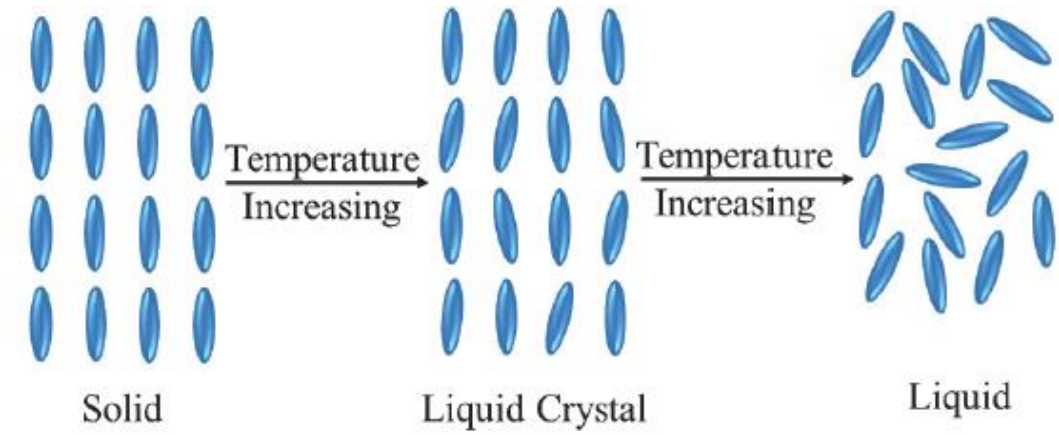

Figure 1.1. Alignment of the molecules in (from left to right) solid, liquid crystals and liquid phases of a matter (4).

Liquid crystals have the properties of anisotropic crystalline solids (i.e., optical, electrical, and magnetic properties) and isotropic liquids (1,5). Because of this, LCs can be termed mesophases (6). Some of the properties that apply to liquid crystal materials can be listed as follows: rod-like molecular structure, stability of their long axes, strong dipoles, or being easily polarized (7). Similar to crystals, liquid crystal materials exhibit anisotropy, which is defined as the change of physical properties depending on the direction. That is, the molecular order in the liquid crystal can be easily changed by the effect of the electric or magnetic field. LCs have weak intermolecular forces and therefore show high sensitivity to external influences. Depending on the features of liquid crystals (orientation and alignment), LCs materials can show extraordinary properties with various external stimulants (i.e., temperature, pressure, light, electromagnetic fields, surface effects, optical properties, chemical analytes, and mechanical forces) (8). For scientists, liquid crystal materials have become preferred in technological fields, thanks to their adaptability to external stimuli and their matchless physical properties. LCs are preferred in biosensor applications thanks to their property of orientability because these properties avoid the need for complicated instrumental analysis to detect certain biomolecular entities (9). Also, compared to the biosensing technologies in use, devices containing liquid crystals are known to be more reliable in detecting binding events (chemical and biochemical). The inherent and incredible properties of LCs, especially lyotropic nematics, have made them notable components in carbon nanotube technology as well, where the carbon nanotubes can be oriented in a particular direction. In addition, lyotropic nematic phases (LNPs) which are a type of liquid crystals can act as a carrier medium for carbon nanotubes and are preferred in nanotube applications due to these properties (10). LCs are also preferred to meet material needs for liquid crystal display (LCD) technology, especially thermotropic liquid crystals (11). In addition, LCs polymers are preferred in the biomimicry of color-producing structures as lenses and muscle-like actuators in biomedical (12). Many studies related to the industries of food, cosmetics, and foams are supported by lyotropic mixtures exhibiting LNPs (13). Depending on these application areas, the determination of the potentials of liquid crystal materials, classification of them and figuring out their physical properties considered important.

LCs are divided into two main classes, thermotropic liquid crystals (TLCs) and lyotropic liquid crystals (LLCs). Although they exhibit similar properties the prominent differences between them are, in general, their molecular arrangements, optical textures, and physical properties (14). Generally, temperature is substantially important a parameter for liquid crystals, and it affects their molecular arrangement. At high temperatures, an isotropic phase is formed due to the disruption of the molecular arrangement of a liquid crystal, while at low temperatures it is observed as an anisotropic phase (15). Liquid crystals formed within a certain temperature range are called TLCs whose structure is formed by the combination of thin-rod and disk-like molecules (16). The orientation of the molecules is near and parallel to each other in TLCs. Thanks to these orientation features, they can illustrate linear and non-linear optical properties, thus there are a lot of studies focused on TLCs (17). TLCs are divided into three groups which are nematic, smectic (SmA, SmC), and cholesteric as seen in Figure 1.2, which is highly dependent on the variation of the temperature (14). The nematic phase is the mesophase in which the molecules are aligned along the director field. There are many different types of smectic phases, usually based on their position and orientation. Smectic phases show a positional alignment in one direction. In the smectic A phase, the molecules are normally oriented on the layer, while in the smectic C phase, they orient at a certain angle. Cholesteric liquid crystal has a helical structure.

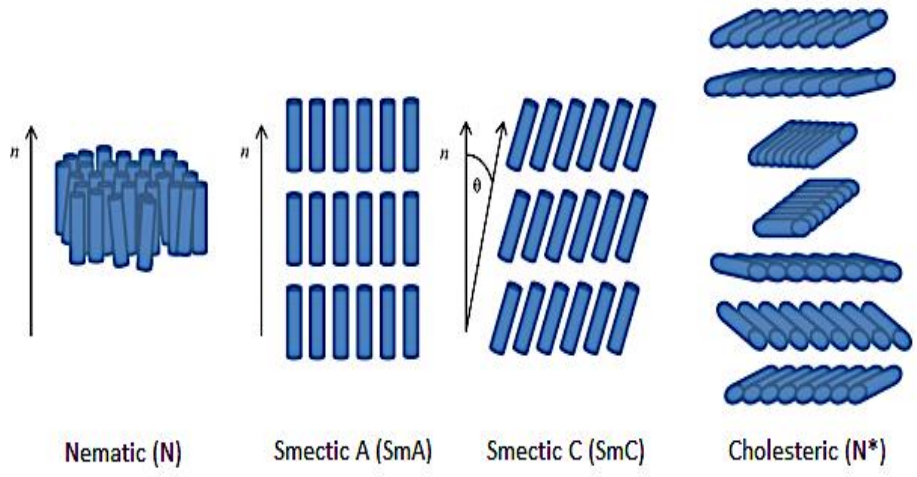

Figure 1.2. Demonstration of molecular arrangement for thermotropic liquid crystal types (18).

The formation of LLCs is related to the concentration of constituents in lyotropic mixtures and the temperature. Lyotropic liquid crystals have a regular structure and exhibit high performance in many applications thanks to their high adaptability, so LLC systems have distinct advantages due to their existing properties (19).

1.1 Lyotropic liquid crystals (LLCs)

LLCs have a significant role in the materials science due to their desirable physicochemical properties, which enable us to produce low-scale structures and high chemical functionality with easy applicability. Because of these properties, LLCs have been found applications in many fields such as biology (20), biotechnology (10), drug delivery systems (21), LCs display, LCs thermometers, optical imaging (22), polymer dispersed LCs, and cosmetics (23), and they have the potential to be used in different fields in the future. In addition, LLCs are present in the molecular structure of the lipids, which act as a biological membrane. Thus, scientists have focused on the production of LLCs with improved properties with proper methods (24).

To prepare different LLC structures, an amphiphilic molecule (surfactant) is dissolved in a suitable solvent. Solvents may be organic liquids or ionic liquids, or water (generally preferred). From this respect, the surfactants are indispensable functional molecules for LLCs. Surfactants are known as surface-active molecules and, they are used to decrease surface free energy of the solutions by entering between the water and air interfaces (25). Surfactant molecules consist of two main segments: **(I)** hydrophilic (water-loving polar terminal head) and **(II)** hydrophobic (long linear or branched hydrocarbon chains), as seen in Figure 1.3. The hydrophilic part provides high solubility to the surfactant molecule in a polar solvent, whereas the hydrophobic part depicts similar behavior in the hydrocarbon-based solvents.

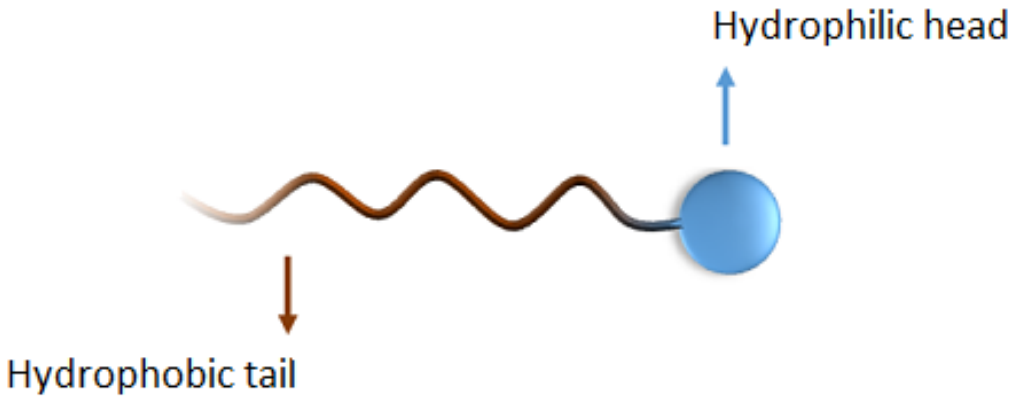

Figure 1.3. Simple representation of the segments of a surfactant (26).

The amphiphilic molecules can possess ionic, nonionic, or zwitterionic characteristics dependent on the hydrophilic fragment. Correspondingly, an ionic surfactant has positively (cationic surfactant) or negatively (anionic surfactant) charged head groups, while zwitterionic surfactants bear both negative and positive charges in the head groups. Moreover, the surfactant molecules with no electrical charge on their head groups are known as non-ionic surfactant (27), Figure 1.4. Also, the ionic surfactants can be classified depending on the type of hydrophilic groups such as carboxylate ($–COO^-$), sulfobetaine ($–N(CH_3)_2C_3H_6SO_3^-$), sulfate ($–OSO_3^-$), carboxybetaine ($–NR_2CH_2COO^-$), sulfonate (SO_3^-) and quaternary ammonium ($–R_4N^+$) (28).

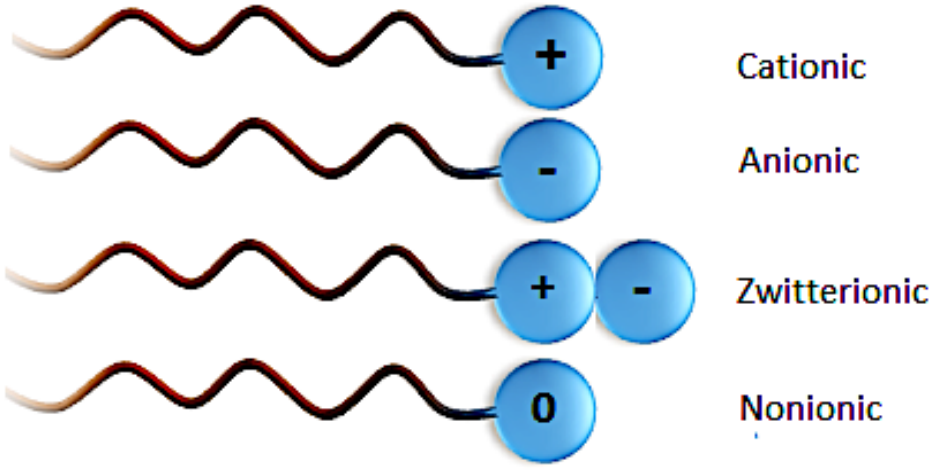

Figure 1.4. Schematic representation of surfactants molecules in terms of charge.

In the light of that mentioned above, amphiphilic molecules show the property of self-assembly with small shape anisotropy at certain conditions through the intermolecular interactions formed between them. This self-assembly creates a peculiar structure called a ***"micelle".*** Thanks to this spontaneously organization, these molecules can form the molecular clusters with various shapes such as spheres, cylindrical, and lamaller with the increasing surfactant concentration (29) as seen in Figure 1.5. Furthermore, adding a co-surfactant or salt to a surfactant solution affects micelle aggregation.

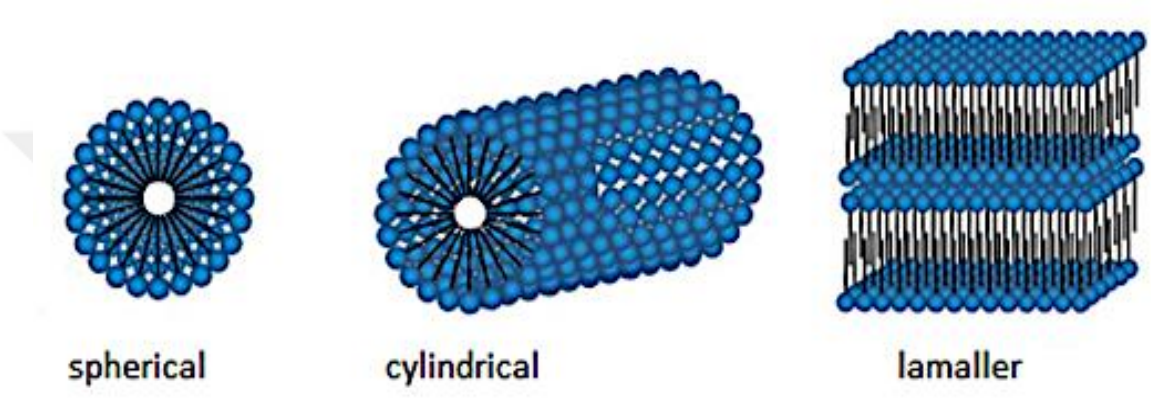

Figure 1.5. Representation of various micelles organizations (29).

In micelle formation, the concentration, temperature, solvent type, chemical structure of the surfactants, use of co-surfactant and additives in the medium are significant parameters since these parameters directly affect the anisotropy during the self-assembly and change the forms (direct or reverse) of the molecular clusters (30). Among them, the most significant one is undoubtedly the concentration of the surfactant. Namely, the concentration must be at the critical value to form the micelle, which is defined as “critical micelle concentration (CMC)" (31). In other words, CMC implies the lowest concentration level, which is necessary for the micelle formation in the solution. The surfactant concentration in the micelle solution higher than the CMC provides aggregation of amphiphilic molecules, and accordingly the increase in the entropy of water (13). There are some theoretical approaches for micelle formation in the literature (32). Because hydrophobic and hydrophilic parts of the surfactants have a significant role in the micelle formation, the CMC values are different for each surfactant types, which depends on the chemical structure of the surfactant, especially characteristics of the terminal functional groups.

Correspondingly, by considering the hydrophobic chain length of surfactant molecules, the CMC value of surfactant molecules decreases as the chain length increases. For example, dodecyltrimethylammonium bromide with 12 carbon atoms have a value of $1.56x10^{-2}$ mol/kg, while decyltrimethylammonium bromide with ionic 10 carbon atoms have a value of 6.5×10^{-2} mol/kg (33). When hydrophobic effect is evaluated, it would be more accurate to classify the surfactants as ionic and non-ionic surfactants. Generally, charged surfactant molecules have larger CMC values than non-ionic molecules because ionic surfactant molecules have greater solubility in water (33).

In the vicinity of CMC, the surfactant solution is isotropic. The surfactant concentration must be much higher than the CMC about $x10^2$ in the micellar solution to obtain anisotropic lyotropic liquid crystals (11). That is, the micelles begin to interact with each other through repulsive electrostatic forces, which result in the formation of an anisotropic solution with a some degree of viscosity. In addition, some studies in the literature stated that the results obtained from dilute aqueous isotropic micellar solutions may be applicable to explain some properties of lyotropic systems obtained at higher surfactant concentrations (34). For example, CMC value of the potassium laurate/water mixture is equal to 0.027 M (35) and the concentration is recorded as c> 2 M at which liquid crystalline phases are observed in the temperature range of 20-350°C (36,37).

Another crucial parameter for the formation of lyotropic liquid crystal phases is temperature. With temperature variation, surfactant molecules move towards each other. Like CMC, there exists a critical minimum temperature value for the micelle formation. This minimum temperature is defined as the Krafft temperature. The solubility at the Krafft point is almost equal to the critical micelle concentration (CMC) (38). However, at temperatures below of the Krafft temperature, which brings about that the solubility of surfactant is less than CMC, micelles cannot be present in the medium (31). Besides, the formation of different types of lyotropic liquid crystals depends on the degree of ordering of the surfactant molecules in the solvent, which can be controlled by change in the temperature and the amphiliphic molecule concentration. In addition to the concentration and temperature, other parameters such as the ionic character of the

polar head, the presence or absence of another surfactant (generally named as co-surfactant) or salt in the mixture, the pH and ionic strength of the solution, the purity of the compounds have a considerable effect on the formation of the lyotropic liquid crystal phases (39). The addition of co-surfactants changes the micellar cluster and its structural features. For instance, the co-surfactant, hexane, in a mixture of cetylpyridinium bromide/salt/water, turns the micelle surface curvature less curved or linear (13). Furthermore, adding a salt to this mixture also leads to difference in the micelle shapes, i.e., the shape of the micelle becomes relatively more anisometric (15). Figure 1.6. shows the temperature-surfactant concentration phase diagram. The critical micelle concentration line implies the representation of micelles formed by crossing the CMC concentration of free amphiphilic molecules. The micelles can be cylindrical or spherical in shapes. As observed in Figure 1.6., a Krafft line is the line which seperates the crystalline phase region from the liquid crystals one. Below Krafft line, a crystalline phase may include coagel or gels (28).

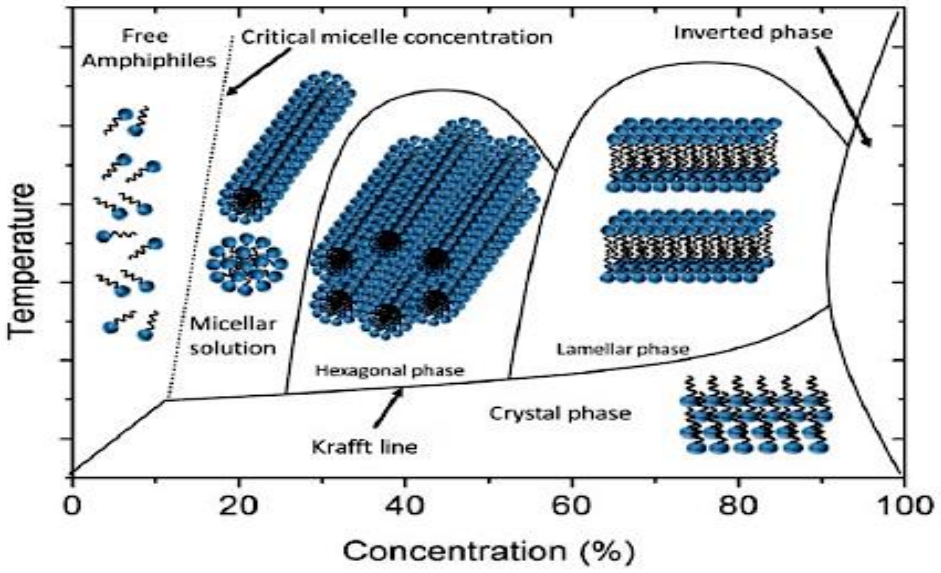

Figure 1.6. The phase diagrams of the surfactants depending on the temperature and concentration changes in the solvent during the formation of lyotropic phase (39).

As seen from the graph, the diversity of liquid crystal phases can be observed with the increase in the surfactant concentration. The increasing of the surfactant concentration reduces the distance between the micelles, and also affects the phase diversity in the hydrophobic effect caused by long-range repulsive forces between the micelle interface (40). Different LLC structures such as hexagonal, lamellar, nematic, cholesteric (chiral nematic) and cubic are formed with increasing surfactant concentration. The hexagonal phase is composed of rod-shaped micelle clusters of infinite length, and the packing of the parallel cylinders is in the form of a two-dimensional hexagonal lattice on the axes. The hexagonal lyotropic liquid crystal phase has two different structures: the direct hexagonal phase **(H_1)** and the inverted hexagonal phase **(H_2)** (41). In direct structure the hydrocarbon chains in the inside of the cylinders show a liquid-like arrangement, Figure 1.7a. It has a high-water content, but it is a dense phase (42). In an inverted structure the polar solvent is placed in the inside of the cylinders and the carbonic chains are outward, Figure 1.7b. The inverted structure is observed in a narrower nonpolar solvent concentration range compared to the direct hexagonal structure (13). With increasing surfactant concentration, a lamellar or a nematic phase may be observed.

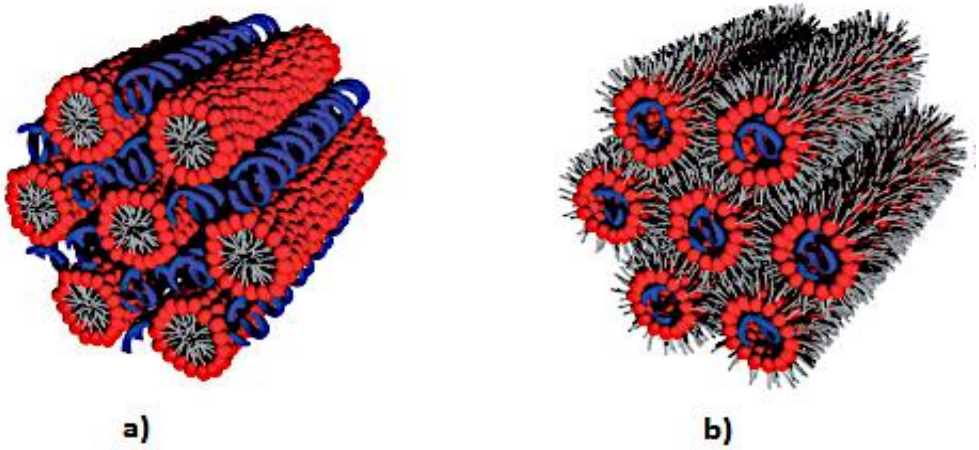

Figure 1.7. The hexagonal phase structures: (a) direct and (b) inverted (43).

The structural units of the lamellar phase are bilayers formed by the surfactant and water molecules. In the bilayers, surfactant molecules are sandwiched between two water layers. In other words, these bilayers are separated from each other by water, Figure 1.8. The surfactant head groups interact with the aqueous medium, but the hydrocarbon chains do not interact in this bilayer. About twice the length of the surfactant molecule is equivalent to the thickness of the bilayer. Also, the thickness of the double layer can be increased by adding a non-polar solvent, and another factor affecting the thickness is the temperature (14) . The lamellar phases can be characterized in two ways, neat soap (**L_α**) (25) and gel phase (**L_β**) (44). The difference between these phases arises from the properties of the carbonic chains of the surfactants. The surfactant molecules exhibit liquid-like properties in L_α phase but has less chain motions such as solid in L_β phase. Furthermore, in the L_β state, the hydrocarbon chains in the surfactant often have an all-trans alkyl-chain conformation in the bilayers (45).

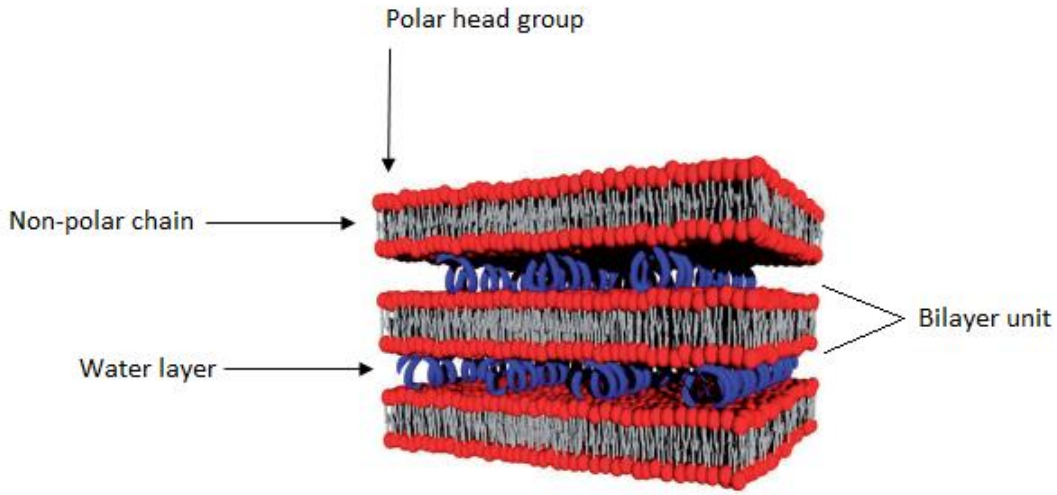

Figure 1.8. Schematic representation of the structure of lamellar phase (43).

The cubic phase is formed by the collection of micelles in a cubic order with a three-dimensional repetition pattern. According to their molecular assembly, they produce two types of structures: bicontinuous cubic phase and simple cubic phase in three dimensions, Figure 1.9 (46).

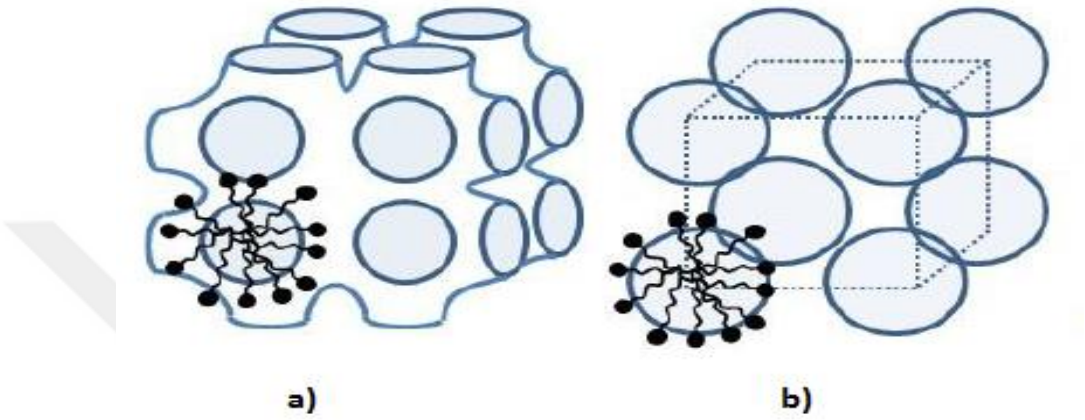

Figure 1.9. Schematic illustration of (a) bicontinuous cubic and (b) simple cubic (47).

As depicted in Figure 1.10, the simple cubic phase may be in body-centered or face-centered arrangements by spherical micelles (40). These phases include curved regions (negatively and positively) (47). Cubic phases are very viscous compared to hexagonal and lameller phases. Therefore, they can act as the solid at certain conditions. Hence, they are called ‘viscous isotropic phases’ (48). Generally, the cubic phase is usually located between the lamellar and hexagonal phases in the phase diagrams. Moreover, depending on the surfactant concentration, the shapes and types of micelles can be modified by using a suitable solvent, Figure 1.10.

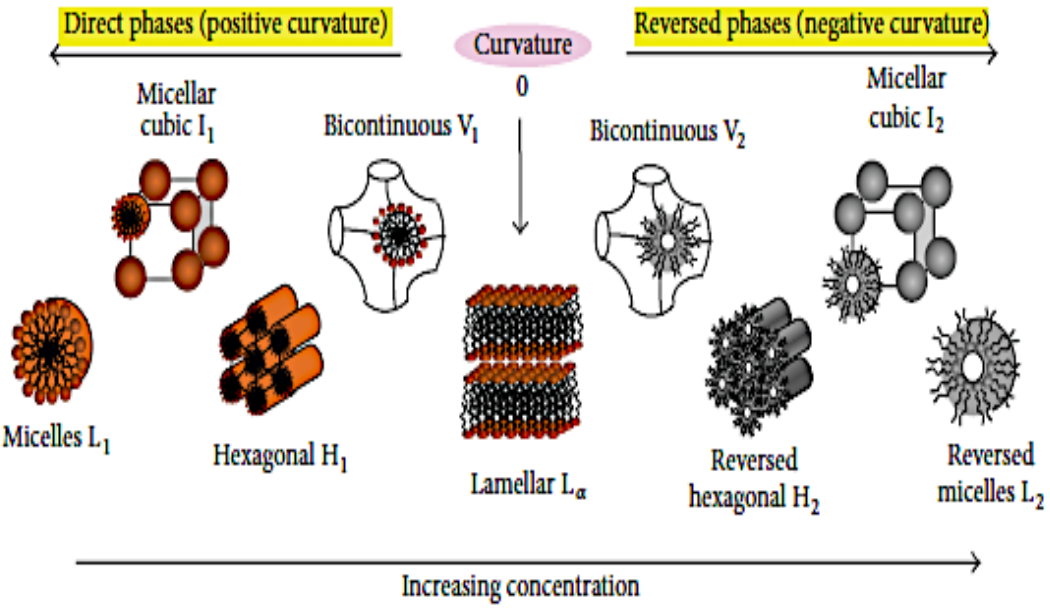

Figure 1.10. Schematic illustration of typical phase progression based on surfactant concentration in a certain solvent and micellar surface curvature (48).

The cholesteric phase consists of the stacking layers showing little angle deviations between the layers where the molecules in the layers are at different intervals but in the same direction. Cholesteric phases are obtained by adding a chiral molecule to a mixture exhibiting nematic phase properties (49). The addition of both chiral amphiphilic or non-amphiphilic molecules to the nematic phase can be seen as a practical route to obtain cholesteric phase. For this purpose, L-n-lauroyl potassium alaninate and 2-sodium dodecyl sulfate, and L/D-octanol can be utilized as chiral amphiphilic molecules, whereas brucine sulfate, tartaric acid, cholesterol, l-sorbose, diacetone-sorbose and diacetone-2-ceto potassium gulonate can be given as examples of the non-amphiphilic chiral molecules (13). Additionally, the use of enantiomers of a racemic mixture (L- or D-enantiomers of DL- forms) as well as a chiral solvent are another way to form the cholesteric phase. Moreover, the cholesterics phases are divided into two types depending on the characteristics of the chiral molecule in the nematic mixture, and these are the intrinsic and extrinsic cholesterics phases. For example, the mixture composed of the potassium laurate, decanol, water, and L-N-lauroyl potassium alaninate depicted an intrinsic cholesteric phase (50), while the mixture formed by the combination of the ammonium decylsulfate, ammonium, sulfate, decanol, water and brucine sulfate shown extrinsic cholesteric phase (51). Additionally, it can be

said that the cholesteric phases are structurally formed by the helical arrangement of micelles as seen in Figure 1.11. In the helical organization, the local directors of the micelles, which are perpendicular to the largest micelle surfaces in the discotic cholesteric phase (Ch_D) and parallel to the longest micelle dimension (Ch_C), rotate with 360° around the helical axis by remaining their initial position. The helical axis can also be called the optical axis of the cholesteric phase. Another important property of the cholesteric phase is the pitch length (P) which is described as the distance required for the phase director to make a full turn along the helix axis. The relative molar concentration of the chiral molecules (C_m) depending on the level of the main amphiphiles in the medium and the shape anisotropy of the micelles (S_a) are the main factors affecting the pitch of the cholesteric structure (P) (52).

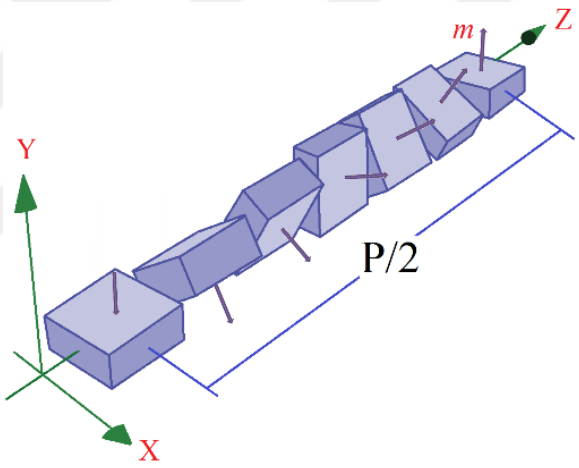

Figure 1.11. Representation of organization of orthorhombic micelles with their local directors along the helix axis (53).

Three types of cholesteric phases have been recognized, namely discotic (Ch_D), calamitic (Ch_C), and biaxial (Ch_B) (54,55). The texture differences in the cholesteric phases vary depending on the optical axis orientation as seen in Figure 1.12. In the Ch_D phase, the local optical axes of the micelles are oriented perpendicular to the magnetic field, while the helix axis is oriented parallel to the magnetic field. The black regions indicated by the arrow in Figure 1.12a are called the pseudo-isotropic or homeotropic regions located in the Ch_D phase. The change in the homeotropic region is an indication of the phase transition between Ch_D and Ch_B, and this region is not seen as black in the Ch_B phase as seen Figure 1.12b. Homeotropic alignment does not occur in Ch_B because it has two optical axes. In the Ch_C phase as seen in Figure 1.12.c, the local axis of the micelles is oriented parallel to the magnetic field direction and the helix structure is unwound.

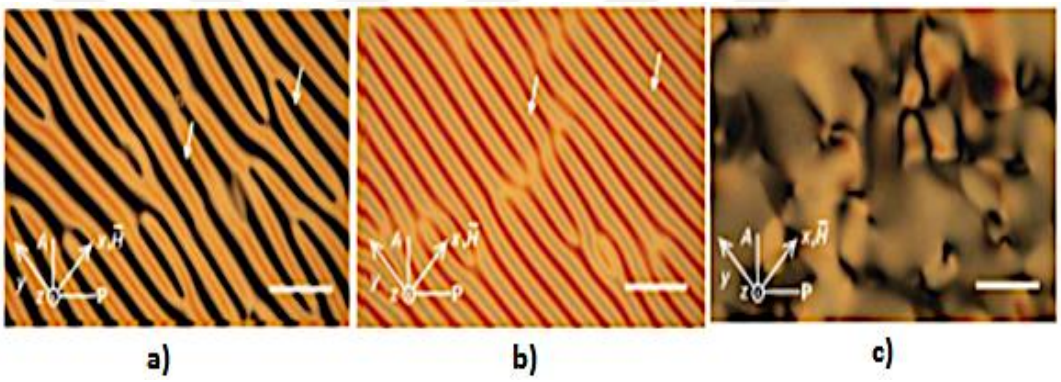

Figure 1.12. Characteristic cholesteric phase texture identified using polarizing optical microscopy for KL/Brucine/DeOH/H_2O mixture. Fully oriented a) ChD and b) ChB phases in the magnetic field, homeotropic regions are shown with arrows in the texture. c) ChC phase, without magnetic field. *x*, *y*, and *z* are representative of the laboratory frame axes (52).

Considering all the LLC types, the structural change between lyotropic phases depends on factors such as the length, structure and nature of hydrophobic chains, nature and charge in hydrophilic parts, electrolyte concentration, and also some thermodynamic factors such as temperature and pressure (56).

1.1.1 Lyotropic nematic phases (LNPs)

Nematic liquid crystals are the simplest and most common liquid crystal structures. The structural units of nematic liquid crystals are characterized by long-range orientational order. The director field orientation of nematic liquid crystals can be modified or controlled by applying different surface anchoring conditions on the walls or external fields (57).

In 1967, Flautt and Lawson discovered that a mixture formed by combining a surfactant, salt, water, and alcohol in certain concentration ranges yielded a surfactant-based lyotropic liquid crystal nematic phase (58). After the discovery, lots of studies were made to explain the formation mechanisms, phase diagrams, and physicochemical properties of LNPs depending on temperature and concentration (59,60). In general, the mixture exhibiting lyotropic nematic phase properties is obtained by dissolving the surfactant molecules in water. Furthermore, in many cases, an electrolyte, a co-surfactant, or both together can be added to such mixtures (61–63).

LNPs have attracted the attention of the researchers because of the arrangement of the local director of the micelles concerning a preferred direction. This direction is called phase director or optical axis of the nematic phases. Optically, nematic phases are divided into two uniaxial nematic phases (N_D, N_C) and biaxial nematic phase (N_B). Uniaxial lyotropic phases have only one optical axis, while biaxial nematic phases have three orthogonal and two-fold symmetry axes **($\vec{l}, \vec{m}$** and **$\vec{n}$, $\vec{n} = \vec{l} \times \vec{m}$)** and two optical axes perpendicular to each other (64). Due to having two optical axes, the N_B phases are optically more advantageous over the other uniaxial nematic phases because one of the optical axes can be oriented instead of the other in the magnetic field, and this is a prominent and important feature for faster switching (65), especially for display technology. Also, N_B phases have diamagnetic properties, and magnetic field strengths (H) must be high (~10kG) to be able to orient in experimental processes (59). When the laboratory frame axes are chosen as perpendicular to each other in directions 1, 2, and 3, and axis-3 is perpendicular to plane 1-2, the refractive indices along the three axes can be shown in Figure 1.13.

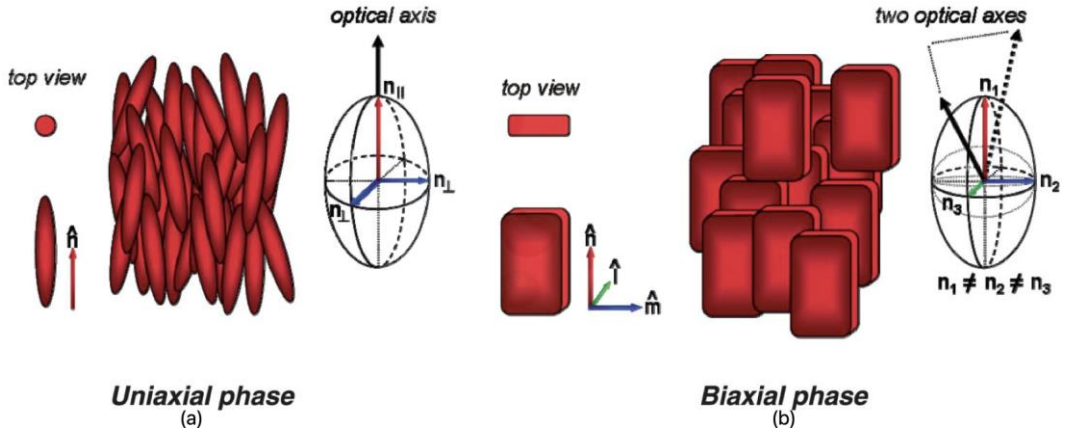

Figure 1.13. Schematic representation of molecular orientation for (a) uniaxial and (b) biaxial nematic phases (66).

Some applications of lyotropic nematic phases were reported in the literature. They are used in the production of carbon nanotubes which have applications in the fields of nanoscale electronics (67,68), field-emission sources (69–73), actuators (74), and nanosensors for both biological molecular determination (75) and drug release in molecular level (76). It is known that it is important to direct carbon nanotubes in a certain direction in carbon nanotubes/LLC hybrid systems (77). Indeed, lyotropic nematic phases act as a carrier (78) or directing solvent/medium (34) for carbon nanotubes and control the direction of alignment of nanotubes with their director (10,79–81). As a result of their independent studies, Lagerwall (34) and Okano (82) stated that LLC/CNT systems may have advantageous in directing carbon nanotubes compared to thermotropic liquid crystal/CNT systems with an approach developed for the orientation of CNTs dispersed in the lyotropic nematic phase (83). Although, in another important study on carbon nanotubes, uniaxial and biaxial single-wall CNT and multi-wall CNT films could be obtained in different lengths and film thicknesses using thermotropic nematic liquid crystals (79), however, it is not reported in the literature that any single-wall and multi-wall CNT films can be obtained by using lyotropic biaxial nematic phase.

As seen from some applications of the lyotropic nematic phases summarized above, lyotropic nematic phases, especially biaxial ones, may play a crucial role.

The main property of N_D and N_C phases is that the local symmetry axes of their structural units, micelles, shows an orientation in a preferred direction (director) in the magnetic field. It can also be said that they exhibit different

structural anisotropy. In early studies it was assumed that, the N_C phase consists of cylindrical-like micelles, while N_D is composed of planar disk-like micelles (84), Figure 1.14.

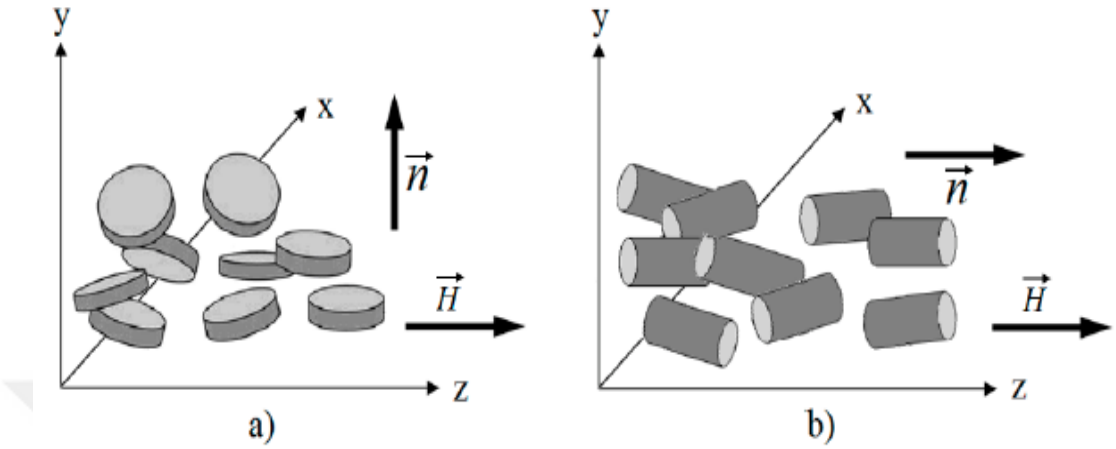

Figure 1.14. The orientations of the micelles in the a) discotic and b) calamitic phases, considering the presence of magnetic field and phase director ($\vec{n}$) (59).

The biaxial nematic phase was first detected in a mixture of potassium laurate, decanol, water by Yu and Saupe (85). The biaxial nematic phases usually occur between the uniaxial N_D and N_C phases in the phase diagrams (86,87). The transitions from the uniaxial phase to the biaxial phase are of second order as experimentally substantiated (88,89) and theoretically proven (90). After the exploration of the biaxial phase, the studies (88) continued by focusing on the investigations of the N_B phase regions in the partial phase diagrams by obtaining novelmixtures. Contrary to uniaxial phases, questions about the stability of biaxial phases have come to the about in studies of lyotropic nematic phases. The biaxial phases were found to be thermodynamically stable, and this result was supported experimentally (62). However, to explain the interpretations of the nature and structure of the biaxial phase more clearly, considering that the biaxial nematic phases are intermediate phase, some approaches have claimed that the N_B is caused by the coexistence of uniaxial phases. To interpret this approach, some models to explain the formation of nematic biaxial phases have been proposed in the literature. Stroobants and Lekkerkerker, in 1984, put forward a mixture of cylindrical and disk-like, MCD, model, which is compatible with Onsager theory to explain the formation mechanism of the biaxial nematic phases (91). Their model proposes that disk- and cylindrical-like micelles coexist to form the biaxial

nematic phase. In 2000, Kooij and Lekkerkerker showed that rod or cylindrical-like and disk-like micelles cannot coexist in a mixture, which gives the N_B phase, and the phase separation occurs. In addition, theoretical and experimental studies showed that the MCD-type models are not sufficient to explain the formation mechanism of the biaxial nematic phase (92,93).

Another important model was proposed by Neto and Galerne in 1985. This model is called “the intrinsically biaxial micelle, (IBM)” model. The IBM model emphasizes that both the uniaxial and biaxial phases are composed of micelles with orthorhombic symmetry. An X-ray diffraction study on the KL/DeOH/D_2O mixture confirmed that the micelles were similar in terms of local symmetry in the uniaxial and biaxial phases, as proposed in the IBM model (94). The IBM model is based on two basic assumptions: micelle symmetry and micelle orientational fluctuations. The orthorhombic micelles in the nematic phases can be sketched with the dimensions *A′*, *B′*, and *C′*, Figure 1.15a. The micelle bilayer formed by the surfactant molecule corresponds to *C′*. The symmetry axes of the local coordinate system fixed in the micelles are *α, β*, and *γ*. According to the IBM model, changes in orientational fluctuations around these coordinate axes are responsible for the formation of different types of LNPs. The N_D phase is caused by changes in orientational fluctuations around the axis (along the γ-axis) perpendicular to the largest micelle surface, Figure 1.15b. In this case, the micelle size *A′* has approximately the same values as the micelle size *B′*. At the transition from N_D to N_B phase, the size of the micelle along the axis of symmetry α (*A′*) begins to elongate, and the orientational fluctuations along three symmetry axes with small amplitude lead to the formation of the N_B phase, Figure 1.15c. In the N_C phase, the micelle size along the axis of symmetry *α* continues to get longer and the orientational fluctuations around the *α*-axis become dominant and the N_C phase is formed, Figure 1.15d. The reliability of the IBM model has also been supported by some studies in the literature (59,87,95).

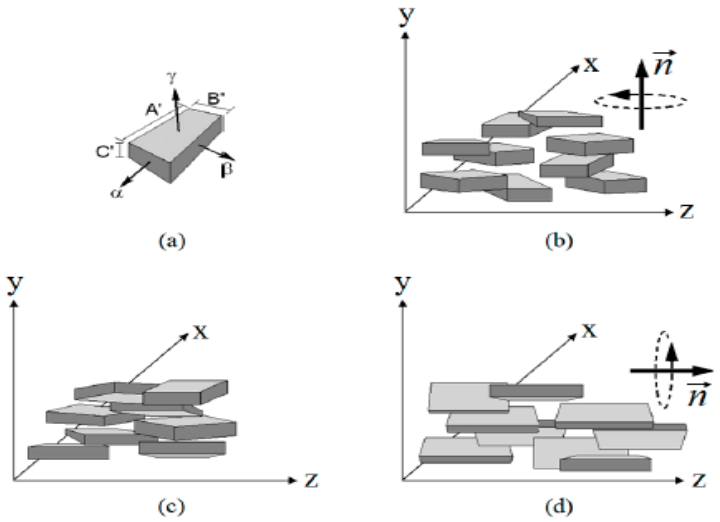

Figure 1.15. (a) Representation of an orthorhombic micelle. Formation of (b) discotic nematic (N_D), (c) biaxial nematic (N_B) and (d) calamitic nematic (N_C) phases due to different directional fluctuations in the IBM model (94).

To obtain lyotropic nematic phases, if necessary, a cosurfactant (e.g., 1-decanol) or an electrolyte (e.g., NaCl) may be added to the mixtures (59). Both components screen the repulsions between the surfactant headgroups at micelle surfaces and cause efficient packing of the surfactants in the micelles. Furthermore, they modify the micelle surface curvature, which is an important control parameter to obtain different nematic phases, especially the biaxial phase. In a very recent study, it was reported that a dye molecule Sunset Yellow, which produces lyotropic chromonic liquid crystals (LCLCs), may also use in lyotropic mixtures to form nematic phases, behaving as an electrolyte (96). It has been shown that dye molecules may be doped into the lyotropic mixtures to obtain biaxial nematic phases and be more efficient compared to the electrolytes. The advantage of the use of the dye molecules arises from the surfactant-dye interactions. However, there are no sufficient studies in the literature on obtaining lyotropic surfactant-based and dye-included mixtures to obtain lyotropic nematic phases. So, it would be, scientifically, useful to clarify the mechanism of the surfactant-dye interactions in lyotropic mixtures on the formation of different nematic phases.

1.2 Optical and magnetic properties of liquid crystals

Because liquid crystals are anisotropic materials, their physical properties change depending on the direction of the average alignment of their structural units with respect to the phase director. When a polarized light beam is passed through a liquid crystal sample, it travels in it by splitting into two plane-polarized rays, so-called "ordinary and extraordinary rays", Figure 1.16. While the electrical vector of the ordinary ray vibrates perpendicular to the $\vec{n}$, that of extraordinary one vibrates along the $\vec{n}$. The velocities of these two rays are different, which leads to the existence of two principal refractive indices, and the difference between these two refractive indices corresponds to " birefringence" or "optical anisotropy" (Δn):

$$\Delta n = n_e - n_o = n_{//} - n_{\perp} \quad (1.1)$$

where n_e and n_o are the refractive indices of the extraordinary and ordinary rays, respectively. For an anisotropic sample, there are two possibilities: $n_e > n_o$ or $n_e < n_o$.

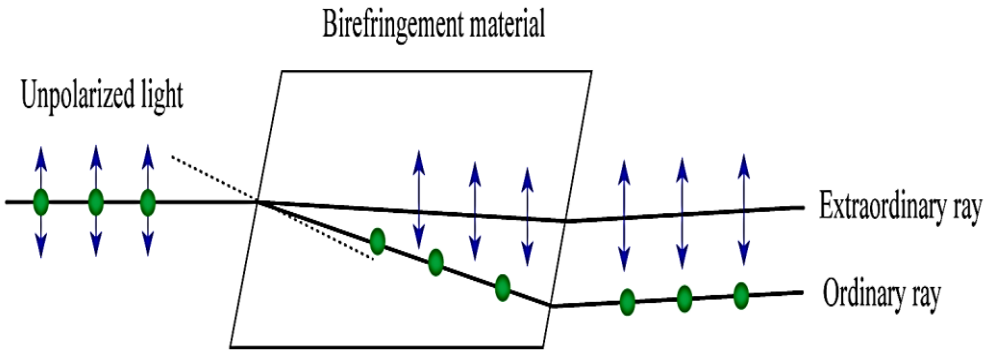

Figure 1.16. Light passing through a birefringent material travel in two paths as o-ray and e-ray (ordinary and extra ordinary) (97).

The sign of Δn for the nematic phases can be determined by conoscopic investigations under the polarizing optical microscope. The uniaxial nematics (N_D or N_C) are described by two different refractive indices. If we choose the laboratory frame axes along three orthogonal 1, 2, and 3 directions, where axis-3 is perpendicular to the 1-2 plane, $\Delta n = n_2 - n_1$ ($n_1 \neq n_2 = n_3$). Thus, the uniaxial nematics are described with only one birefringence (Δn). In general, the optical

birefringence is positive ($\Delta n>0$) for the N_D phase but negative ($\Delta n<0$) for the N_C phase. However, the biaxial nematics have two different birefringences with three refractive indices, n_1, n_2 and n_3: $\Delta n = n_2–n_1$ and $\delta n = n_3–n_2$, where $n_1 \neq n_2 \neq n_3$. If $n_3–n_2 > n_2-n_1$, the biaxial phase has positive birefringence. If $n_3–n_2 < n_2–n_1$, the biaxial phase is described with negative birefringence (89).

The behavior of materials under the effect of a magnetic field is an important physical property. Magnetic materials are classified as diamagnetic, paramagnetic and ferromagnetic. LCs are diamagnetic materials. The diamagnetic susceptibility leads to a coupling between external magnetic fields and the orientation of the anisotropic part of LC molecules (98). LCs are sensitive to application of the external magnetic fields, enabling them to be used in many technological advances (99).

The magnetization, M, for diamagnetic materials is proportional to the magnetic field strength H,

$$M=\chi H \tag{1.2}$$

where χ is the magnetic susceptibility and, for diamagnetics materials, χ is always negative. The difference between the components of magnetic susceptibilities, measured taking into account the direction of the applied magnetic field, determines the sign of the diamagnetic susceptibility anisotropy. If the direction of the applied magnetic field is parallel (perpendicular) to that of the optical axis of the phase, the resultant magnetic susceptibility is indicated as $\chi_{//}$ ($\chi_{\perp}$). Thus, the diamagnetic susceptibility anisotropy $\Delta\chi$ of a liquid crystal sample can be defined by $\chi_{//}$ and $\chi_{\perp}$ with the following equation:

$$\Delta\chi = \chi_{//} - \chi_{\perp} \tag{1.3}$$

When a LC sample has a positive diamagnetic susceptibility anisotropy ($\Delta\chi>0$), the optical axis of the LC aligns parallel to the magnetic field. When it is negative ($\Delta\chi<0$), the direction of the optical axis is perpendicular to the magnetic field. When it equals zero, the system is isotropic.

Similar to the sign of Δn, $\Delta\chi$ is also a criterion for characterization of nematic phases, i.e., in general, Δn and $\Delta\chi$ have opposite signs. For instance, if the optical axis of a uniaxial nematic liquid crystal sample aligns perpendicular to the magnetic field direction, $\Delta\chi<0$ but $\Delta n>0$, and vice versa.

The N_B phases exhibit three two-fold magnetic susceptibilities. In the presence of the magnetic field, $\Delta\chi$ of the N_B phase is

$$\Delta\chi = \chi_{33} - \frac{1}{2}(\chi_{11} + \chi_{22}) \quad (1.4)$$

where the subscripts 11, 22 and 33, correspond to the three orthogonal directions. If a N_B phase aligns with the axis of the largest diamagnetic susceptibility parallel (perpendicular) to the magnetic field direction, $\Delta\chi>0$ ($\Delta\chi<0$) (100).

2. AIM AND SCOPE OF THE STUDY

In the literature, various studies have been carried out to explain the formation mechanisms and physicochemical properties of surfactant-based LNPs (60,101,102). Especially, it has become important to define the formation mechanisms of the N_B phase regions in the phase diagrams and to reveal the factors that cause the formation of biaxial nematic phases.

In lyotropic mixtures, the main component is surfactant molecules. In general, strong/weak electrolytes and/or long-chain alcohols (e.g decanol) can be added to the mixtures. The types of electrolytes and the alkyl chain length of alcohols determine the properties of the nematic phases. In 2020, it was reported the lyotropic nematic phase properties of dodecyltrimethylammonium bromide (DTMABr)/dodecanol (DDeOH)/water ternary mixture by doping with an anionic azo dye Sunset Yellow. That study showed that Sunset Yellow molecule is more effective for obtaining different nematic phases, especially the biaxial one, than conventional inorganic electrolytes (e.g. NaCl, NaBr, etc.). Furthermore, for the first time, it was shown that Sunset Yellow molecule has a chaotropic character and it can be sequenced in the Hofmeister series of ions. However, novel lyotropic mixtures with different dyes have to be found, investigated and characterized to clarify the effect of surfactant-dye interactions on the formation of different nematic phases.

In the present thesis, we concentrate on finding novel lyotropic mixtures including different dyes (amaranth and tartrazine) and a drug molecule (DSCG) to examine their relative effects on finding different nematic phases via laser conoscopy, polarizing optical microscopy and small-angle X-ray scattering (SAXS). All molecules gave similar partial phase diagrams. However, they affected the nematic-nematic phase transitions and biaxial phase temperature range differently. Furthermore, we classified those molecules in the Hofmeister series of ions by considering the number of ionic groups in their structures. Consequently, the results indicated that dye/drug molecules can also be used to obtain different nematic phases.

3. MATERIALS AND METHODS

3.1 Materials used in the thesis.

Surfactant molecule (DTMABr) was commercially available with a minimum purity of 98% (Sigma), and characterized by FTIR (Perkin-Elmer Spectrum Two FTIR Spectrometer) and ^{1}H-NMR (JEOL NMR spectrometer, 400 MHz), Figure 3.1. and Figure 3.2., respectively. The FTIR spectrum is quite compatible with the literature (103), and the chemical shift values obtained from the NMR spectrum also agree with the expected values. In particular, the NMR spectrum shows that DTMABr is pure enough.

The dye molecules amaranth (85-95%), and tartrazine (85%) and the drug molecule disodium cromoglycate (>95%) were purchased from Sigma-Aldrich. The purification method applied for Sunset Yellow in the literature was also applied for amaranth and tartrazine (96,104,105). Disodium cromoglicate (DSCG) was used as purchased without purification as in the literature. The ultrapure water required for the preparation of lyotropic liquid crystal samples was obtained from the Millipore Direct-Q3 UV purification system (18.2 MΩ.cm resistivity at 25ºC). 1-dodecanol (DDeOH) used in lyotropic mixtures was purchased from Sigma-Aldrich with 99% purity.

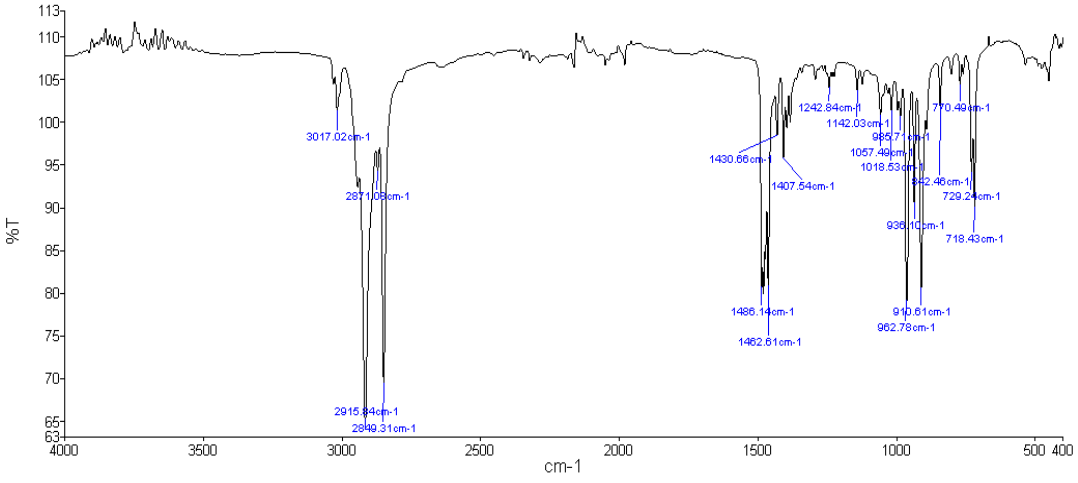

Figure 3.1. FTIR spectrum of the DTMABr molecule (103).

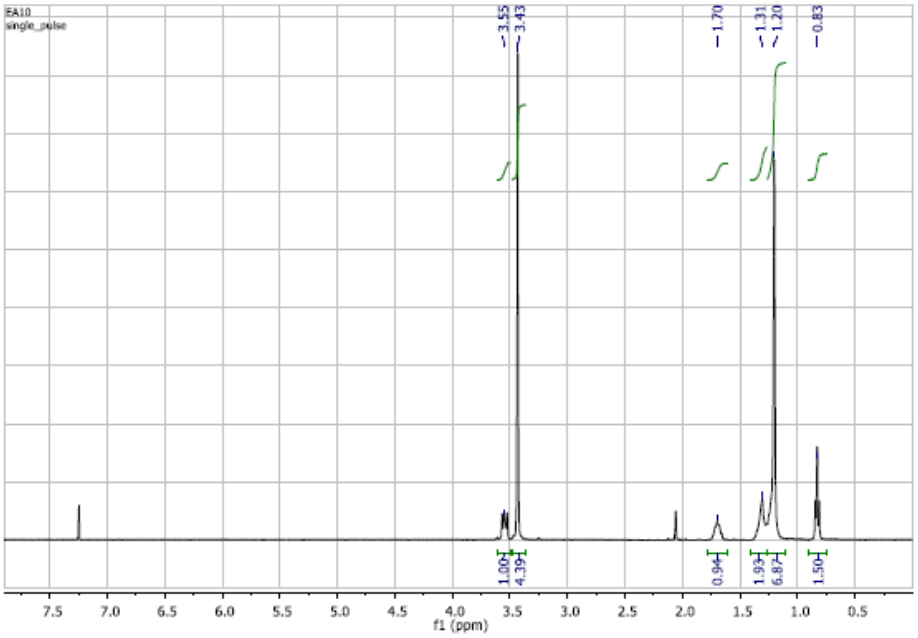

Figure 3.2. [1] H-NMR spectrum of DTMABr in $CDCl_3$ solvent; 1H NMR (400 MHz), δ (ppm, $CDCl_3$): 0.83 (CH_3, 3H, t), 1.20 (CH_2, 14H, br m), 1.30 (CH_2, 4H, br m), 1.70 (CH_2, 2H, br m), 3.40 (N^+CH_3, 9H, s), 3.55 (N^+CH_2, 2H, t). s=singlet, t=triplet, q=quartet, m=multiplet, br s=broad singlet, br m=broad multiplet (103).

3.2 Experimental techniques

3.2.1 Preparation of liquid crystal samples

Lyotropic liquid crystal mixtures were prepared by weighing the constituents of the desired mixtures (surfactant, co-surfactant, electrolyte, amaranth/tartrazine/DSCG, water) in pyrex glass tubes with caps. A high-precision balance (Radwag, ±0.00001 mg) was used in the weighing procedure. Then, samples were homogenized by applying vortex (Ika) and centrifuge (Hettich). Because well-oriented nematic phases in the presence of the magnetic field (~2.0, ~1.0 kG, respectively) are required for laser conoscopy, polarizing optical microscopy and small-angle X-ray scattering measurements, a water-based ferrofluid (Ferrotec, EMG-605) was added at a ratio of 1 μL ferrofluid per 1 g of lyotropic mixtures. Previous experiments in the literature showed that the addition of this amount of ferrofluid did not cause any deformation in the phase topology or an error in the measurements (102).

In this thesis, a total of 41 new lyotropic mixtures were prepared by adding amaranth, tartrazine and DSCG molecules separately to the dodecyltrimethylammonium bromide (DTMABr)/dodecanol (DDeOH)/water host mixture at different concentrations. However, to better understand the experimental results, some mixtures containing the Sunset Yellow molecule examined in the reference study (96) were also examined within the scope of the thesis. The total number of lyotropic mixtures studied was 52, including 1 main mixture, 10 mixtures containing Sunset Yellow, 13 mixtures containing amaranth, 18 mixtures containing tartrazine, and 10 mixtures containing DSCG. The reason for the different number of mixtures studied for the molecules is that they interact with the DTMABr surfactant molecule at different level as intended in the thesis, and different numbers of mixtures are needed to obtain clear phase diagrams. The compositions of the mixtures obtained by adding guest molecules to the main mixture are given in Tables of “Results and Discussions”.

3.2.2 Laser conoscopy

As mentioned before, lyotropic nematic phases are defined by two different optical birefringences, Δn and δn (Δn =n_2−n_1 and δn = n_3−n_2, where n_1, n_2, and n_3 are the refractive indices of the medium along the three selected perpendicular laboratory frame axes (1, 2 and 3). While only birefringence Δn can be measured using a Berek compensator under polarizing optical microscope, both Δn and δn can be evaluated by laser conoscopy. In addition, laser conoscopy is a method that provides very useful and sensitive results in determining the phase transition temperatures between uniaxial nematic phases and biaxial nematic phases, which is of second order according to the "mean-field theory". Laser conoscopy measurements were started from the well-oriented N_D phase, Figure 3.3a. In these measurements, it is very important to start with the well-oriented N_D phase. Uniaxial-biaxial nematic phase transitions were determined from the temperature dependence of the birefringence values of the nematic phases. The interference patterns observed for all three nematic phases are given in Figure 3.3.

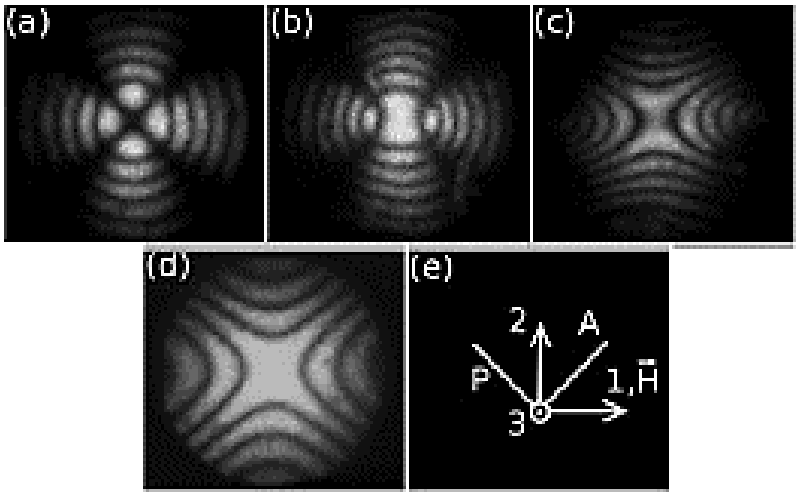

Figure 3.3. Characteristic conoscopic interference patterns of LNPs by laser conoscopy (106). Interference patterns of (a) N_D, (b) N_B around N_D-N_B phase transitions, (c) N_B around N_B-N_C phase transitions, and (d) N_C phases obtained by changing temperature. (d) 1, 2, 3 selected laboratory coordinate axes; A and P are the analyzer and polarizer direction, respectively; H indicates the direction of the magnetic field. The optical direction of the laser light beam directed on the sample is parallel to the axis-3 direction.

In laser conoscopy measurements, lyotropic liquid crystal samples are placed between two 2.5 cm diameter round optical glasses (Helma) using a 2.5 mm thick hollow glass ring, Figure 3.4. Afterward, the prepared sample is placed in the specially designed sample holder and measurements are performed. The experimental setup of laser conoscopy is roughly given in Figure 3.5. After the measurements are completed, the birefringence values are calculated with specially developed computer software depending on the temperature Figure 3.6.

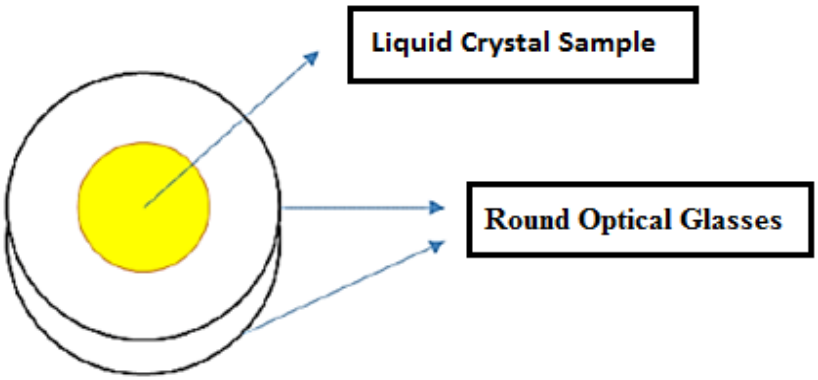

Figure 3.4. A lyotropic liquid crystal sample prepared between two round optical glasses.

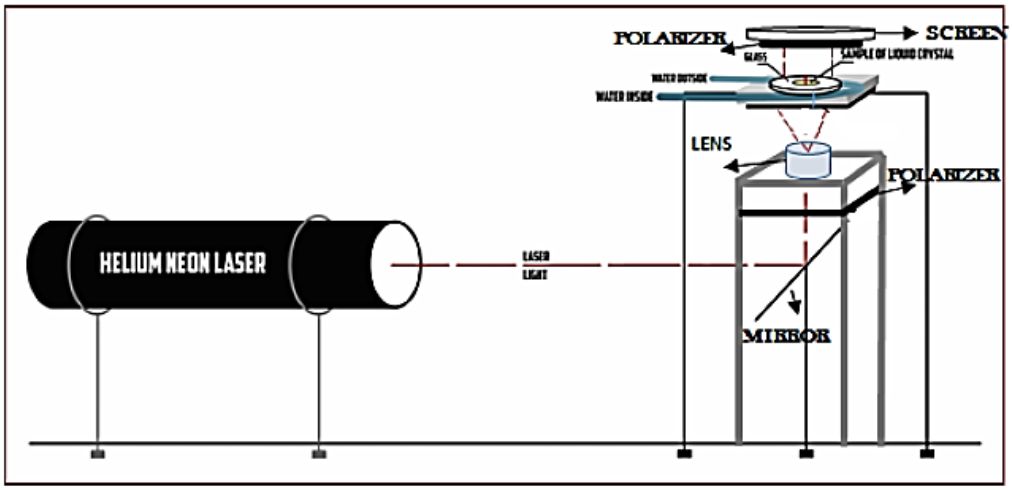

Figure 3.5. Laser conoscopy setup. The light from the HeNe (632.8 nm) laser source is reflected vertically to the lens by passing through the polarizer with a 45° angled mirror. Laser light passing through the lyotropic nematic sample passes through a second polarizer (in this case, the analyzer) perpendicular to the first polarizer, creating an interference pattern on the screen.

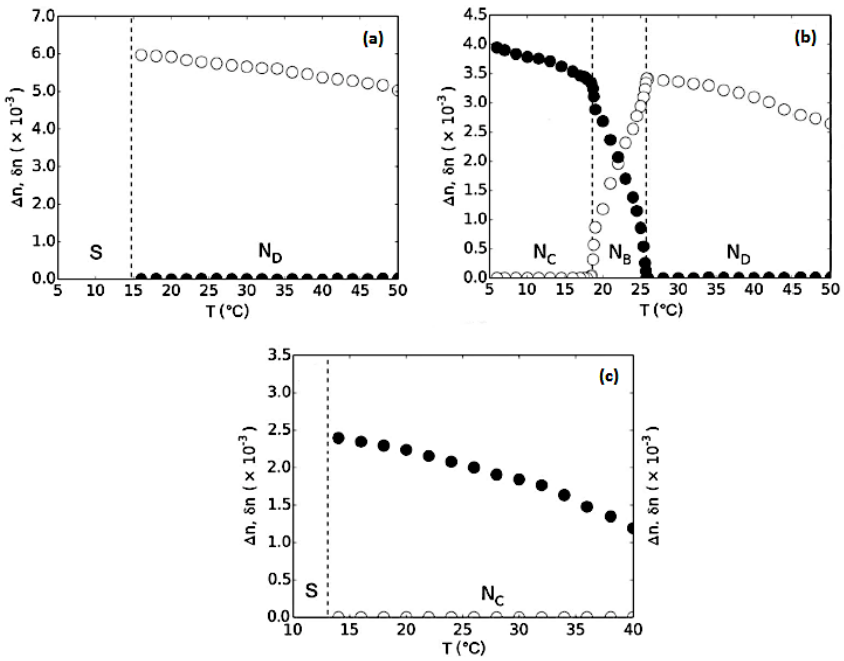

Figure 3.6. The change of birefringence values of nematic phases with temperature for potassium alkanoate/Rb_2SO_4/DeOH/water mixtures obtained from studies (86): (a) giving only uniaxial N_D phase; (b) yielding three nematic phases depending on temperature; (c) giving only uniaxial N_C phase.

Temperature control is very important in the laser conoscopy system. For this purpose, a temperature controller (Lakeshore 335) with a sensitivity of 0.001°C and a Pt102 sensor were used. A water-circulating bath (Polyscience AD07R) with a sensitivity of 0.01° C was used for a homogeneous distribution of the temperature in the system. The strength of the magnetic field (2.2 kG) in the system was controlled with a gaussmeter (Lakeshore, Model 455) during the measurements.

3.2.3 Polarizing optical microscopy

The phase textures of the lyotropic liquid crystals were characterized by Nikon Eclipse Ci-POL (Nikon, Japan) polarizing optical microscope (POM), Figure 3.7. For POM measurements, well-homogenized liquid crystal samples were transferred into a 0.2, 0.3, and/or 0.4 mm rectangular microslide (Vitrocom, Japan). Both ends of the microslides were coated with a special fluid nanocomposite (DLine, Lithuania), and then UV light was applied to the ends. Microslides containing lyotropic liquid crystal samples were placed in a temperature control unit (Linkam LTS120E, 0.1°C sensitivity) and homogeneous heat distribution was provided by a water bath with a circulator connected to this temperature control unit. The phase textures of the lyotropic liquid crystal samples were recorded with a color camera (DFK41AU02, The Imaging Source, Germany) and characterized with special software (NIS-Element-D computer software, Nikon). The experimental measurement configuration in the polarizing optical microscope is shown in Figure 3.8.

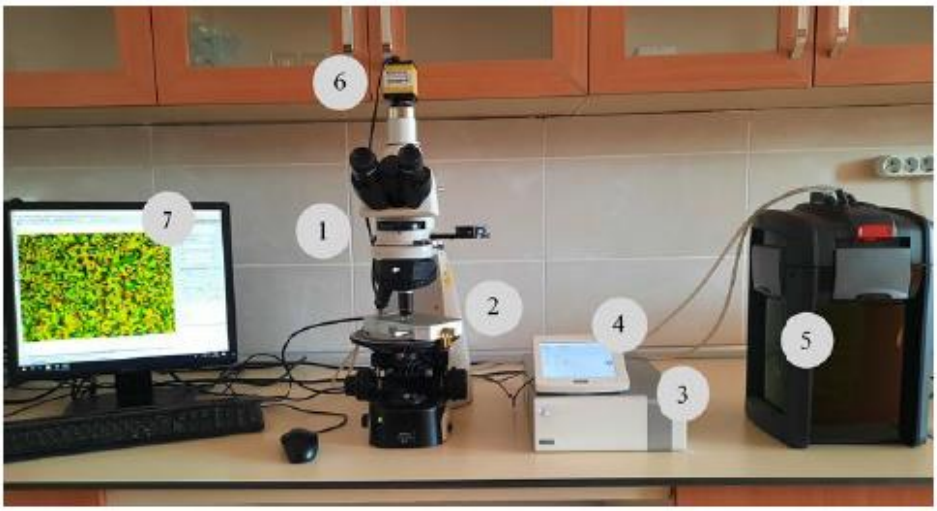

Figure 3.7. Polarizing optical microscopy measurement setup. 1: polarizing optical microscopy; 2: Linkam LTS120E heater/cooler plate; 3: Linkam T95-PE heating/cooling controller; 4: connector and display of parts 2 and 3 (Linkpad); 5: water bath; 6: camera; 7: NIS-Element-D computer software.

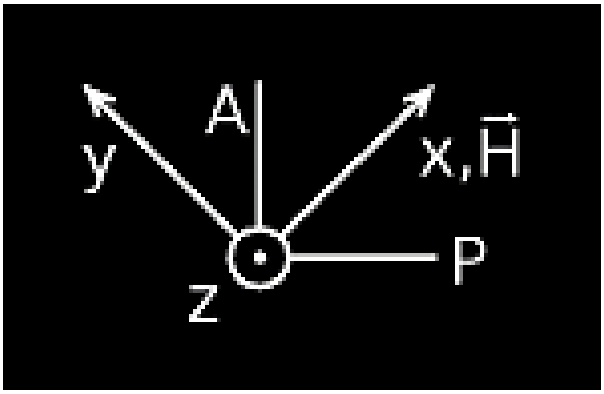

Figure 3.8. The measurement configuration chosen for the examination of phase under polarizing optical microscopy: x, y, z selected laboratory coordinate axes; A and P are the analyzer and polarizer direction, respectively; H indicates the direction of the magnetic field. The long axis of the capillary containing the lyotropic liquid crystal samples is placed parallel to the y-axis (perpendicular to the magnetic field direction).

3.2.4 Small-angle x-ray scattering (SAXS)

Small-angle X-ray scattering (SAXS) is a very useful and strong experimental technique to evaluate micelle structure parameters (micelle dimensions, intermicellar distances, surfactant aggregation numbers, packing parameter, etc.). In this thesis, the small-angle X-ray scattering (SAXS) measurements procedure and data treatment were based on those given in the Supplementary Information of Ref. (53). The experimental part of the SAXS can be summarized as follows. A Xeuss 2.0 laboratory-based system (Xenocs, France) was applied to lyotropic mixtures. The monochromatic and collimated incident X-ray beam has a square cross section with 0.7 mm side in sample's position and wavelength of 1.5419 Å. A Genix3D beam delivery system was used to generate the beam. This systems consists of a Cu anode microfocus' X-ray source and a FOX3D X-ray mirror. A sample-to-detector distance was 936 mm. A Pilatus 300K detector (Dectris, Switzerland) enabled to measure the images of the two-dimensional X-ray scattering patterns. Lyotropic samples were transferred into cylindrical Mark-capillary of 1.5 mm diameter (Hilgenberg, Germany). The end of capillary was closed with a UV-sensitive photopolymer. During the SAXS measurement, a capillary was placed in a temperature-controlled sample holder with precision of ±0.2 °C. Rectangular bars of permanent NdFeB magnets (~1 kG) were attached to the sidewalls of the sample holder to generate a sufficiently homogeneous magnetic field.

4. RESULTS AND DISCUSSIONS

4.1 Polarizing optical microscopy and phase transitions

Figure 4.1. shows the molecular structures of dye/drug molecules Sunset Yellow, amaranth, tartrazine, and DSCG. Note that we recently investigated the uniaxial and biaxial nematic phase properties of lyotropic mixtures including Sunset Yellow in another study (96,107), thus the investigation of the nematic phase properties of Sunset Yellow-included mixtures has been repeated in the present study just for the comparison with other dye/drug molecules.

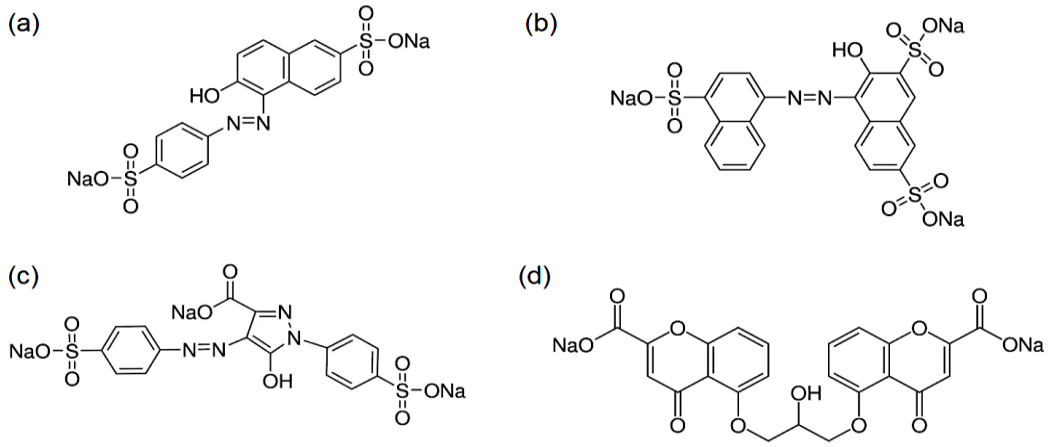

Figure 4.1. Molecular structures of dye/drug molecules: (a) Sunset Yellow, (b) amaranth, (c) tartrazine, and (d) DSCG.

The compositions of lyotropic mixtures of DTMABr/DDeOH/water doped with Sunset Yellow, amaranth, tartrazine, and DSCG are given in Tables 4.1-4.4, respectively, at different dye/drug concentrations. The nematic textures of the mixtures were confirmed by polarizing optical microscopy investigations with characteristic “schlieren textures” of nematic phases, and also their homeotropic and planar alignments in the presence of a magnetic field (Figures 4.2-4.5). Notice that the N_D (N_C and N_B) phase(s) is (are) characterized by homeotropic (planar) alignment. While the N_D phases may be easily distinguished from other nematics, the birefringence measurements by optical conoscopy with compensators or laser conoscopy help to distinguish the N_C phase from the N_B one. The latter was used in the present study to evaluate the second-order uniaxial-to-biaxial nematic phase transitions from the temperature dependence of the birefringences of three nematic phases and to determine the temperature range of the biaxial nematic phase domain in the partial phase diagrams.

Table 4.1. Compositions of the lyotropic host mixture DTMABr/DDeOH/water (D0) and the mixtures obtained from doping it with Sunset Yellow (SSY), nematic-nematic phase transition temperatures, and biaxial nematic phase range observed in the partial phase diagram -ΔT_{N_B}. X corresponds to the percent mole fraction of each component of the mixtures. Similar results were reported in our recent study and repeated in the present study for comparison (96).

Mixture	$\mathbf{X_{DTMABr}}$	$\mathbf{X_{SSY}}$	$\mathbf{X_{DDeOH}}$	$\mathbf{X_{water}}$	**Phase transitions**	ΔT_{N_B}/℃
D0	4.988	0.000	1.794	93.218	N_C	---
s1	4.986	0.026	1.794	93.194	N_C	---
s2	4.985	0.053	1.793	93.169	N_C	---
s3	4.984	0.079	1.793	93.144	N_C	---
s4	4.982	0.106	1.792	93.120	$N_D \xrightarrow{26.4℃} N_B \xrightarrow{24.5℃} N_C$	1.90
s5	4.980	0.132	1.791	93.097	$N_D \xrightarrow{21.2℃} N_B \xrightarrow{17.1℃} N_C$	4.10
s6	4.980	0.144	1.792	93.084	$N_D \xrightarrow{19.3℃} N_B \xrightarrow{14.7℃} N_C$	4.60
s7	4.979	0.158	1.791	93.072	$N_D \xrightarrow{17.1℃} N_B$	---
s8	4.978	0.184	1.791	93.047	$N_D \xrightarrow{14.5℃} N_B$	---
s9	4.977	0.211	1.790	93.022	N_D	---
s10	4.975	0.237	1.790	92.998	N_D	---

Table 4.2. Compositions of the lyotropic mixtures obtained from doping the host mixture with amaranth, nematic-nematic phase transition temperatures, and biaxial nematic phase range observed in the partial phase diagram -ΔT_{N_B}.

Mixture	**X_{DTMABr}**	**$X_{Amaranth}$**	**X_{DDeOH}**	**X_{Water}**	**Phase transitions**	ΔT_{N_B}/℃
a1	4.985	0.036	1.793	93.186	N_C	---
a2	4.984	0.056	1.793	93.167	N_C	---
a3	4.983	0.066	1.793	93.158	$N_D \xrightarrow{27.2℃} N_B \xrightarrow{25.4℃} N_C$	1.8
a4	4.983	0.070	1.793	93.154	$N_D \xrightarrow{26.6℃} N_B \xrightarrow{24.5℃} N_C$	2.1
a5	4.983	0.079	1.792	93.146	$N_D \xrightarrow{23.0℃} N_B \xrightarrow{20.7℃} N_C$	2.3
a6	4.982	0.088	1.792	93.138	$N_D \xrightarrow{21.4℃} N_B \xrightarrow{19.0℃} N_C$	2.4
a7	4.982	0.096	1.792	93.130	$N_D \xrightarrow{18.9℃} N_B \xrightarrow{15.7℃} N_C$	3.2
a8	4.981	0.106	1.792	93.121	$N_D \xrightarrow{16.8℃} N_B \xrightarrow{13.7℃} N_C$	3.1
a9	4.981	0.114	1.792	93.113	$N_D \xrightarrow{15.2℃} N_B$	---
a10	4.980	0.126	1.792	93.102	$N_D \xrightarrow{13.3℃} N_B$	---
a11	4.980	0.129	1.792	93.099	$N_D \xrightarrow{13.4℃} N_B$	---
a12	4.980	0.141	1.791	93.088	N_D	---
a13	4.979	0.153	1.791	93.077	N_D	---

Table 4.3. Compositions of the lyotropic mixtures obtained from doping the host mixture with tartrazine, nematic-nematic phase transition temperatures, and biaxial nematic phase range observed in the partial phase diagram -ΔT_{N_B}.

Mixture	$\mathbf{X_{DTMABr}}$	$\mathbf{X_{tartrazine}}$	$\mathbf{X_{DDeOH}}$	$\mathbf{X_{water}}$	**Phase transitions**	$\Delta T_{N_B}/℃$
t1	4.985	0.036	1.793	93.186	N_C	---
t2	4.984	0.057	1.793	93.166	N_C	---
t3	4.983	0.066	1.793	93.158	N_C	---
t4	4.983	0.070	1.793	93,154	N_C	---
t5	4.983	0.078	1.792	93.147	$N_D \xrightarrow{29.0℃} N_B \xrightarrow{28.4℃} N_C$	0.6
t6	4.982	0.088	1.792	93.138	$N_D \xrightarrow{27.6℃} N_B \xrightarrow{26.8℃} N_C$	0.8
t7	4.982	0.095	1.792	93.131	$N_D \xrightarrow{24.9℃} N_B \xrightarrow{23.7℃} N_C$	1.2
t8	4.981	0.106	1.792	93.121	$N_D \xrightarrow{24.2℃} N_B \xrightarrow{22.5℃} N_C$	1.7
t9	4.981	0.114	1.792	93.113	$N_D \xrightarrow{22.0℃} N_B \xrightarrow{19.9℃} N_C$	2.1
t10	4.980	0.130	1.792	93.098	$N_D \xrightarrow{19.2℃} N_B \xrightarrow{16.8℃} N_C$	2.4
t11	4.980	0.141	1.791	93.088	$N_D \xrightarrow{17.5℃} N_B \xrightarrow{14.8℃} N_C$	2.7
t12	4.979	0.153	1.791	93.077	$N_D \xrightarrow{15.7℃} N_B \xrightarrow{12.6℃} N_C$	3.1
t13	4.978	0.165	1.791	93.066	$N_D \xrightarrow{15.2℃} N_B$	---
t14	4.978	0.177	1.791	93.054	$N_D \xrightarrow{14.0℃} N_B$	---
t15	4.977	0.189	1.790	93.044	N_D	---
t16	4.977	0.200	1.790	93.033	N_D	---
t17	4.976	0.212	1.790	93.022	N_D	---
t18	4.975	0.224	1.790	93.011	N_D	---

Table 4.4. Compositions of the lyotropic mixtures obtained from doping the host mixture with DSCG, nematic-nematic phase transition temperatures, and biaxial nematic phase range observed in the partial phase diagram -ΔT_{N_B}.

Mixture	$\mathbf{X_{DTMABr}}$	$\mathbf{X_{DSCG}}$	$\mathbf{X_{DDeOH}}$	$\mathbf{X_{water}}$	**Phase transitions**	ΔT_{N_B}/℃
d1	4.984	0.053	1.793	93.170	N_C	---
d2	4.983	0.084	1.792	93.141	N_C	---
d3	4.982	0.099	1.792	93.127	$N_D \xrightarrow{24.2℃} N_B \xrightarrow{22.9℃} N_C$	1.3
d4	4.981	0.105	1.792	93.122	$N_D \xrightarrow{22.9℃} N_B \xrightarrow{21.3℃} N_C$	1.6
d5	4.981	0.118	1.792	93.109	$N_D \xrightarrow{20.9℃} N_B \xrightarrow{18.6℃} N_C$	2.3
d6	4.980	0.132	1.791	93.097	$N_D \xrightarrow{18.6℃} N_B \xrightarrow{15.8℃} N_C$	2.8
d7	4.979	0.143	1.791	93.087	$N_D \xrightarrow{18.0℃} N_B \xrightarrow{15.2℃} N_C$	2.8
d8	4.979	0.158	1.791	93.072	$N_D \xrightarrow{16.4℃} N_B$	---
d9	4.978	0.171	1.791	93.060	$N_D \xrightarrow{15.9℃} N_B$	---
d10	4.977	0.189	1.790	93.044	N_D	---

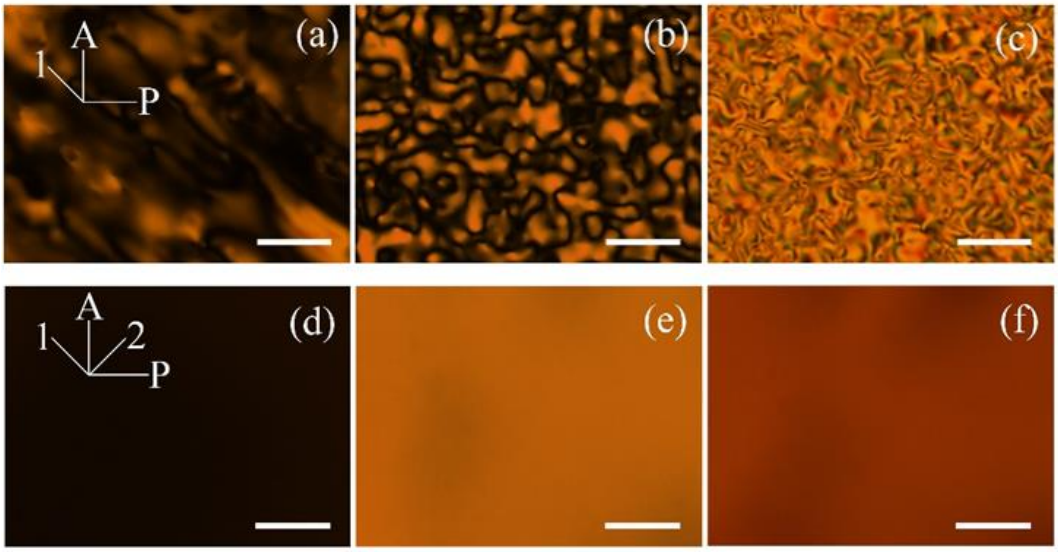

Figure 4.2. Polarizing optical microscope textures of magnetically non-aligned lyotropic nematic phases for DTMABr/Sunset Yellow/DDeOH/water mixture, s5: (a) N_D at 22.0°C, (b) N_B at 18.0°C, and (e) N_C at 14.0°C. After applying the magnetic field of 0.9 kG to those nematic phases at the corresponding temperatures: (d) homeotropic N_D, (e) planar N_B and (f) planar N_C. Objective is 10x and the white bars corresponds to 200 μm. A, P, 1 and 2 are the directions of analyzer, polarizer, long capillary axis and magnetic field (only for d, e and f) for all textures, respectively. Similar experimental set-up was applied to amaranth, tartrazine and DSCG-included mixtures. The observed textures were very similar to the ones in Ref (96).

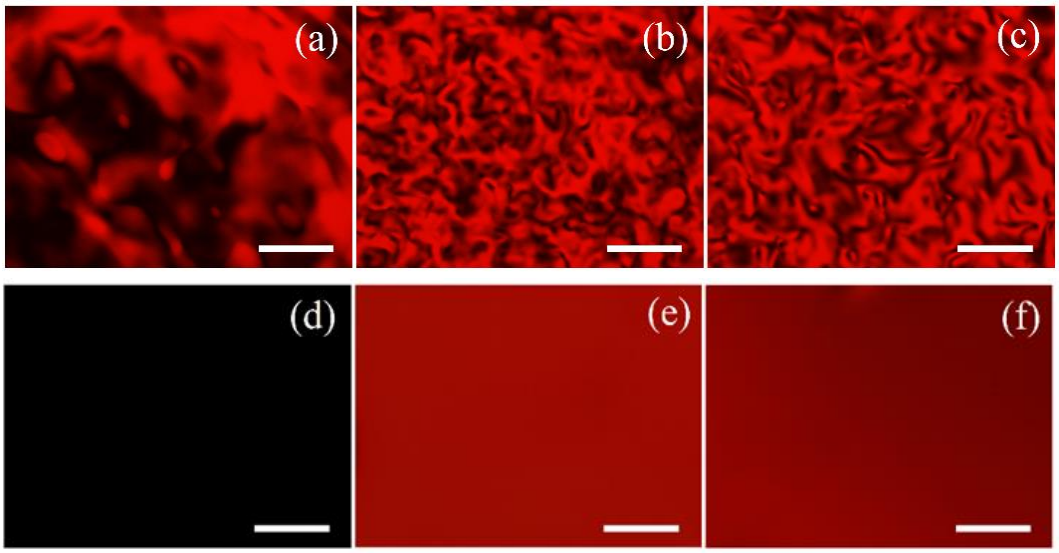

Figure 4.3. Polarizing optical microscope textures of magnetically non-aligned lyotropic nematic phases for DTMABr/amaranth/DDeOH/water mixture, a6: (a) N_D at 22.0°C, (b) N_B at 20.0°C, and (e) N_C at 15.0°C. After applying the magnetic field of 0.9 kG to those nematic phases at the corresponding temperatures: (d) homeotropic N_D, (e) planar N_B and (f) planar N_C.

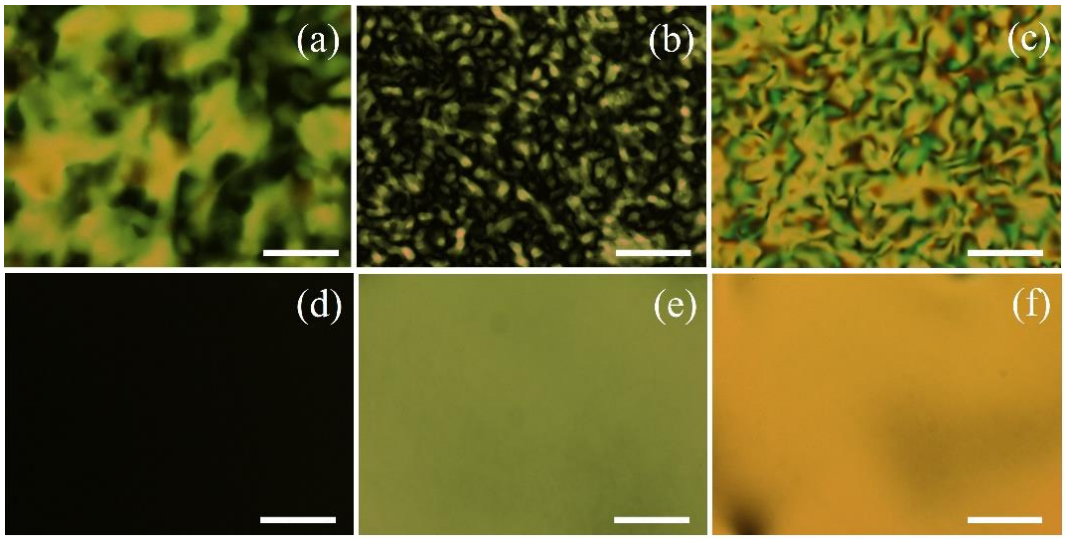

Figure 4.4. Polarizing optical microscope textures of magnetically non-aligned lyotropic nematic phases for DTMABr/tartrazine/DDeOH/water mixture, t6: (a) N_D at 30.0°C, (b) N_B at 27.3°C, and (e) N_C at 22.0°C. After applying the magnetic field of 0.9 kG to those nematic phases at the corresponding temperatures: (d) homeotropic N_D, (e) planar N_B and (f) planar N_C.

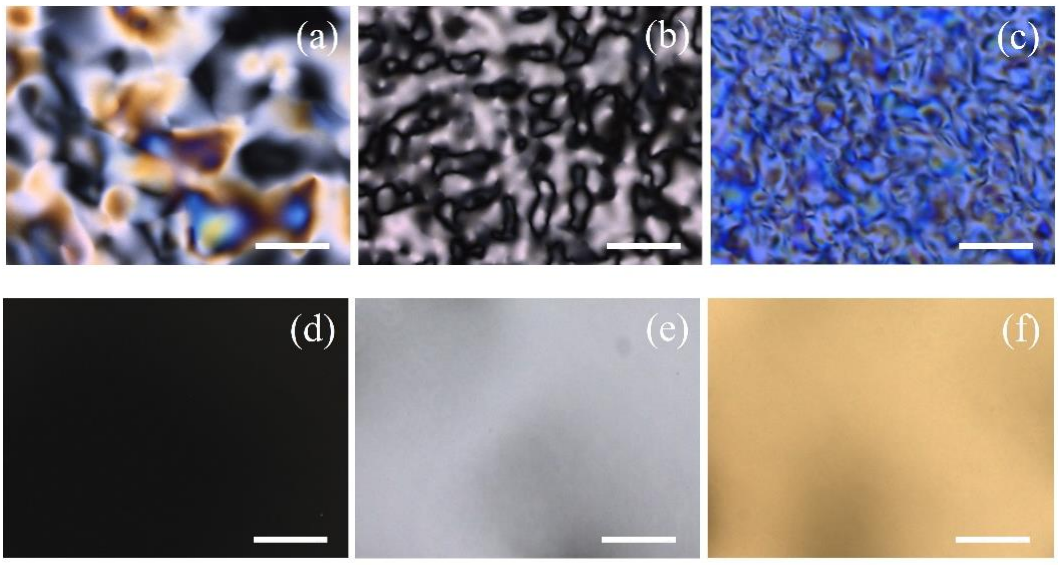

Figure 4.5. Polarizing optical microscope textures of magnetically non-aligned lyotropic nematic phases for DTMABr/DSCG/DDeOH/water mixture, d6: (a) N_D at 25.0°C, (b) N_B at 17.0°C, and (e) N_C at 14.0°C. After applying the magnetic field of 0.9 kG to those nematic phases at the corresponding temperatures: (d) homeotropic N_D, (e) planar N_B and (f) planar N_C.

4.2 Laser conoscopy: nematic-nematic phase transitions

The birefringences of the three nematic phases as a function of temperature for the mixtures given in Tables 4.1-4.4 were determined from the laser conoscopy. The results are presented in Figures 4.6-4.9 for each dye/drug molecule.

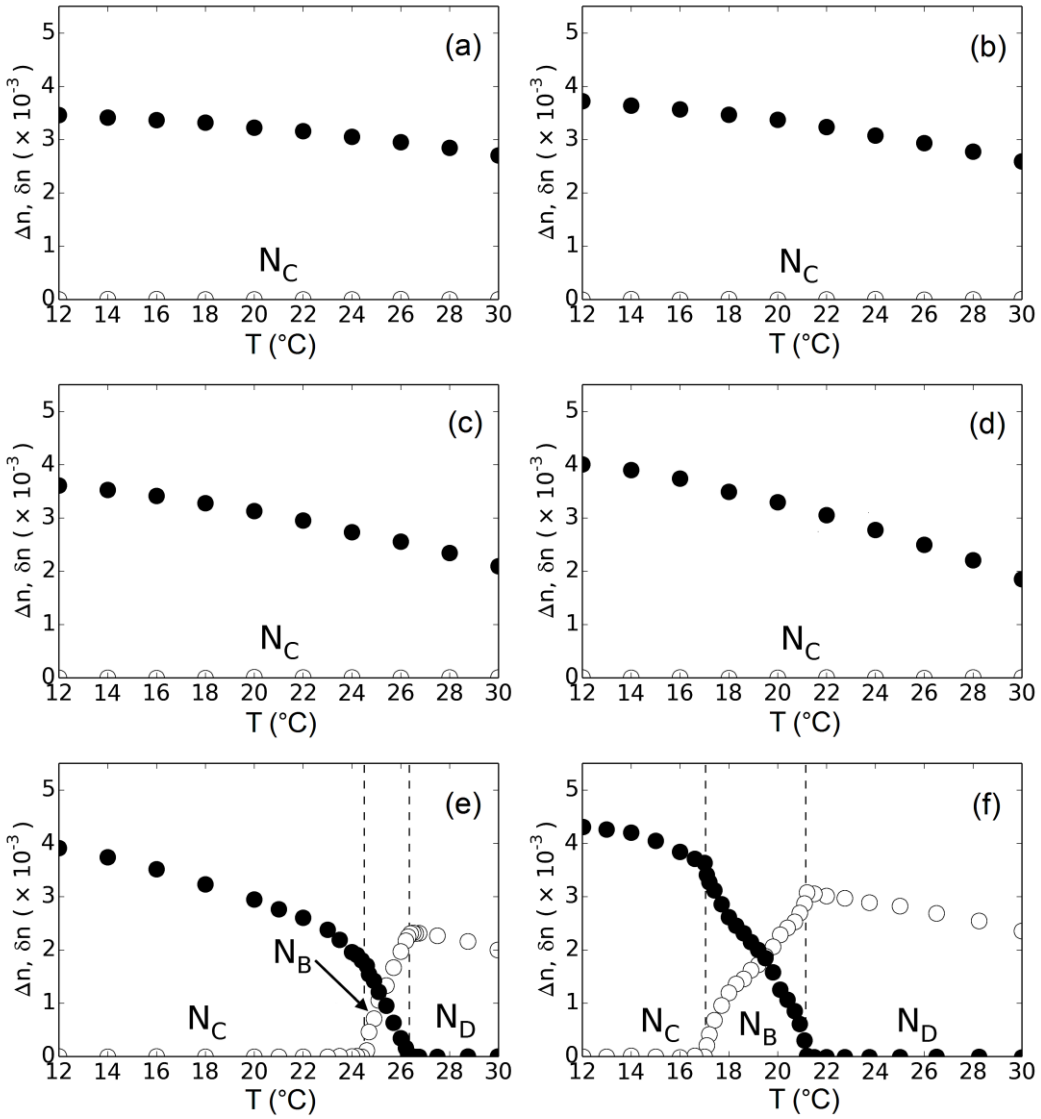

Figure 4.6. Continuing.

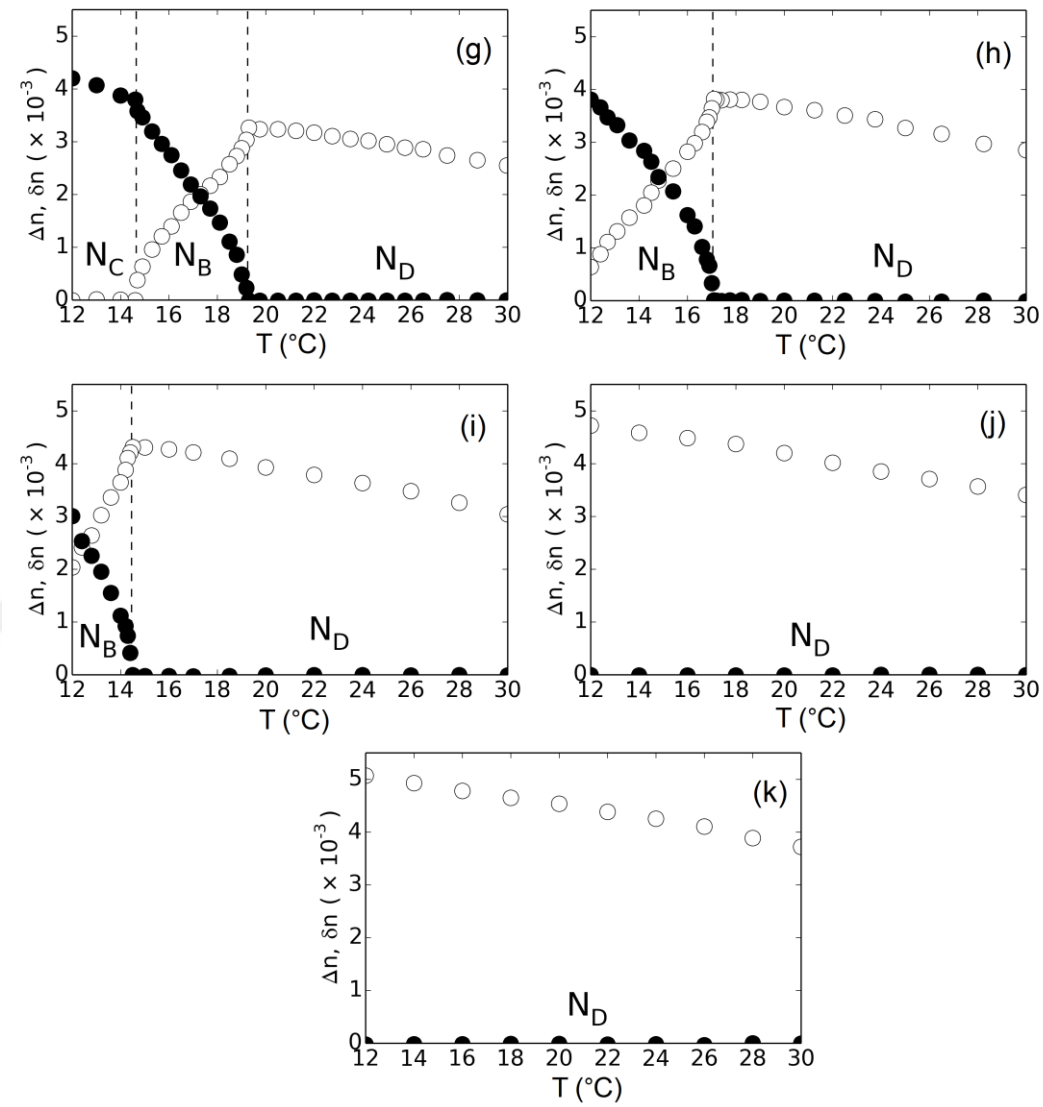

Figure 4.6. The temperature dependences of the birefringences of the nematic phases for (a) the host mixture DTMABr/DDeOH/water (D0) and DTMABr/Sunset Yellow/DDeOH/water (Table 4.1): (b) s1, (c) s2, (d) s3, (e) s4, (f) s5, (g) s6, (h) s7, (i) s8, (j) s9, and (k) s10. Similar results were obtained in Ref. (96).

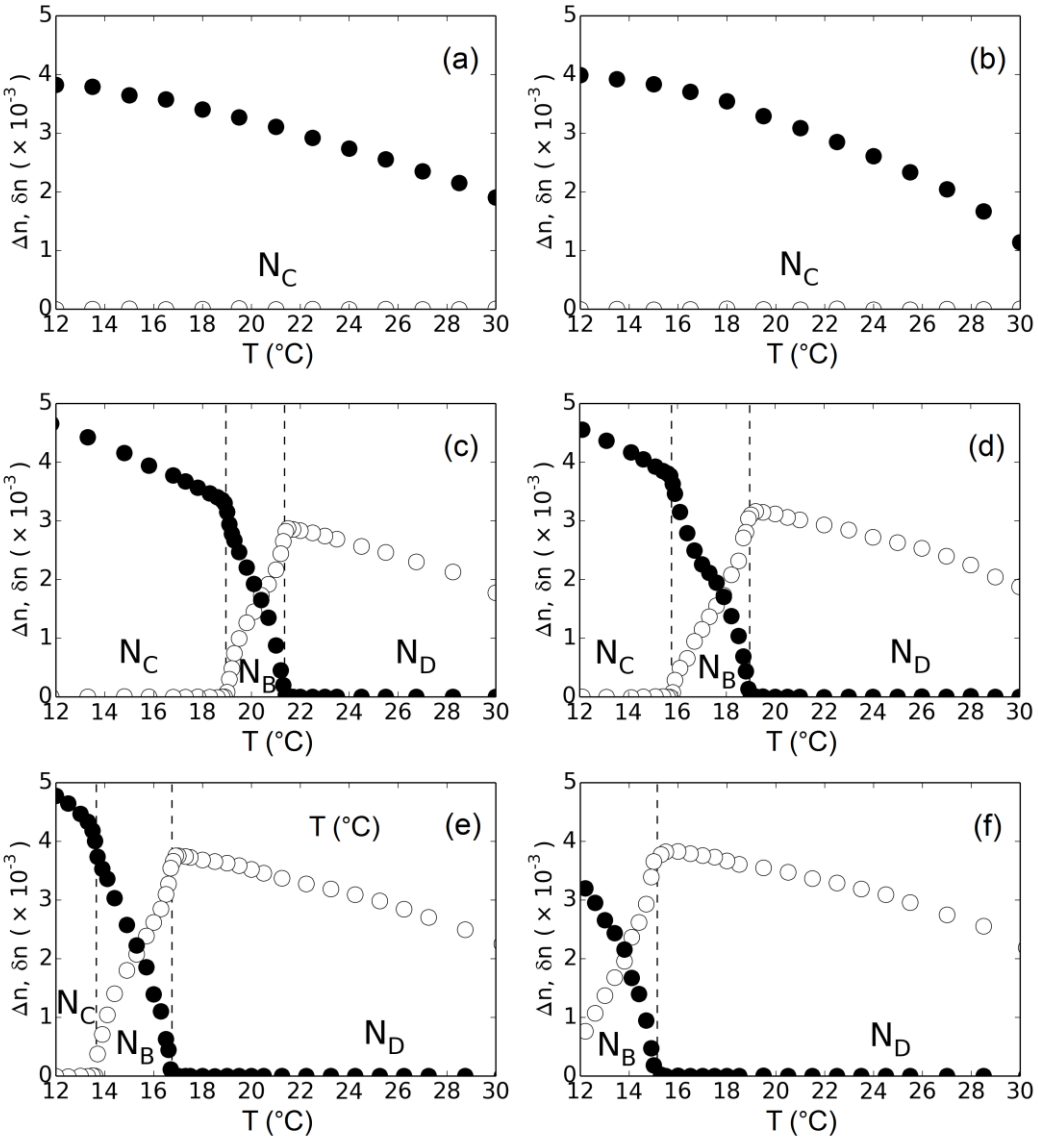

Figure 4.7. Continuing.

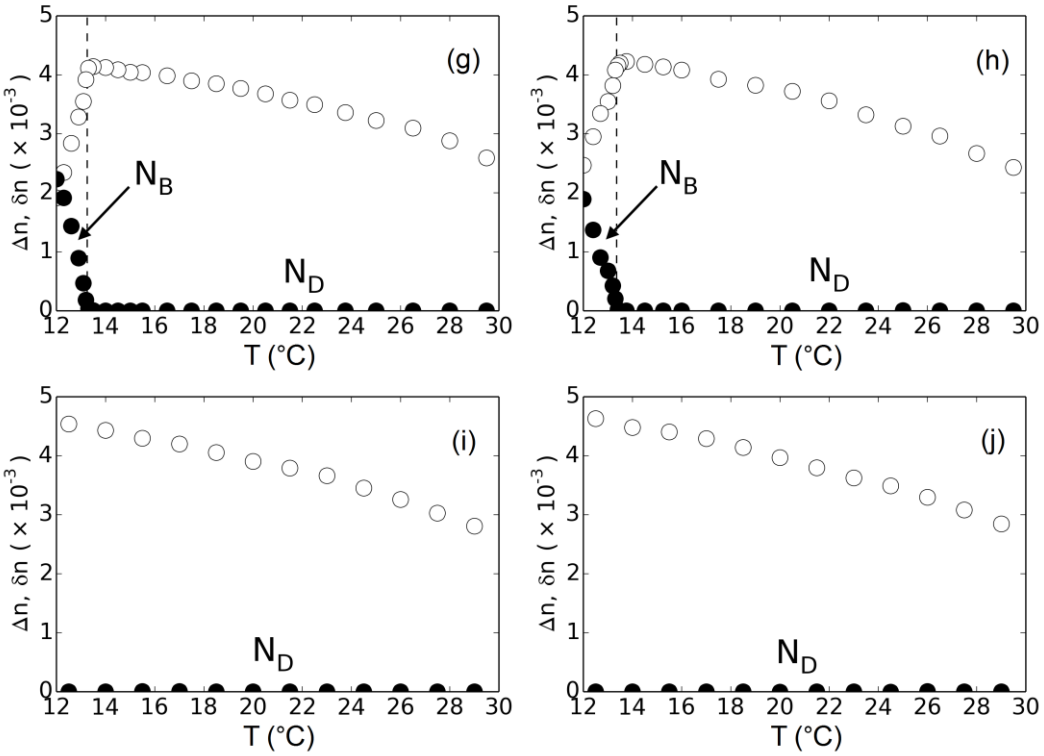

Figure 4.7. The temperature dependences of the birefringences of the nematic phases for DTMABr/amaranth/DDeOH/water mixtures (Table 4.2): (a) a1 (b) a2, (c) a6, (d) a7, (e) a8, (f) a9, (g) a10, (h) a11, (i) a12, and (j) a13.

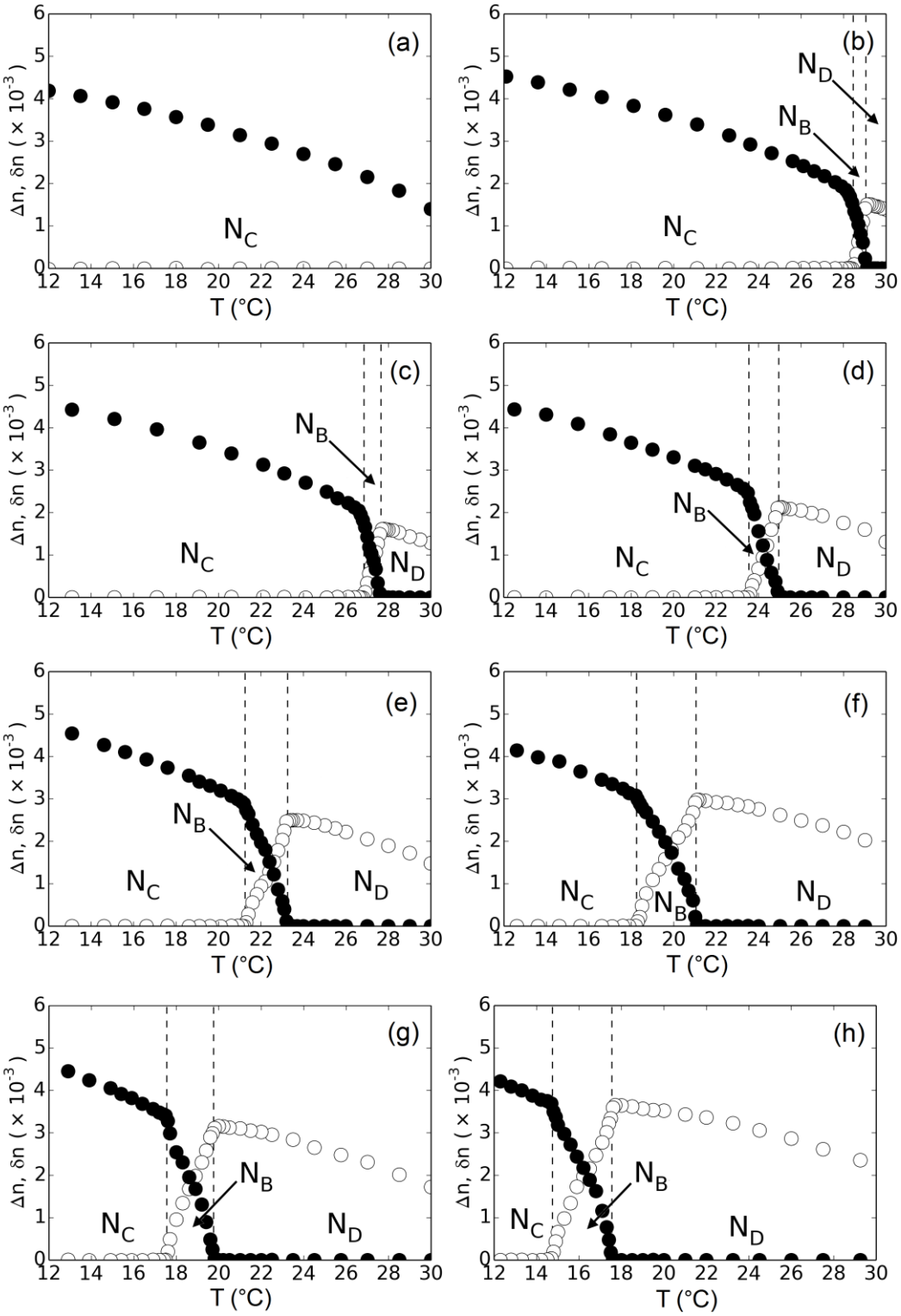

Figure 4.8. Continuing.

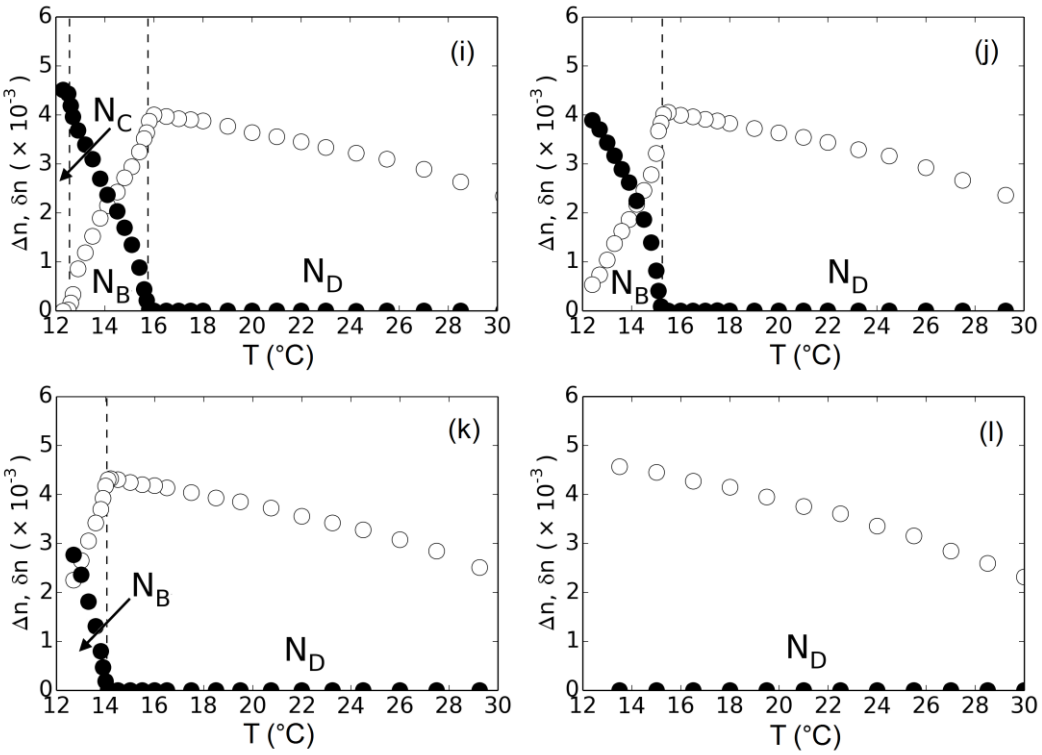

Figure 4.8. The temperature dependences of the birefringences of the nematic phases for DTMABr/tartrazine/DDeOH/water mixtures (Table 4.3.): (a) t4 (b) t5, (c) t6, (d) t7, (e) t8, (f) t9, (g) t10, (h) t11, (i) t12, (j) t13, (k) t14, and (l) t15.

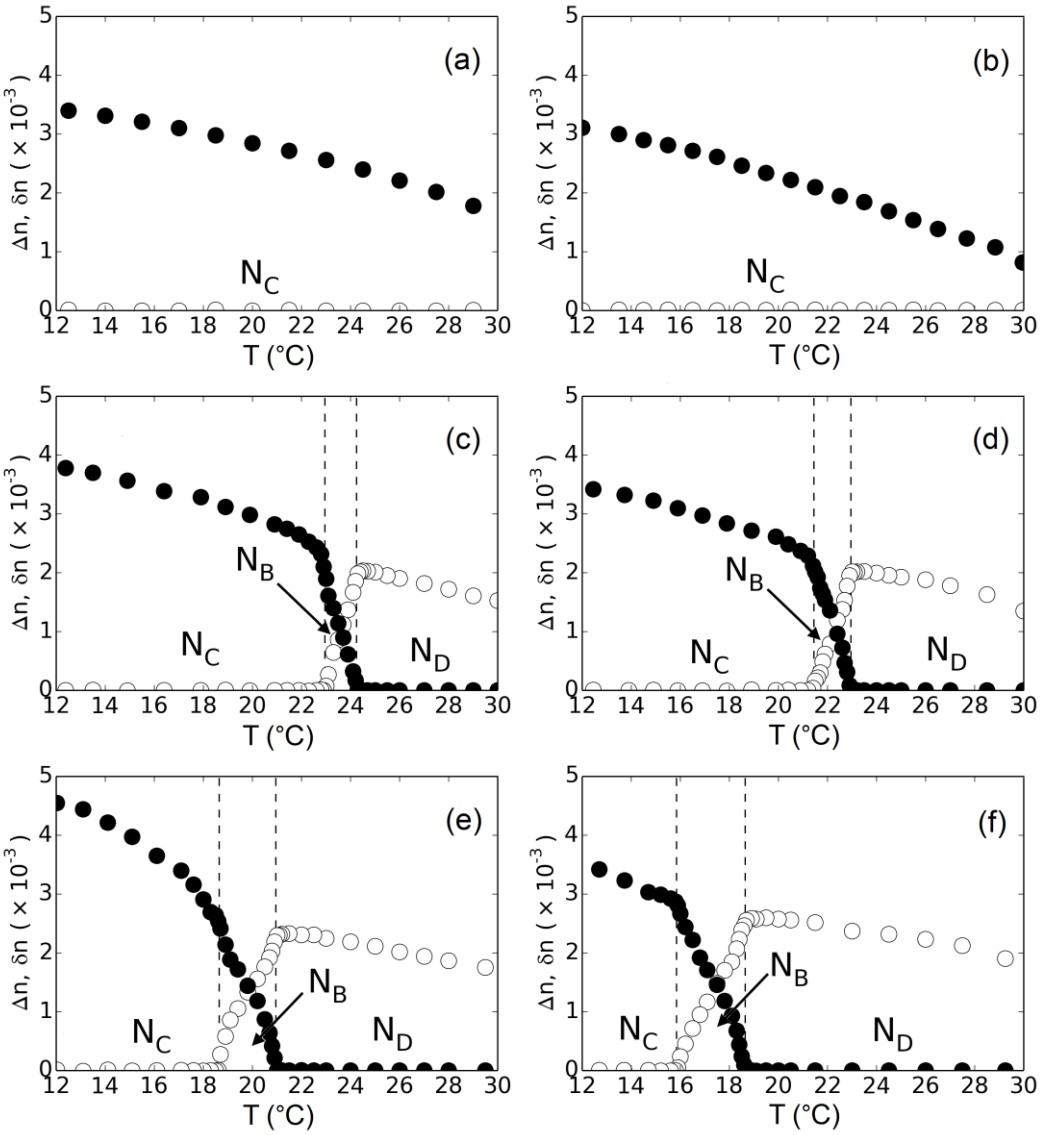

Figure 4.9. Continuing.

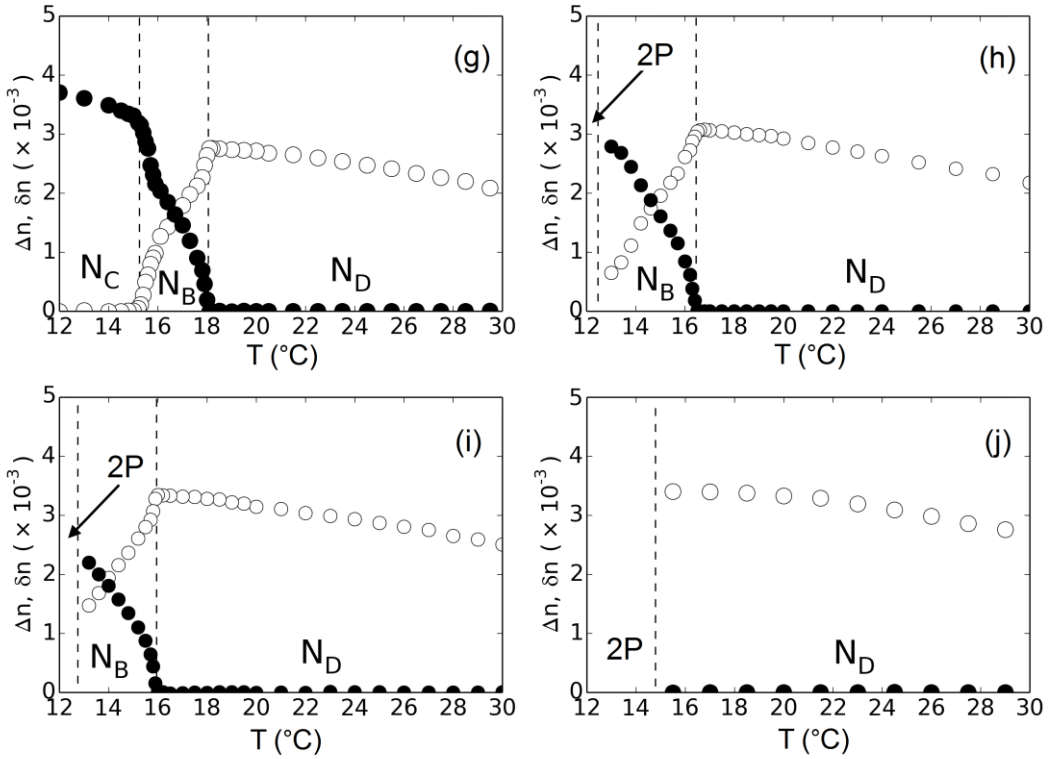

Figure 4.9. The temperature dependences of the birefringences of the nematic phases for DTMABr/DSCG/DDeOH/water mixtures (Table 4.4.): (a) d1 (b) d2, (c) d3, (d) d4, (e) d5, (f) d6, (g) d7, (h) d8, (i) d9, and (j) d10.

4.3 Phase diagram

Considering the polarizing optical microscopy investigations and the laser conoscopy results together, the temperature-concentration partial phase diagrams for each guest molecule, i.e., dye and drug molecules, were constructed, Figures 4.10-4.13. The partial phase diagram of DTMABr/Sunset Yellow/DDeOH/water is, within the experimental error limits, very similar to the one reported before (96). Because it was aimed to compare the effect of each guest molecule on the host mixture DTMABr/DDeOH/water under the same conditions, the phase diagrams were studied in the temperature range of 12.0-30.0°C.

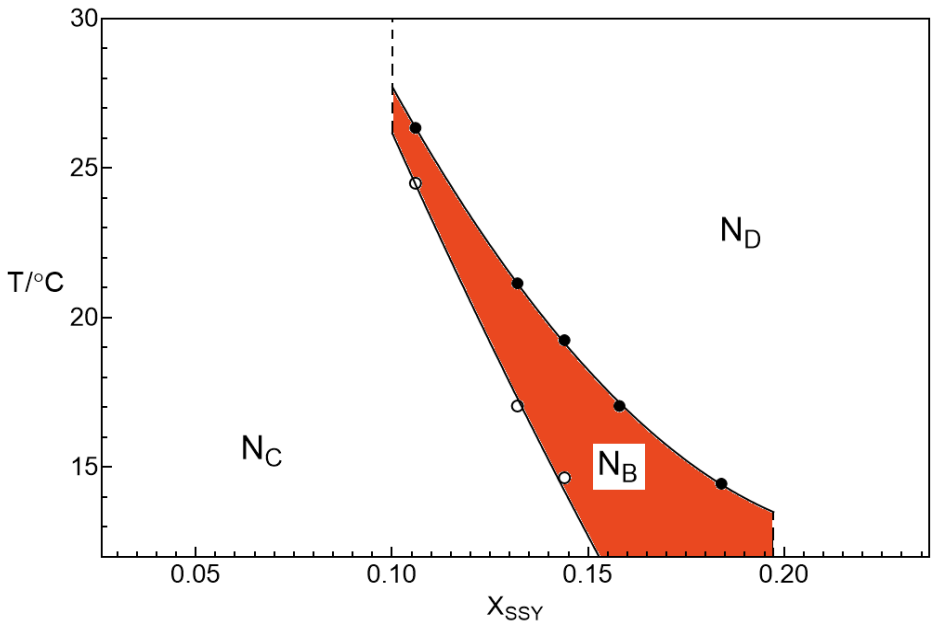

Figure 4.10. The partial phase diagram of DTMABr/Sunset Yellow/DDeOH/water mixtures whose compositions were given in Table 4.1. Similar partial phase diagram were reported in Ref. (96).

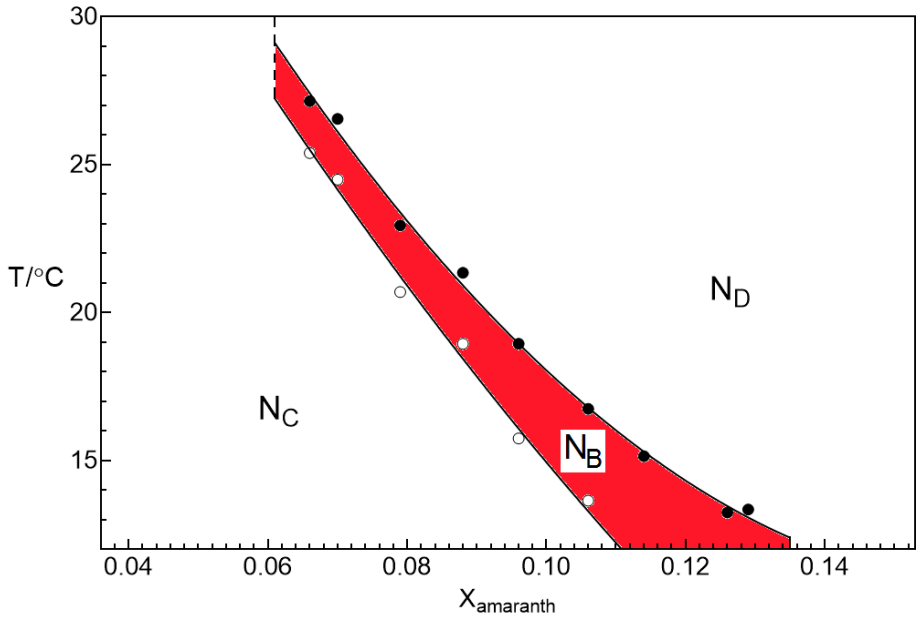

Figure 4.11. The partial phase diagram of DTMABr/amaranth/DDeOH/water mixtures whose compositions were given in Table 4.2.

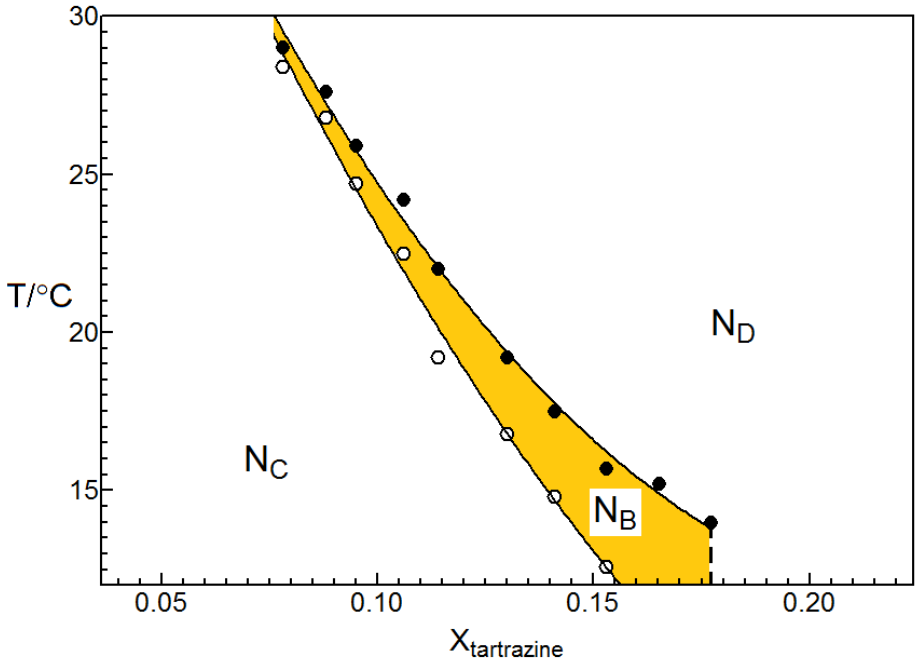

Figure 4.12. The partial phase diagram of DTMABr/tartrazine/DDeOH/water mixtures whose compositions were given in Table 4.3.

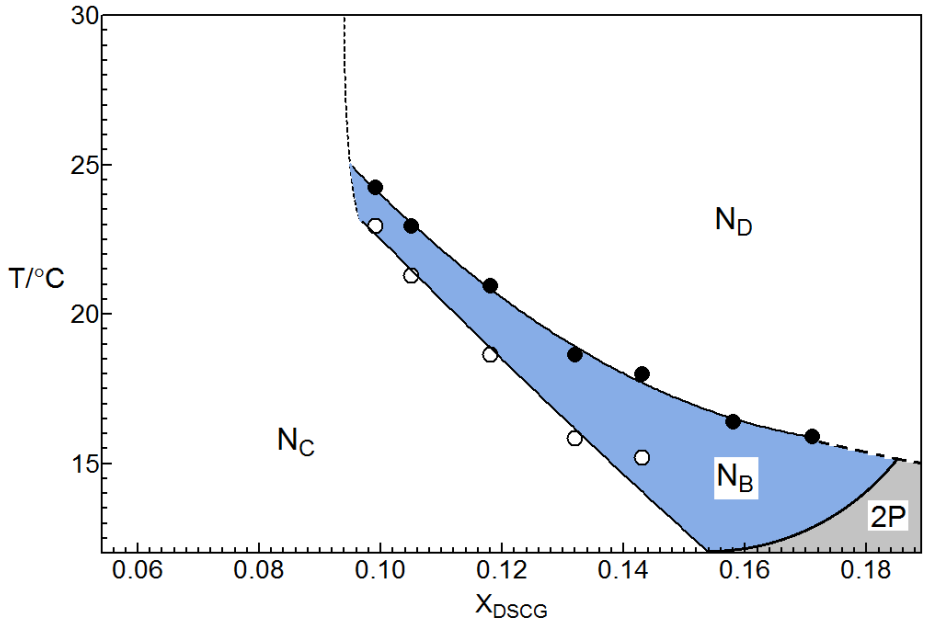

Figure 4.13. The partial phase diagram of DTMABr/DSCG/DDeOH/water mixtures whose compositions were given in Table 4.4. 2P: two-phase region.

As can be seen from the phase diagram of each of the four selected guest molecules, the N_D-N_B and N_B-N_C phase transitions shift to lower temperatures with the addition of guest molecules to the main mixture (D0), which gives only the lyotropic N_C phase depending on the temperature.

This means that the dye/drug guest molecules interact with the micelles by acting as electrolytes in lyotropic mixtures (61). In addition, with the increase in the concentration of guest molecules, the N_C phase region narrows in the partial phase diagrams, while the N_D and N_B phase regions expand. This can only be possible if the anionic groups of dyes and drug molecules on the micelle surfaces interact with the cationic head groups of DTMABr surfactant. As it is known, electrolyte ions added to the medium in micellar systems interact with surfactant head groups on the micelle surfaces and change the micelle surface curvature or micellar shape (108,109). This change is actually a result of the shielding of the repulsive forces between the surfactant head groups on the micelle surfaces by electrolyte ions (110). In a study that we recently brought to the literature, it was demonstrated with strong experimental results (laser conoscopy and small-angle X-ray scattering) that it is possible to obtain different types of nematic phases by controlling the micelle surface curvatures in lyotropic nematic phases (107). In that study, it was revealed that the micelle surface curvatures were different in all three nematic phases.

In the partial phase diagrams, the least and highest micelle surface curvatures are observed in the N_D and N_C phases, respectively, remaining in the nematic phase region. In the case of micelle surface curvature at moderate levels, the N_B phase is most likely to occur, Figure 4.14. So, if we go back to the partial phase diagrams; since guest molecules cause N_D and/or N_B phase formation, they interact effectively with the head groups of DTMABr surfactant molecules on the micelle surfaces and change the micelle surface curvatures.

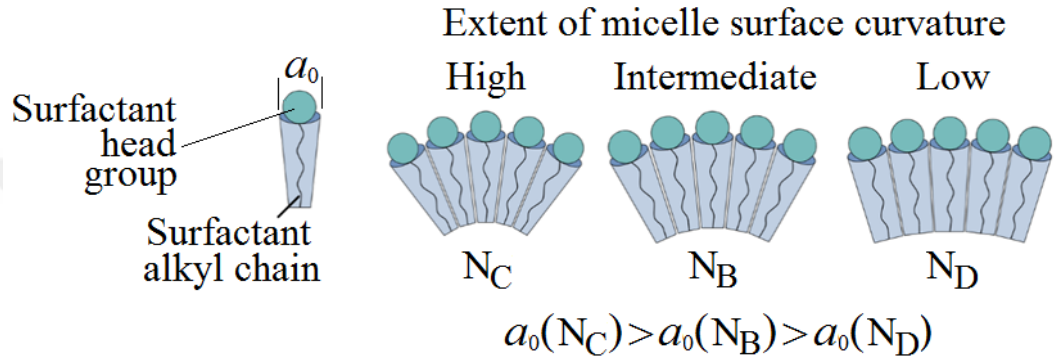

Figure 4.14. Relationship between the possible extent of micelle surface curvature and the formation of lyotropic nematic phases.

4.4 Determination of the sequence of dye/drug molecules in Hofmeister series

It is important in the present thesis to determine which guest molecule is more effective in obtaining different types of nematic phases. Among the mixtures given in Table 4.1- 4.4, the concentrations of guest molecules in percent mole fractions (X: 0.13) and the total mixture compositions in the mixtures of s5 (Sunset Yellow), a11 (amaranth), tartrazine (t10), and d6 (DSCG) are same within the experimental error limits. Therefore, by comparing the lyotropic nematic liquid crystal properties of these mixtures, the effects of those molecules and their places in the Hofmeister series can be relatively determined. Among the selected molecules, only Sunset Yellow's place in the Hofmeister series has been determined by us before (96), and there is no information about the others in the literature, to the best of our knowledge. However, before starting a relative comparison as intended, it would be appropriate to thoroughly examine the molecular structures of the guest molecules given in Figure 4.1. Sunset Yellow and amaranth have two and three, respectively, chaotropic $–SO_3^-$ anionic groups. While tartrazine has two $–SO_3^-$ and one kosmotropic $–COO^-$, DSCG includes two $–COO^-$. The nematic-nematic phase transition temperatures and biaxial nematic phase region range in the partial phase diagrams given previously for the mixtures in Tables 4.1-4.4 are summarized in Table 4.5.

Table 4.5. Nematic-nematic phase transitions and biaxial nematic phase range determined without considering the number of ions possessed by the molecules at the same dye/drug molecule concentration (X: 0.13).

Mixture	Number of chaotropic $–SO_3^-$	Number of kosmotropic $–COO^-$	$N_D \rightarrow N_B$ /°C	$N_B \rightarrow N_C$/ °C	ΔT_{N_B}/°C
s5	2	---	21.2	17.1	4.1
a11	3	---	13.4	---	---
t10	2	1	19.2	16.8	2.4
d6	---	2	18.6	15.8	2.8

Before proceeding to the interpretation of the data summarized in Table 4.5, it would be useful to remind some points. It is well known that the interactions between ionic surfactant head groups and electrolyte ions at micelle surfaces play important role on the formation of different lyotropic nematic phases (61,111). If there are strong chaotropic-chaotropic or kosmotropic-kosmotropic interactions between two ionic species, tightly bound ion pairs are formed (112), resulting in the formation of lyotropic N_D phases. In the opposite case, that is, between two types of ions with quite opposite chaotropic or kosmotropic properties, the interactions are weak and ion pairs weakly bound to each other are formed. This indicates weak chaotropic-kosmotropic interactions and favors the formation of the lyotropic N_C phase. If there are relatively moderate chaotropic-kosmotropic interactions between ionic species, then N_B phases are formed. Comparing the a11 mixture with the t10 mixture, it is seen that although amaranth and tartrazine molecules with the same mole number contain the same number of ionic groups, the mixture containing amaranth molecule lowered the N_D-N_B phase transition more than tartrazine (about 5.8°C). In other words, in the studied temperature range, the N_D phase region for the a11 mixture was wider in the partial phase diagrams with respect to that for the t10 mixture. In addition, there is no N_C phase region in the mixture a11. This means that the amaranth molecule interacts more strongly with the chaotropic headgroups of DTMABr surfactant molecule at the micelle surfaces compared to the interactions between DTMABr and tartrazine. Therefore, in terms of chaotropy, amaranth is more chaotropic than the tartrazine molecule. This is an expected situation because the amaranth molecule interacts with the chaotropic DTMABr surfactant headgroups (113) with three chaotropic ionic groups compared to tartrazine, which has two chaotropic and one kosmotropic group, and screens the interactions between the headgroups on the micelle surfaces and then reduces the micelle surface curvature more. As a result, the order of these two molecules in order of increasing chaotropic degree in the Hofmeister series is “amaranth > tartrazine”.

Similarly, the effects of Sunset Yellow and DSCG molecules, each of which has two ionic groups, can be compared. Here, our expectation was that the mixture containing Sunset Yellow molecule with two chaotropic ionic groups would have a wider N_D region and lower nematic-nematic phase transition

temperatures than the mixture containing DSCG with two kosmotropic ionic groups. However, as can be seen in Table 4.5, the opposite situation was observed in our experimental results. This is only possible with a more comprehensive analysis of the molecular structures of both molecules. In the structure of both molecules (Figure 4.1), there are two ionic groups and polar OH groups that can partially interact with the head groups of the surfactant DTMABr on the micelle surfaces. Therefore, from this point of view, the same number of ionic/polar groups are present in the structure of both molecules. The question to be asked at this point is "Why does the DSCG molecule reduce the nematic-nematic phase transitions more and favor the formation (expense) of the N_D (N_C) phase, although the chaotropic ionic groups of the Sunset Yellow molecule interact more strongly with DTMABr head groups than the kosmotropic ionic groups of the DSCG molecule and form tightly bound ion pairs?". The first aromatic structure to which the carboxylate group is attached in the DSCG molecule is the pyran-4-one structure. In this structure, there is one ether and one ketone group. It is known that pyran-2-one, which is a similar structure to the pyran-4-one, has a resonance structure as shown in Figure 4.15 (114). A similar resonance structure is expected in pyran-4-one: as given in Ref. (115). ^{1}H-NMR studies on pyran-4-ones proved the existence of their aromatic nature and resonance structures by observing chemical shifts at 6-8 ppm. Similar chemical shifts in the structure of DSCG were also reported (116). Thus, the formation of resonance structure for DSCG, yielding two more negative charges in its structure, which can also interact with the positively charged surfactant head groups on the micelle surfaces, is most likely possible. Consequently, according to our results, the molecular structure of DSCG may be in the form of the resonance structure in the micellar solutions, Figure 4.16, at least, in the lyotropic mixtures studied in this study.

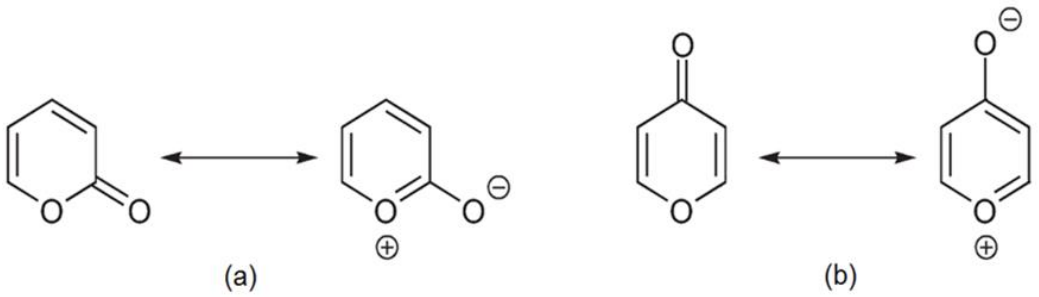

Figure 4.15. Formation of the resonance structures of (a) pyran-2-one and (b) pyran-4-one (114,115).

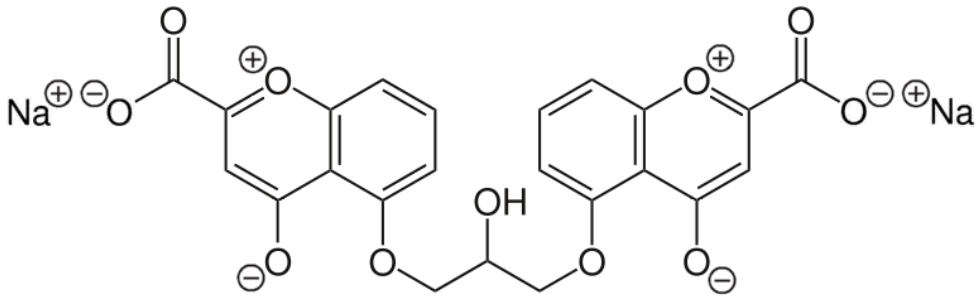

Figure 4.16. Possible resonance structure of DSCG molecule.

Positively charged groups in the resonance structure of DSCG molecule will most likely interact with the free Br^- ions by the ionization of DTMABr in water or water molecules, while four negatively charged ionic groups interact with the head groups of DTMABr. Therefore, it is understandable that such a resonance structure is formed in DSCG molecule and that it remains stable in the presence of positively charged micelles in the solution. As a result, the fact that DSCG is more chaotropic than Sunset Yellow can only be explained by the formation of a resonance structure of DSCG. Thus, in terms of the chaotropic degree, DSCG > Sunset Yellow. Consequently, considering only the mole fractions of the guest molecules in the mixtures, regardless of the number of ions they contain, the ranking in terms of the degree of chaotropy according to the results given in Table 4.5 should be as follows.

Amaranth > DSCG > Tartrazine > Sunset Yellow

Considering the chaotropic properties of Hofmeister series of conventional inorganic anions, the following sequence is valid (117,118).

$$Br^- < NO_3^- < ClO_3^- < I^- < SCN^- < ClO_4^-$$

In some studies, the relationship between Br^- and NO_3^- is also given as Br^- ~ NO_3^- or Br^- < NO_3^- (119) and this can be attributed to the close chaotropic degrees of both ions. To determine the location of the guest molecules in the Hofmeister series, it would be a more accurate approach to compare them as ions with the same electrical charge, because the electrical charge of the ions to be compared in the Hofmeister series is "–1". For this reason, a comparison method followed in our previous study will also be applied here (96). Since the anionic part of the Sunset Yellow molecule has two –1 charged groups, it has a total charge of –2 (S^{2-}). Similarly, amaranth, tartrazine, and DSCG, considering its pyran-4-one structure, have –3 (A^{3-}), –3 (T^{3-}), and –4 (D^{4-}), respectively. As stated earlier, the concentrations of guest molecules in moles or mole fractions are same in the compared mixtures. This means that the same number of guest molecules were added to the host mixture. In the case of the same number of ions, it will be taken as (X_{guest}) x (n_{ion}) = X_{ion} for comparison. Here, since the ionic parts of both the inorganic ions in the Hofmeister series and the dye/drug molecules used in the present thesis have an electrical charge of –1, the total mole fraction values of the ions (X_{ion}) were calculated from the product of the number of the ion (n_{ion}) and the mole fraction values of the guest molecules added to the host mixture (Table 4.6). Thus, the presence of the same amount of ionic species as the ions in the Hofmeister series in the mixtures and interacting with the surfactant head groups on the micelle surfaces were ensured. The DTMABr/Sunset Yellow/DDeOH/water mixture (named s5 in this study), which we brought to the literature from our previous studies, was chosen as the starting point for the comparison. In the same study, laser conoscopy measurements of some Hofmeister series ions given above were performed, and nematic-nematic phase transition temperatures and nematic phase types were determined. The results of the a forementioned study and the present study are given together in Table 4.6 for comparison.

Table 4.6. Considering the number iof ionic parts present in the molecular stuructures of dyes/drug molecules (n_{ion}), nematic-nematic phase transitions and biaxial nematic phase range in the partial phase diagrams.

Ion	n_{ion}	Mixture	X_{guest}	X_{ion}	Observed nematic phase	$N_D \rightarrow N_B$/°C	$N_B \rightarrow N_C$/°C	ΔT_{N_B}/°C
S^{2-}	2	s5	0.13	0.26	N_D, N_B, N_C	21.2	17.1	4.1
A^{3-}	3	a6	0.088	0.26	N_D, N_B, N_C	21.4	19.0	2.4
T^{3-}	3	t6	0.088	0.26	N_D, N_B, N_C	27.6	26.8	0.8
D^{4-}	4	d11[a]	0.066	0.26	N_C	---	---	---
Br^-	1	[b]	0.26	0.26	N_D, N_B, N_C	30.1	29.2	0.9
NO_3^-	1	[b]	0.26	0.26	N_D, N_B, N_C	29.2	28.0	1.2
ClO_3^-	1	[b]	0.26	0.26	N_D, N_B, N_C	24.4	22.4	2.0
I^-	1	[b]	0.26	0.26	N_D, N_B, N_C	24.1	21.3	2.8
SCN^-	1	[b]	0.26	0.26	N_D, N_B, N_C	19.3	14.9	4.4
ClO_4^-	1	[b]	0.26	0.26	N_D	---	---	---

[a] The mole fractions of other components (DTMABr, DDeOH, water) are same given in Table 4.4; [b] From Ref. (96).

The results given in Table 4.6 include some information on the chaotropic degree of Sunset Yellow/amaranth/tartrazine/DSCG relative to the inorganic ions in the Hofmeister series. ClO_4^- (D^{4-}) ion gives only N_D (N_C) phase, which means that it has the strongest (weakest) interaction with the DTMABr head groups on the micelle surfaces. Because the SCN^- ion has the lowest nematic-nematic phase transitions and the largest (smallest) N_D (N_C) phase domain, it follows the ClO_4^- ion in the series. S^{2-} and A^{3-} has very similar N_D-N_B transition, but the N_B-N_C transition for S^{2-} shifts to lower temperature by expensing the N_C phase domain. So, in terms of chaotropic, $S^{2-} > A^{3-}$. The nematic phase properties of the mixtures with I^-, ClO_3^-, NO_3^-, and Br^- obey the Hofmeister series, i.e. the highly (weakly) chaotropic ion I^- (Br^-) gives nematic-nematic phase transitions at lower (higher) temperatures with larger (larger) N_D (N_C) phase domain by the increase in the biaxial phase region.

According to the phase transition temperatures, T^{3-} should be placed between ClO_3^- and NO_3^-. Thus, the following sequence may be obtained, considering the n_{ion} or X_{ion} values of dye/drug molecules:

ClO_4^- > SCN^- > Sunset Yellow > Amaranth > I^- > ClO_3^- > Tartrazine > NO_3^- > Br^- > DSCG

According to the results given in Table 4.5, i.e. if the n_{ion} values are not considered, the following sequence is assumed

ClO_4^- > Amaranth > SCN^- > DSCG > Tartrazine > Sunset Yellow > I^- > ClO_3^- > NO_3^- > Br^-

However, it seems that the former ordering made by considering the ion numbers of dye/drug molecules, nematic-nematic phase transition temperatures, and the biaxial phase regions in the partial phase diagrams, as in our previous study (96), is more accurate.

4.5 Small-angle X-ray Scattering

Small-angle X-ray scattering technique is available to evaluate the micellar structural parameters and to confirm the lyotropic nematic phase types from the scattering pattern point of view. The SAXS patterns of the N_D, N_B, and N_C phases are well-known in the literature. The SAXS patterns for some samples studied in this thesis are given in the following figures. The observed 2D-SAXS patterns of the samples exhibited the characteristic patterns' shape with the pseudo-lamellar structure and the patterns' symmetry in the three aligned nematic phases, when the SAXS tube or capillary is rotated to obtain PP and PR orientations (see the Supplementary Information of the reference, (96), for details). In other words, two different experimental configurations were performed in the SAXS measurements. The first configuration implies that the magnetic field direction (~1.0 kG) is perpendicular to the incident X-ray beam. This configuration is called PP orientation. In the second configuration, the sample was rotated by 90° in the absence of a magnetic field. This configuration is called PR orientation. In the case of the N_D phase, the scattering patterns and related intensity curves of both orientations are very similar. When the N_B phase is obtained, the patterns and

curves for the two configurations are started to be different from one another. While the integration along the vertical direction (VRT) for each pattern gives almost the same q (scattering vector) values in the N_B phase, the one along the horizontal direction (HRZ) starts to change for PP and PR configurations. This situation continues until the N_C phase is obtained. In the N_C phase, sharp (weak) intensity along VRT (HRZ) in the PP orientation is obtained, and a characteristic circular scattering pattern with isotropically distributed intensity for the N_C phase is observed (details are given in Ref. (96).

SAXS patterns for samples s5, a11, t10, d6, a6, and t6 are given in Figures 4.17-4.20, 4.22-4.25, 4.27-4.31, 4.33-4.36, 4.38-4.42, and 4.44-4.49, respectively. Their respected intensity vs q curves is also given in Figures 4.21, 4.26, 4.32, 4.37, 4.43, and 4.50, respectively. The SAXS patterns are in good agreement with the laser conoscopy and polarizing optical microscopy results, i.e., the SAXS results confirm the nematic phase types.

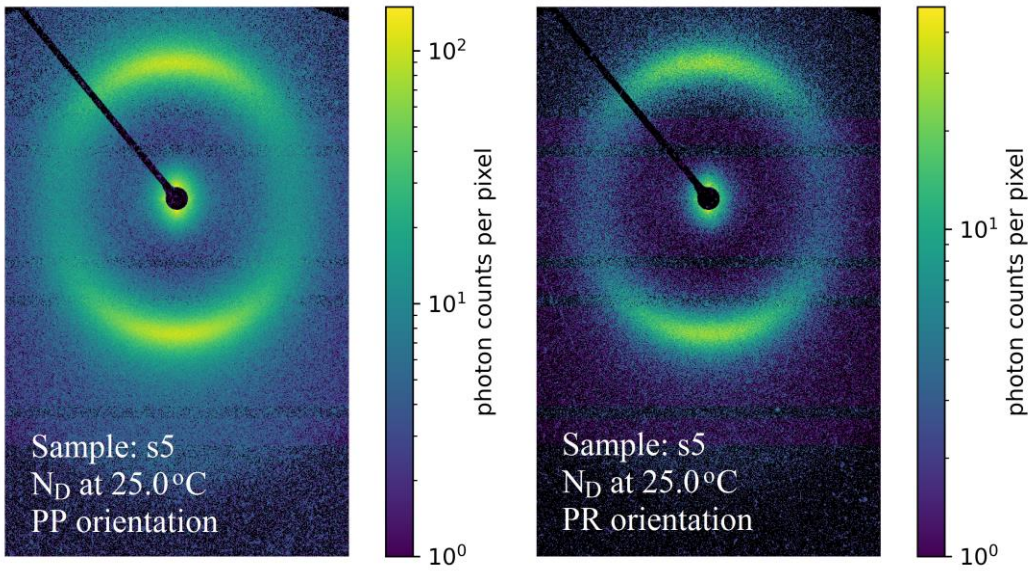

Figure 4.17. SAXS patterns of the N_D phase obtained from the sample with Sunset Yellow (s5) at 25.0°C for PP (left) and PR (right) orientations.

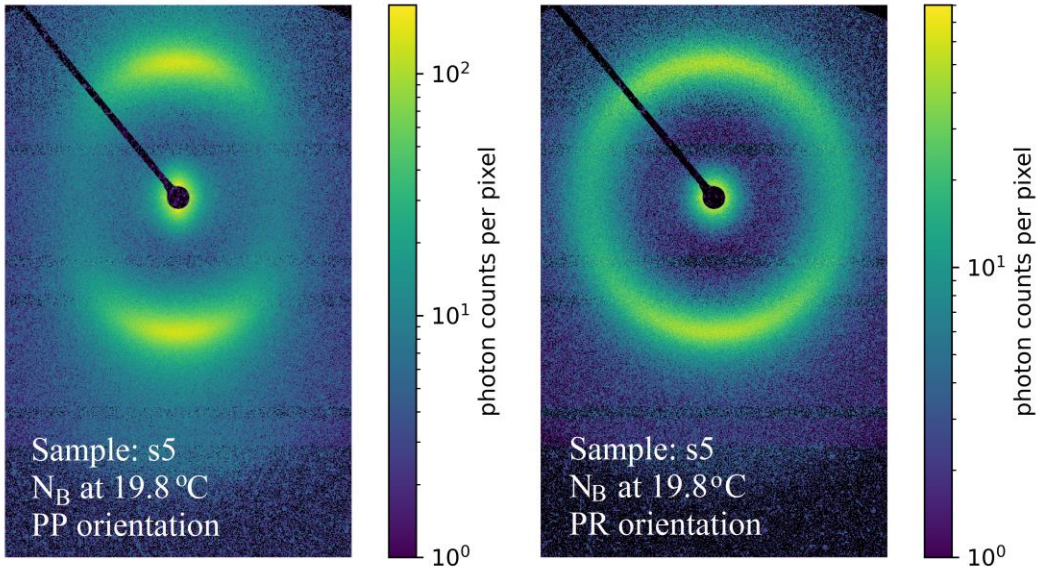

Figure 4.18. SAXS patterns of the N_B phase obtained from the sample with Sunset Yellow (s5) at 19.8°C for PP (left) and PR (right) orientations.

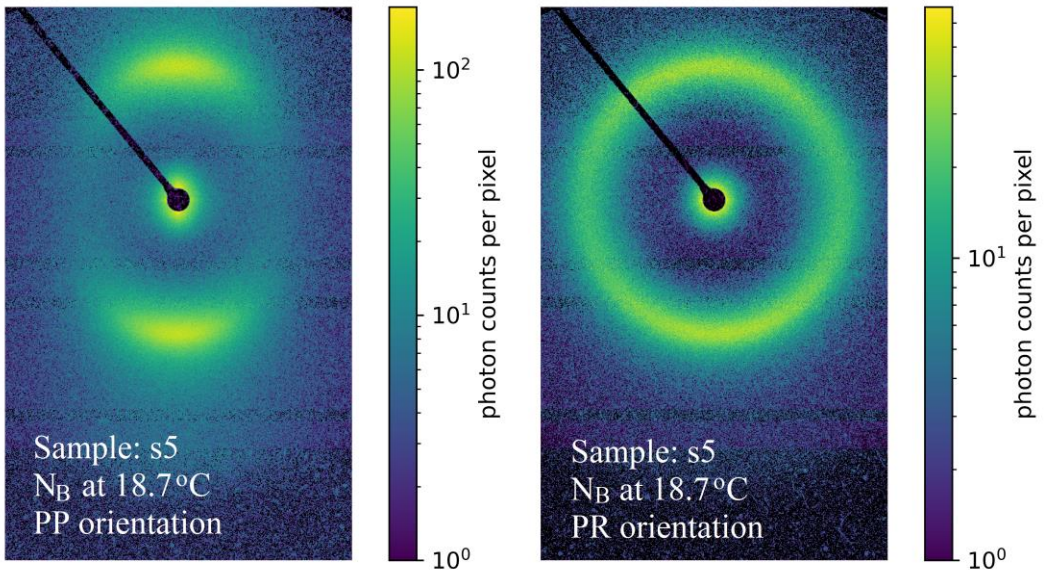

Figure 4.19. SAXS patterns of the N_B phase obtained from the sample with Sunset Yellow (s5) at 18.7°C for PP (left) and PR (right) orientations.

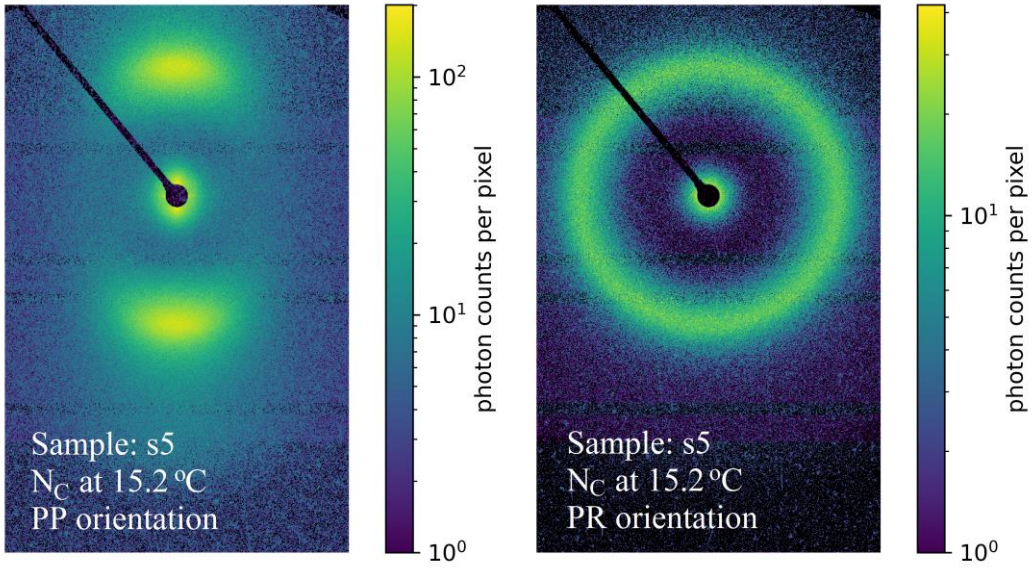

Figure 4.20. SAXS patterns of the N_C phase obtained from the sample with Sunset Yellow (s5) at 15.2°C for PP (left) and PR (right) orientations.

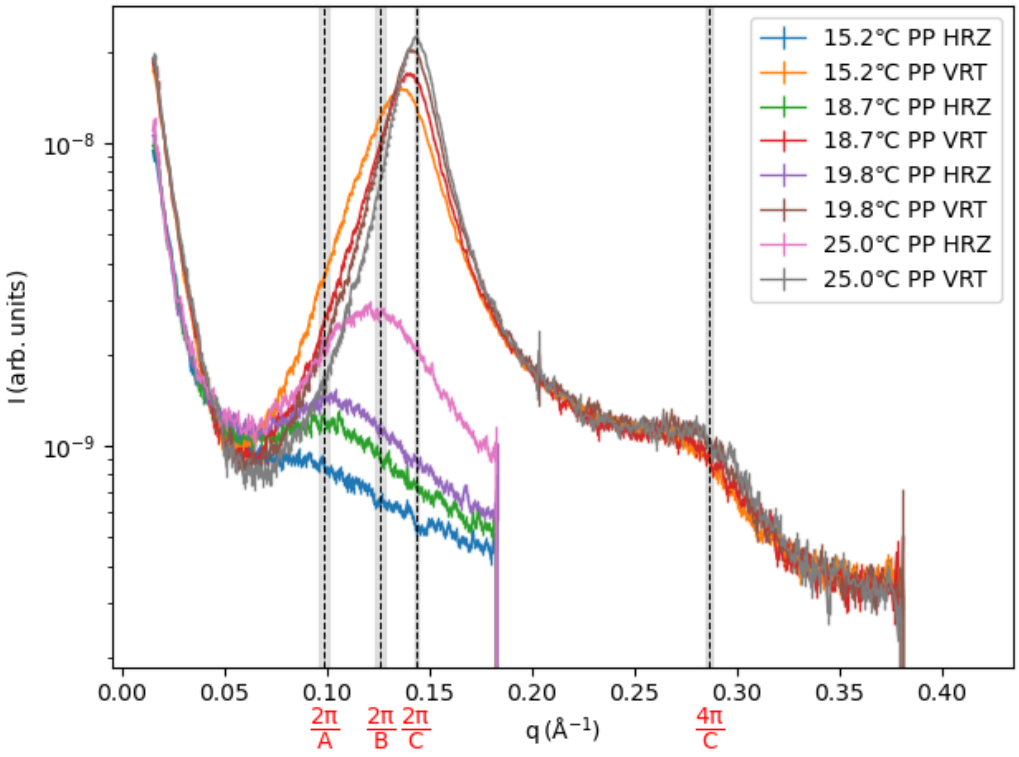

Figure 4.21. Scattering intensity vs scattering vector for the sample s5 at different temperatures. These curves were used to calculate the micellar structural parameters for the nematic phases, considering the analysis model given in the Ref. (96). For other curves (Figures 4.26, 4.32, 4.37, 4.43 and 4.50), same model were applied.

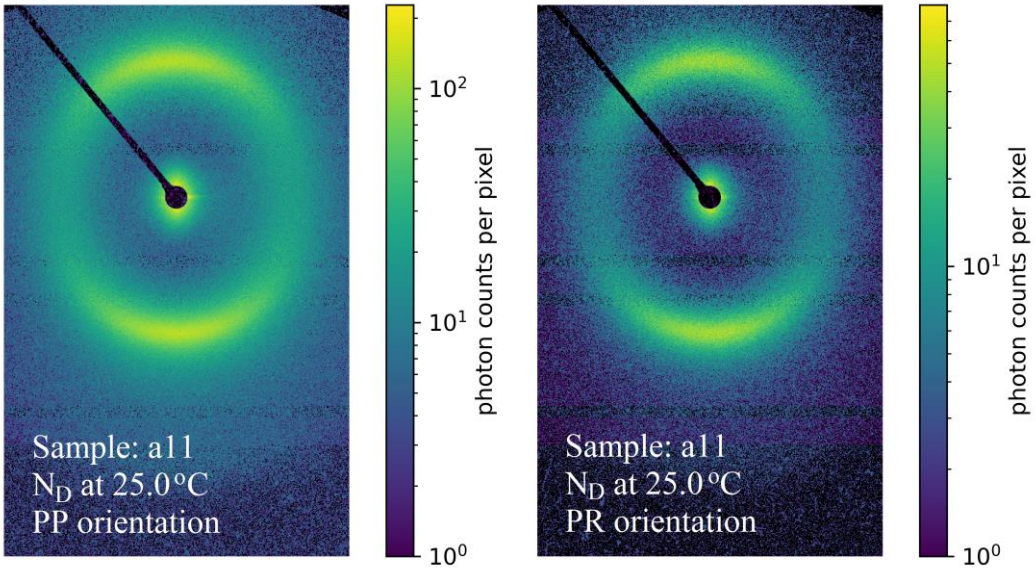

Figure 4.22. SAXS patterns of the N_D phase obtained from the sample with Amaranth (a11) at 25.0°C for PP (left) and PR (right) orientations.

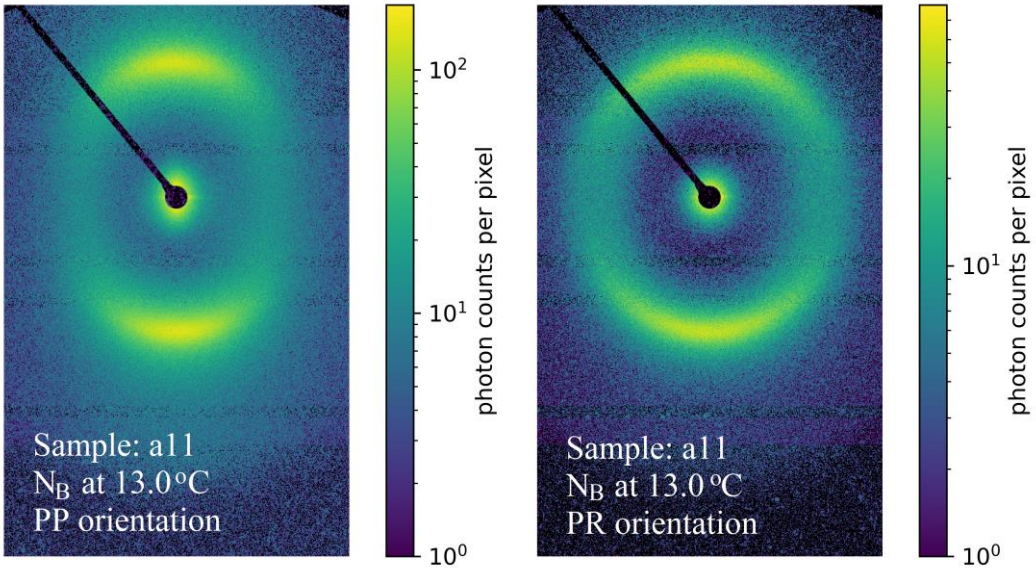

Figure 4.23. SAXS patterns of the N_B phase obtained from the sample with Amaranth (a11) at 13.0°C for PP (left) and PR (right) orientations.

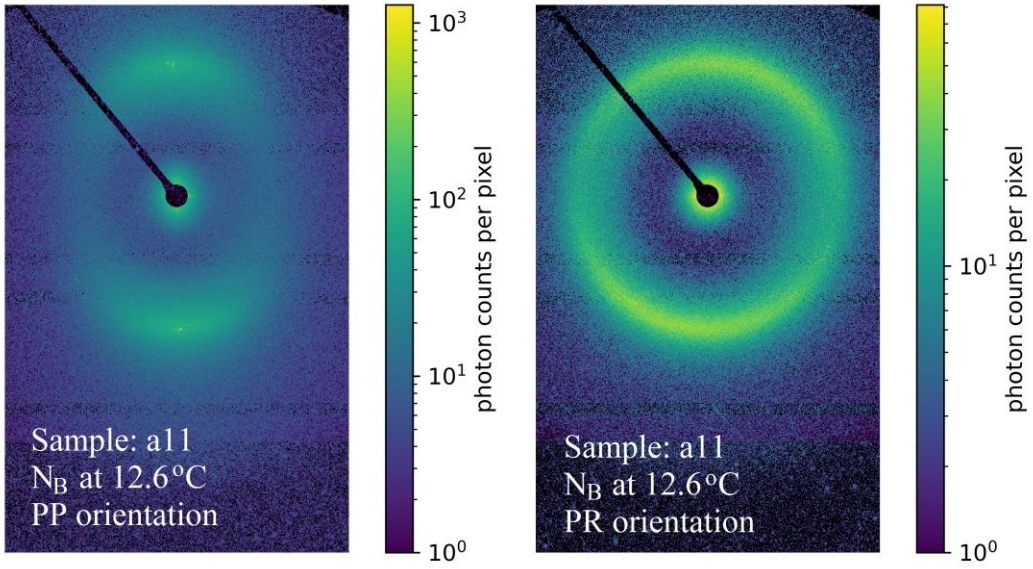

Figure 4.24. SAXS patterns of the N_B phase obtained from the sample with Amaranth (a11) at 12.6°C for PP (left) and PR (right) orientations.

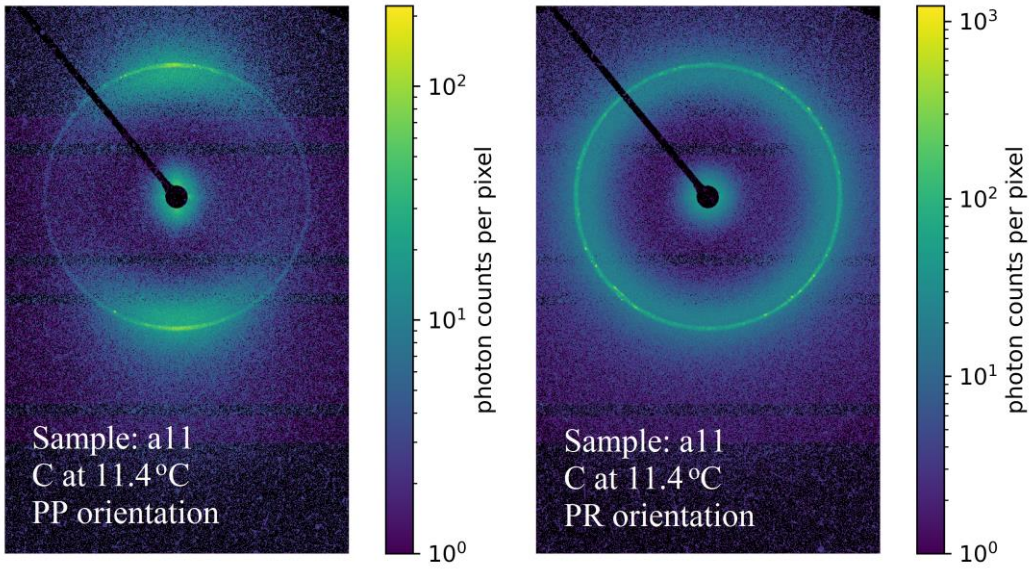

Figure 4.25. SAXS patterns of the C (crystalline-like) phase obtained from the sample with Amaranth (a11) at 11.4°C for PP (left) and PR (right) orientations.

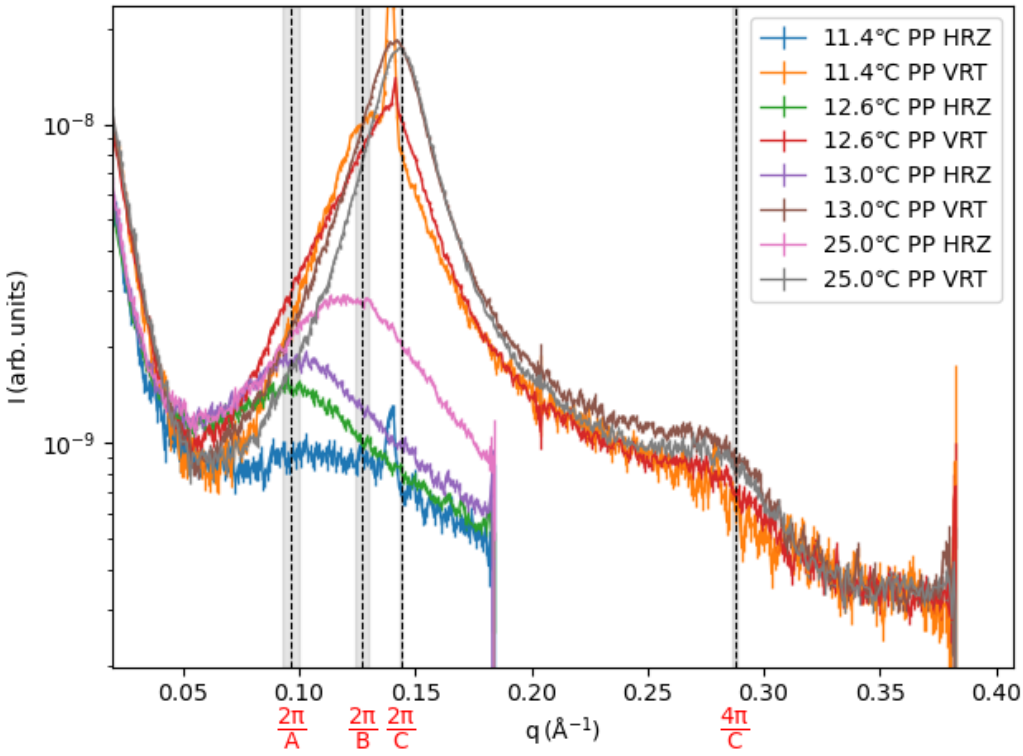

Figure 4.26. Scattering intensity vs scattering vector for the sample a11 at different temperatures to calculate the micellar structural parameters for the nematic phases.

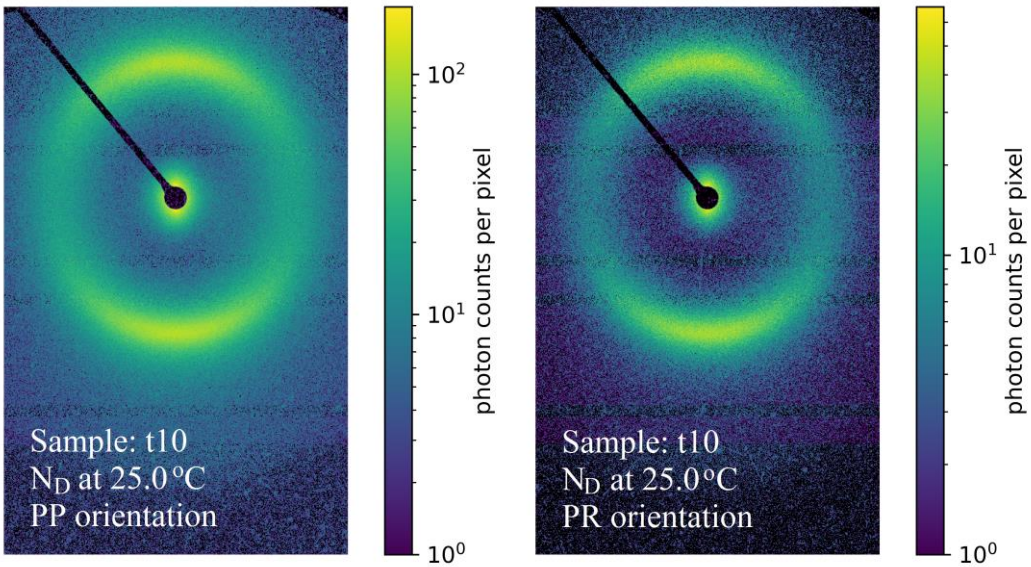

Figure 4.27. SAXS patterns of the N_D phase obtained from the sample with Tartrazine (t10) at 25.0°C for PP (left) and PR (right) orientations.

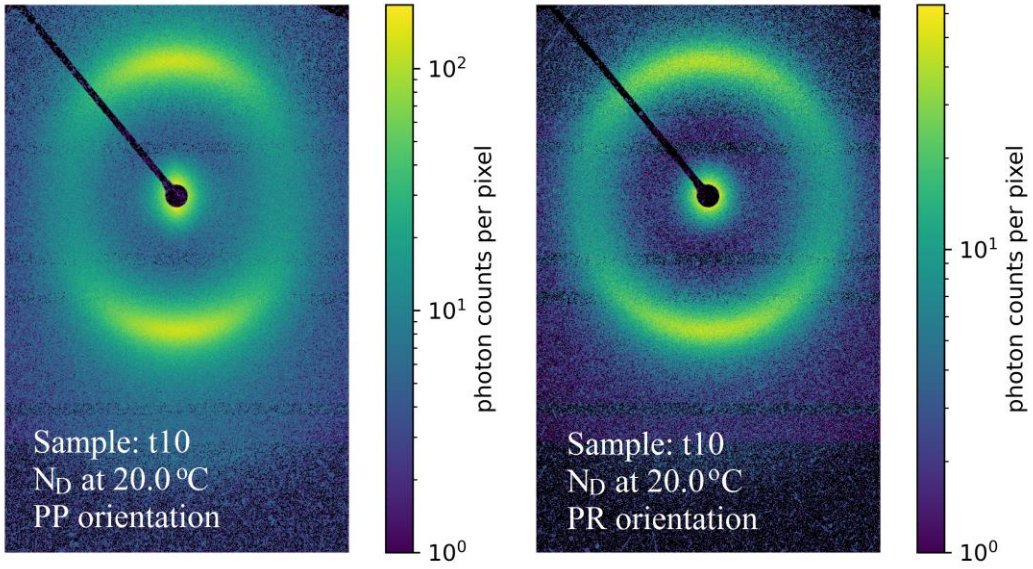

Figure 4.28. SAXS patterns of the N_D phase obtained from the sample with Tartrazine (t10) at 20.0°C for PP (left) and PR (right) orientations.

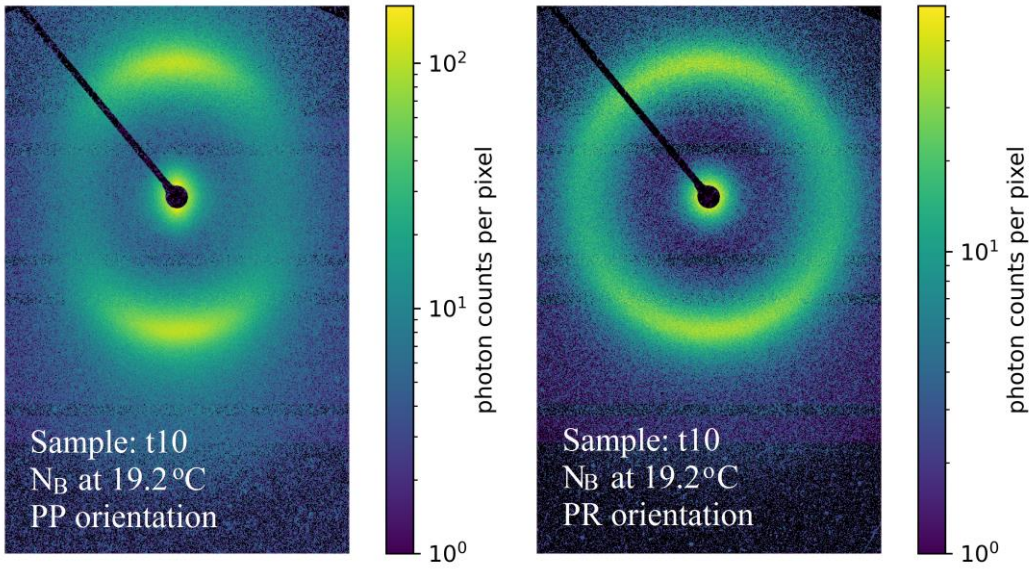

Figure 4.29. SAXS patterns of the N_B phase obtained from the sample with Tartrazine (t10) at 19.2°C for PP (left) and PR (right) orientations.

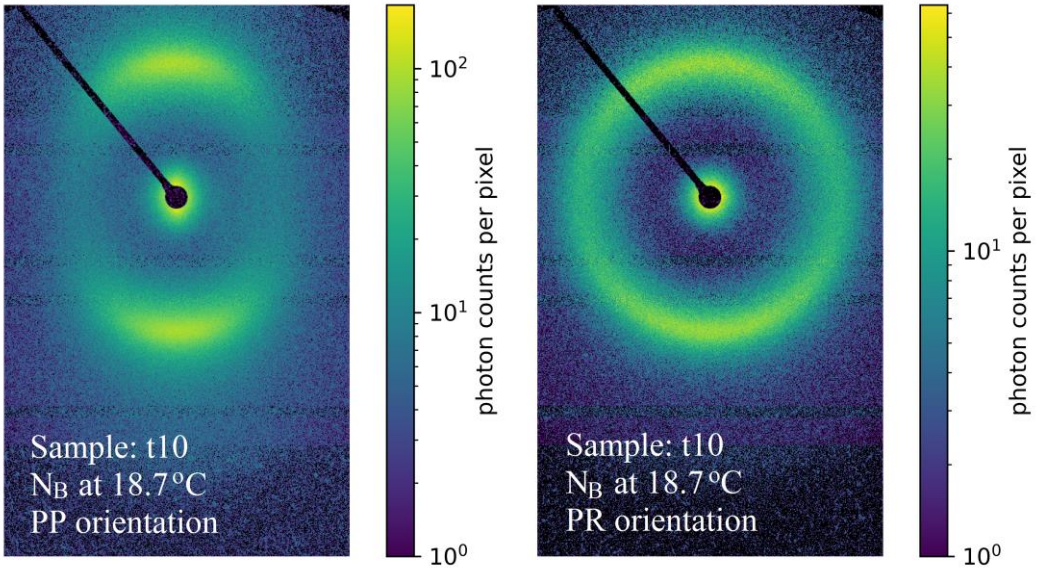

Figure 4.30. SAXS patterns of the N_B phase obtained from the sample with Tartrazine (t10) at 18.7°C for PP (left) and PR (right) orientations.

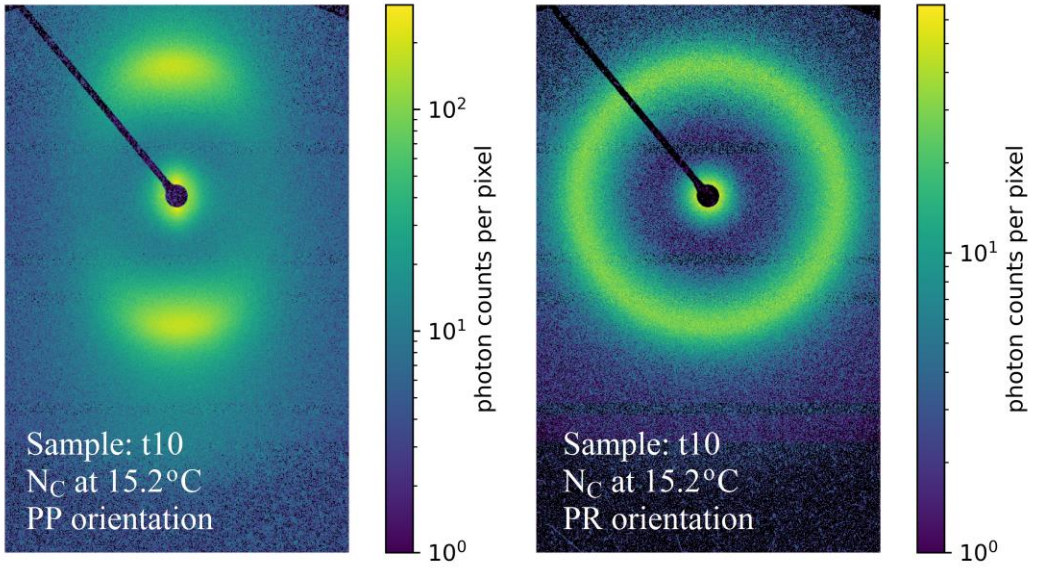

Figure 4.31. SAXS patterns of the N_C phase obtained from the sample with Tartrazine (t10) at 15.2°C for PP (left) and PR (right) orientations.

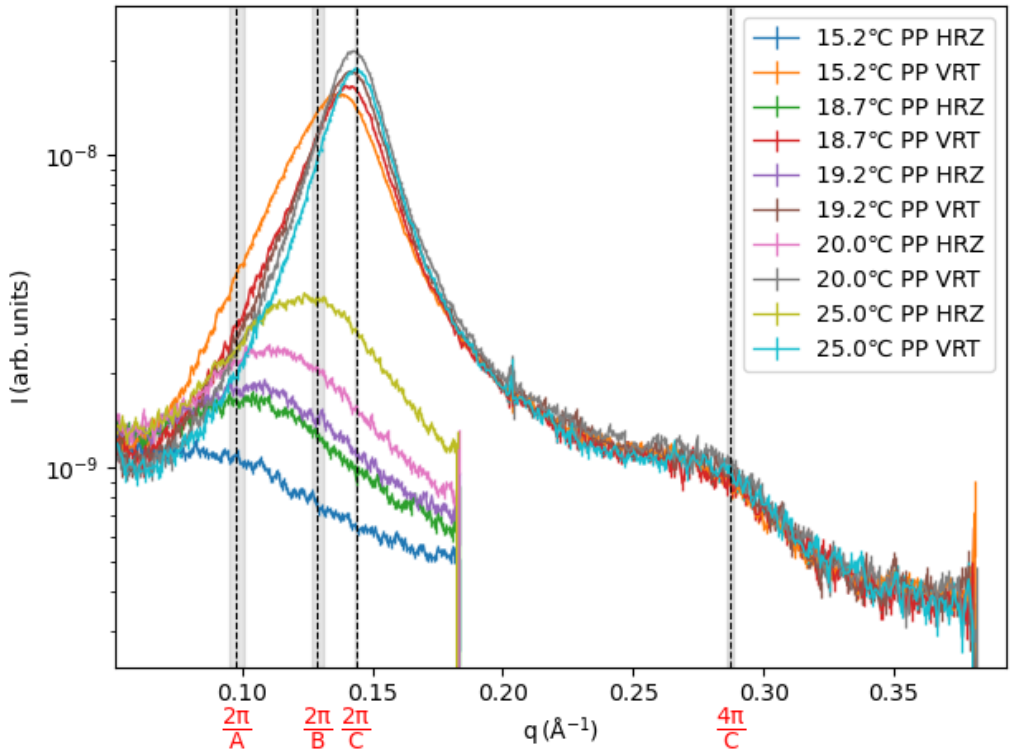

Figure 4.32. Scattering intensity vs scattering vector for the sample t10 at different temperatures to calculate the micellar structural parameters for the nematic phases.

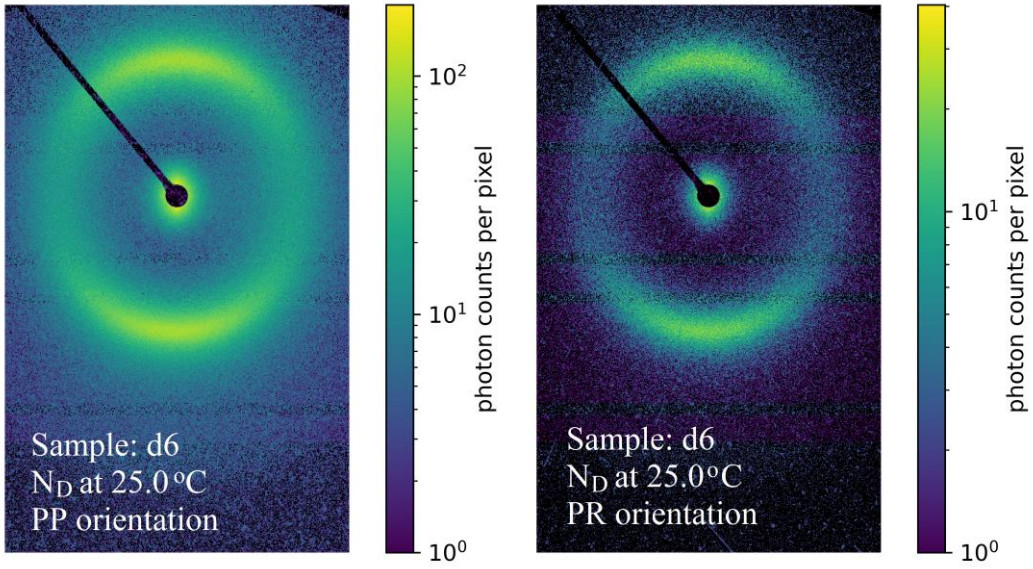

Figure 4.33. SAXS patterns of the N_D phase obtained from the sample with DSCG (d6) at 25.0°C for PP (left) and PR (right) orientations.

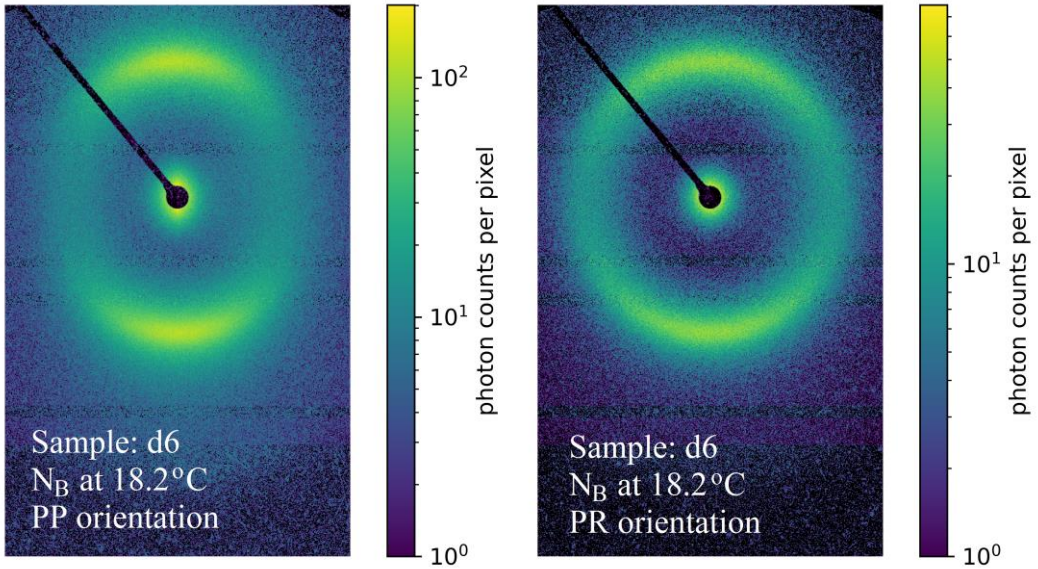

Figure 4.34. SAXS patterns of the N_B phase obtained from the sample with DSCG (d6) at 18.2°C for PP (left) and PR (right) orientations.

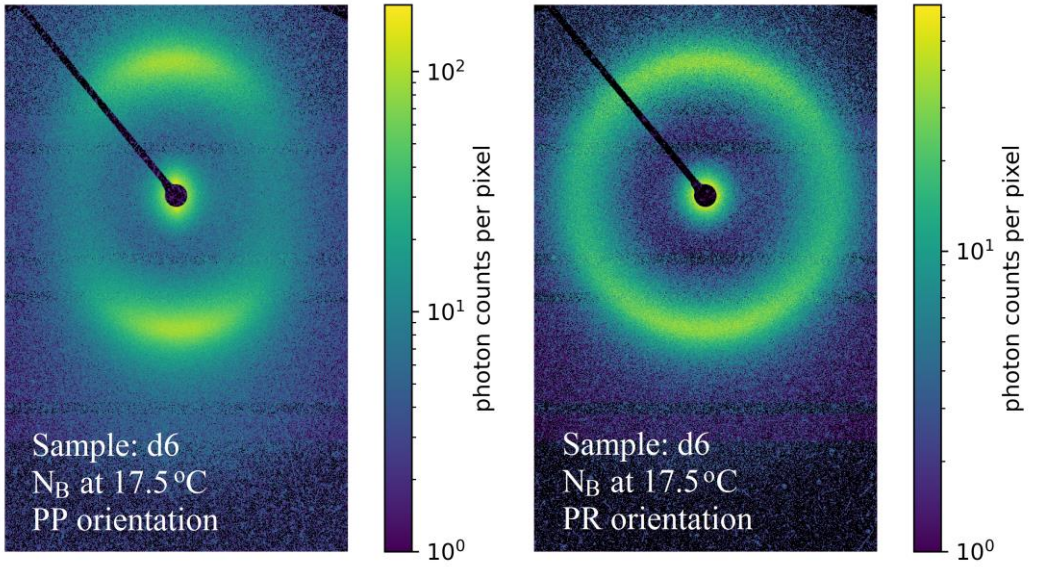

Figure 4.35. SAXS patterns of the N_B phase obtained from the sample with DSCG (d6) at 17.5°C for PP (left) and PR (right) orientations.

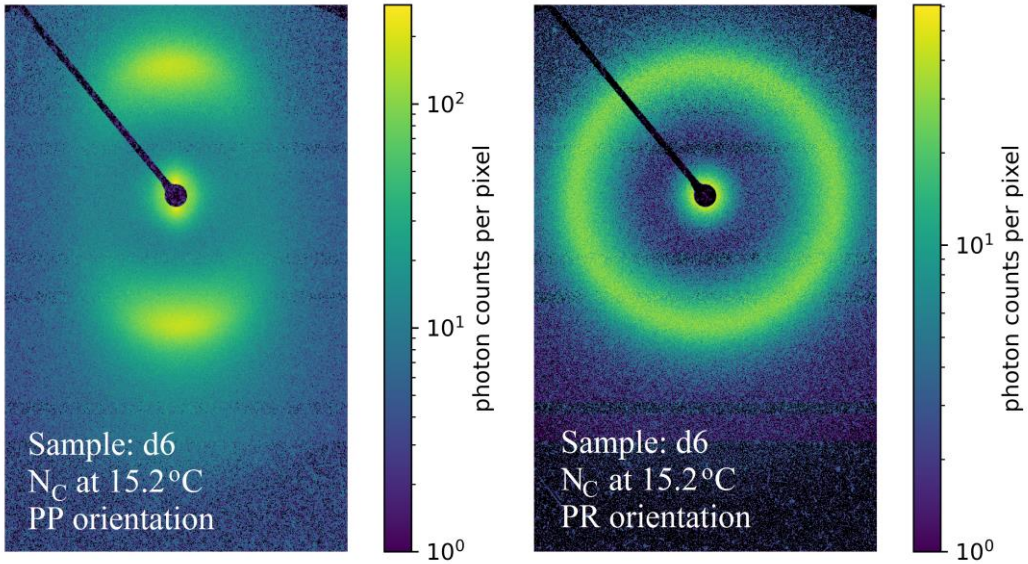

Figure 4.36. SAXS patterns of the N_C phase obtained from the sample with DSCG (d6) at 15.2°C for PP (left) and PR (right) orientations.

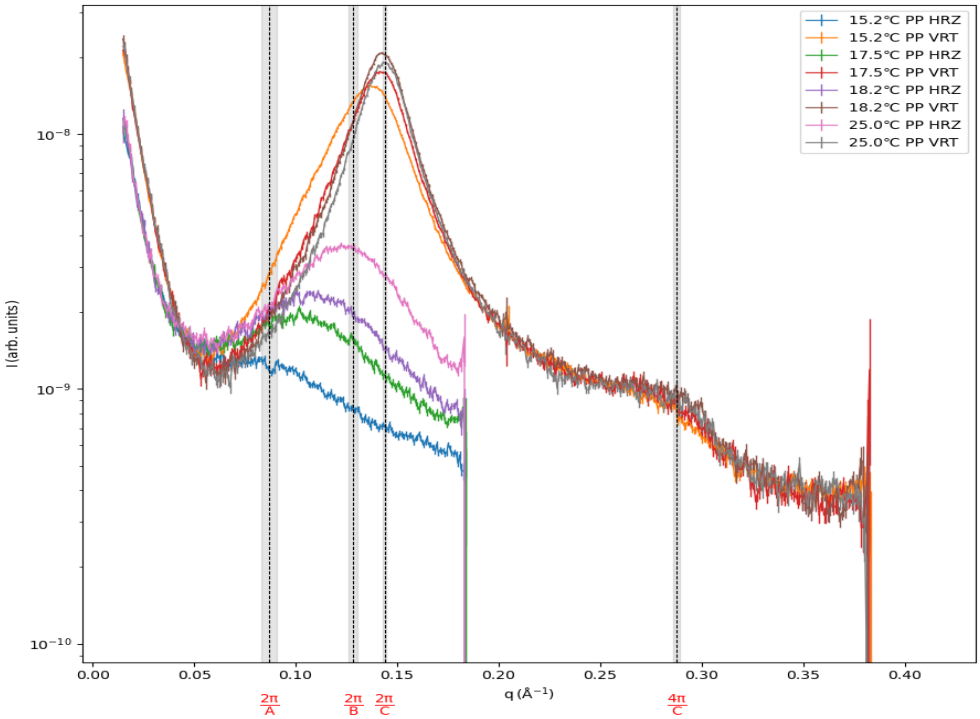

Figure 4.37. Scattering intensity vs scattering vector for the sample d6 at different temperatures to calculate the micellar structural parameters for the nematic phases.

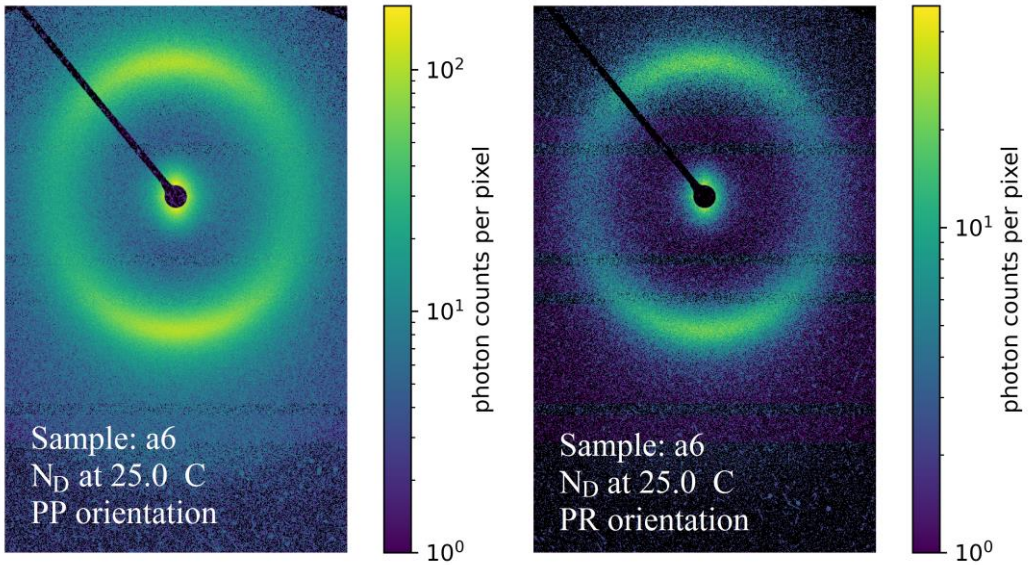

Figure 4.38. SAXS patterns of the N_D phase obtained from the sample with Amaranth (a6) at 25.0°C for PP (left) and PR (right) orientations.

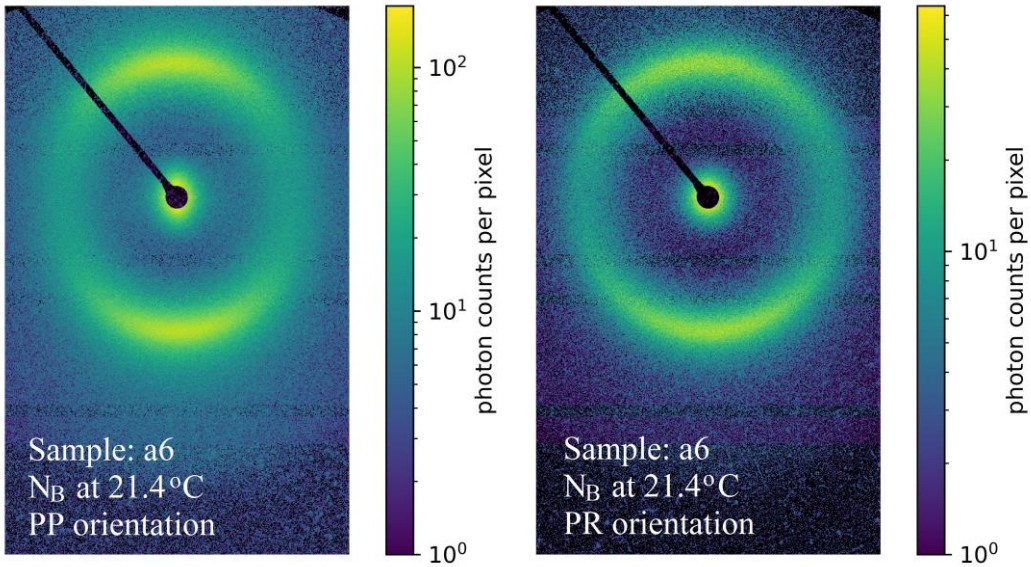

Figure 4.39. SAXS patterns of the N_B phase obtained from the sample with Amaranth (a6) at 21.4°C for PP (left) and PR (right) orientations.

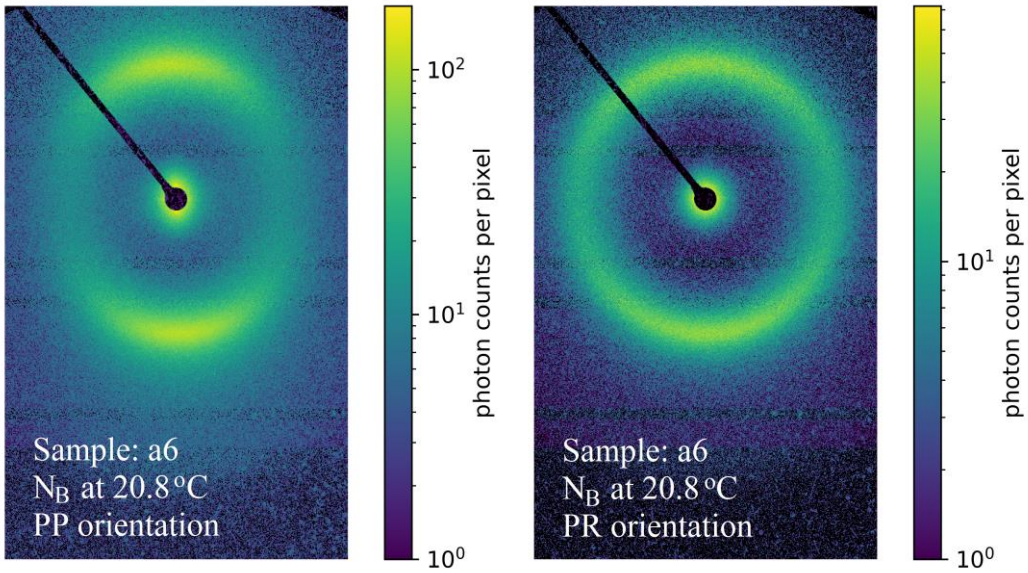

Figure 4.40. SAXS patterns of the N_B phase obtained from the sample with Amaranth (a6) at 20.8°C for PP (left) and PR (right) orientations.

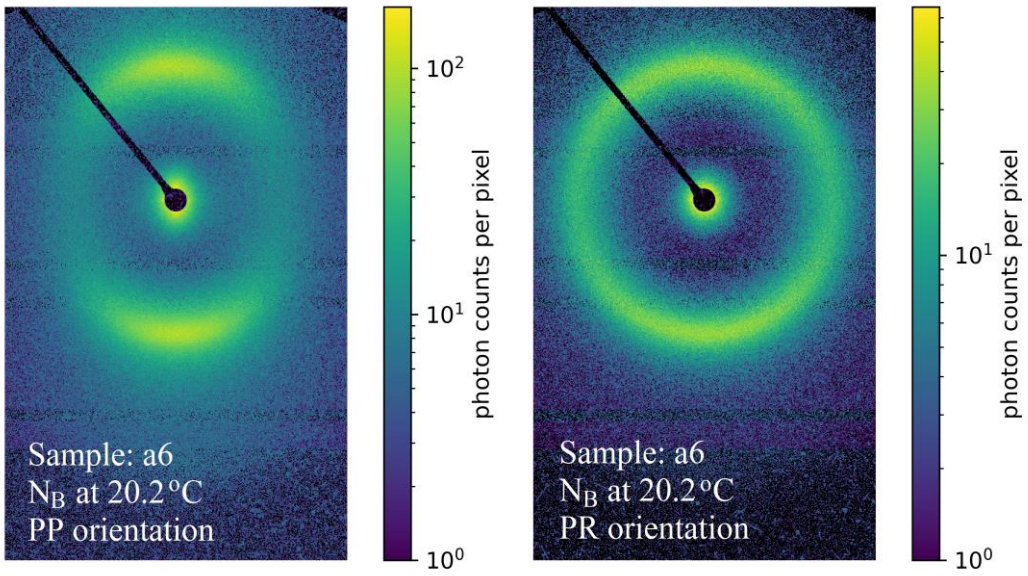

Figure 4.41. SAXS patterns of the N_B phase obtained from the sample with Amaranth (a6) at 20.2°C for PP (left) and PR (right) orientations.

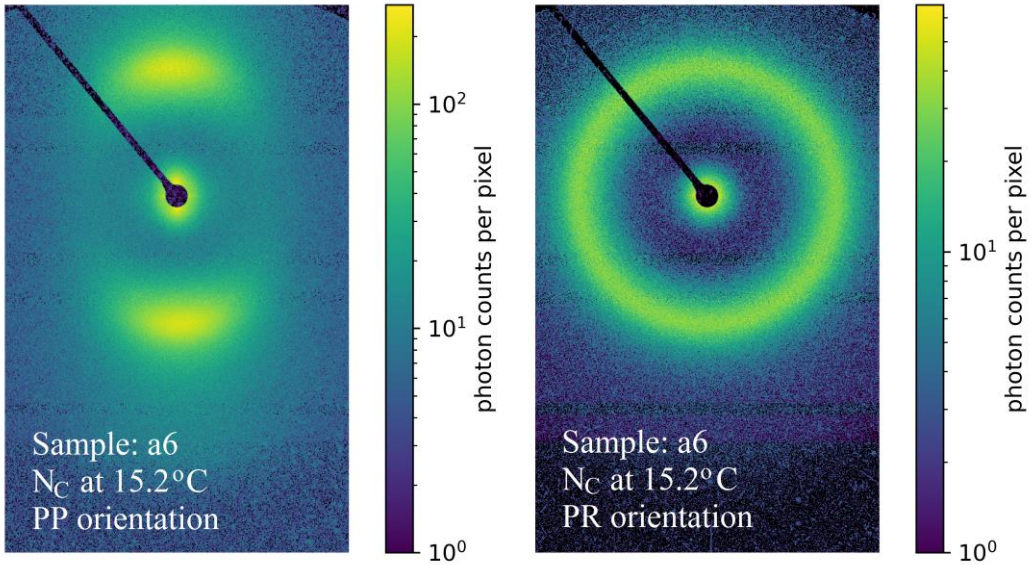

Figure 4.42. SAXS patterns of the N_C phase obtained from the sample with Amaranth (a6) at 15.2°C for PP (left) and PR (right) orientations.

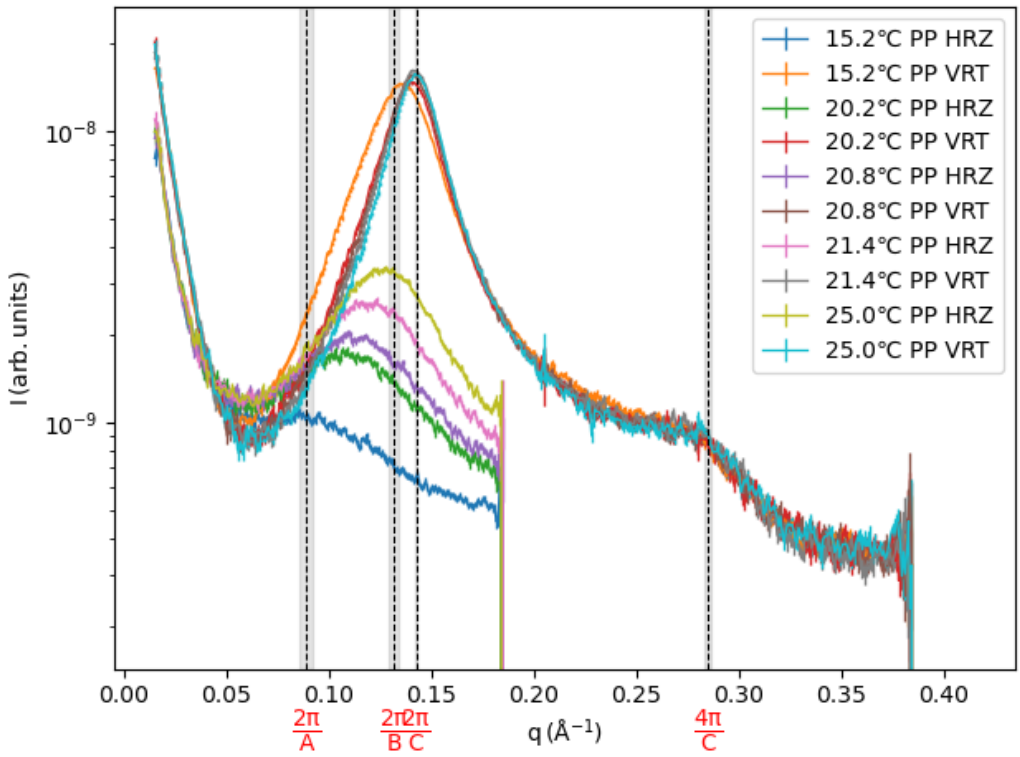

Figure 4.43. Scattering intensity vs scattering vector for the sample a6 at different temperatures to calculate the micellar structural parameters for the nematic phases.

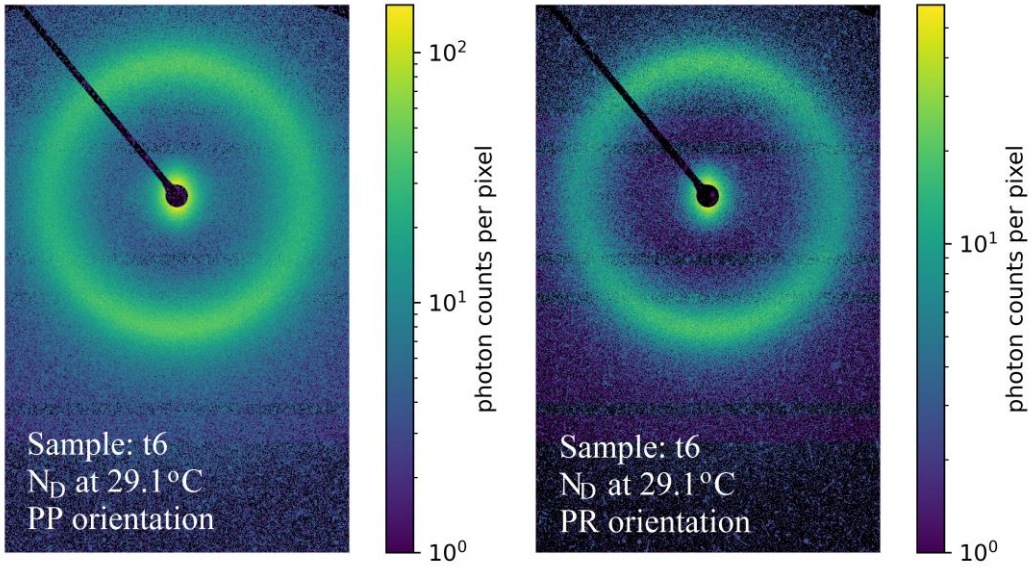

Figure 4.44. SAXS patterns of the N_D phase obtained from the sample with Tartrazine (t6) at 29.1°C for PP (left) and PR (right) orientations.

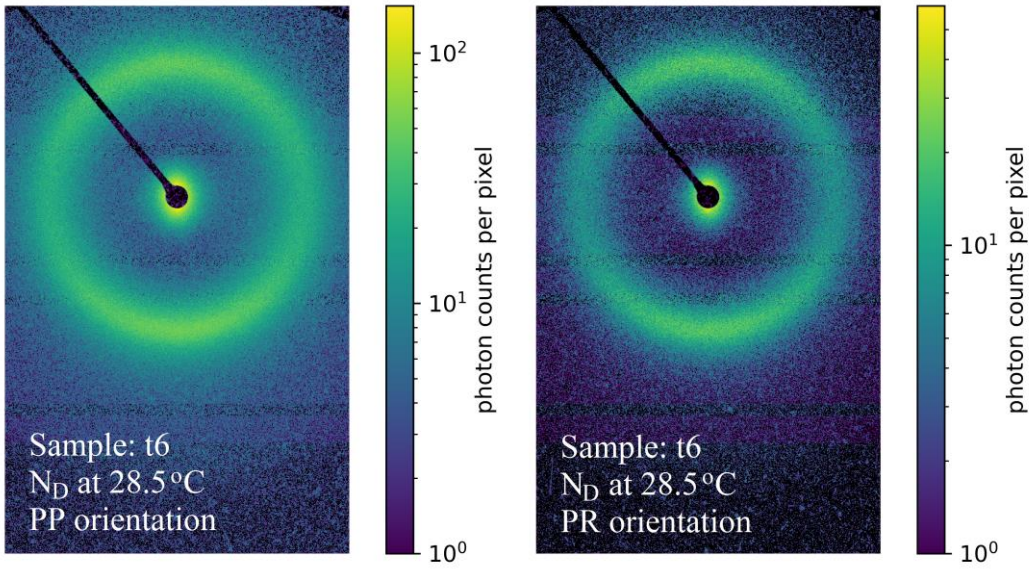

Figure 4.45. SAXS patterns of the N_D phase obtained from the sample with Tartrazine (t6) at 28.5°C for PP (left) and PR (right) orientations.

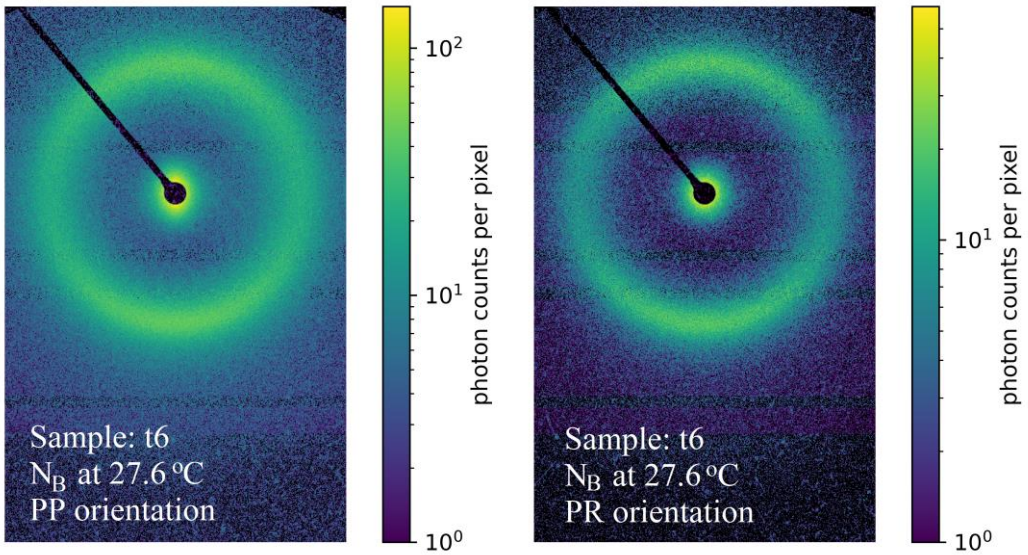

Figure 4.46. SAXS patterns of the N_B phase obtained from the sample with Tartrazine (t6) at 27.6°C for PP (left) and PR (right) orientations.

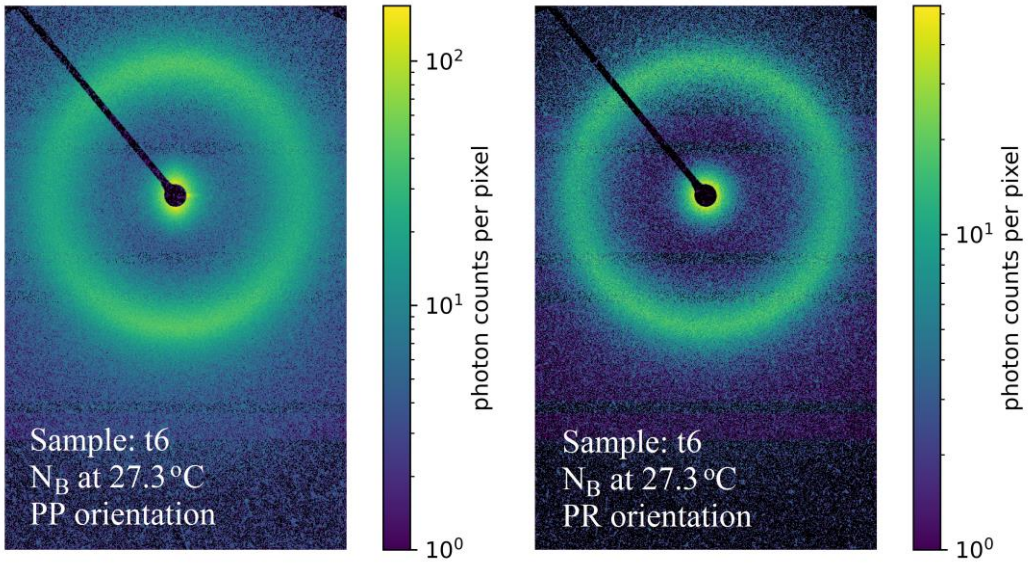

Figure 4.47. SAXS patterns of the N_B phase obtained from the sample with Tartrazine (t6) at 27.3°C for PP (left) and PR (right) orientations.

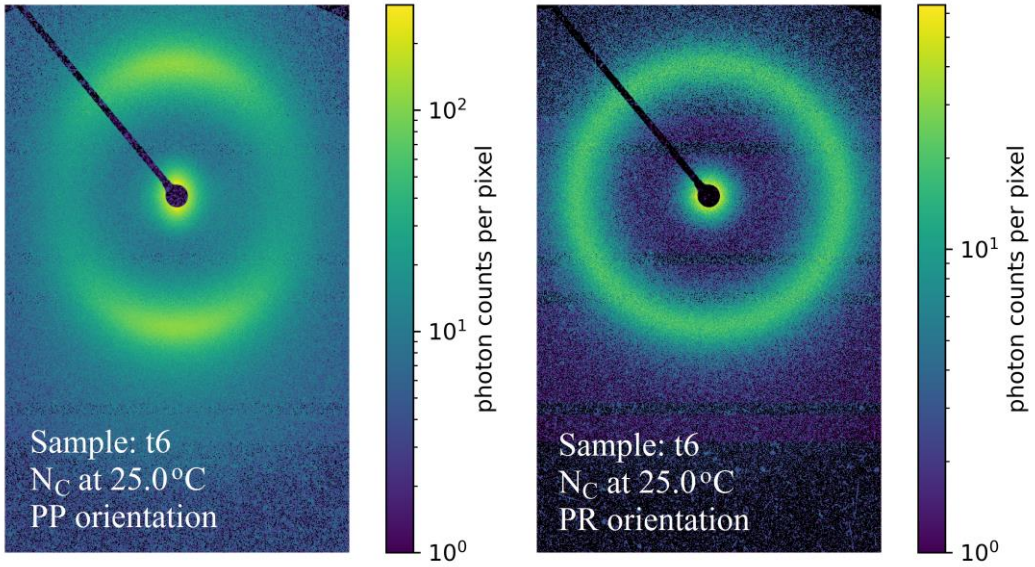

Figure 4.48. SAXS patterns of the N_C phase obtained from the sample with Tartrazine (t6) at 25.0°C for PP (left) and PR (right) orientations.

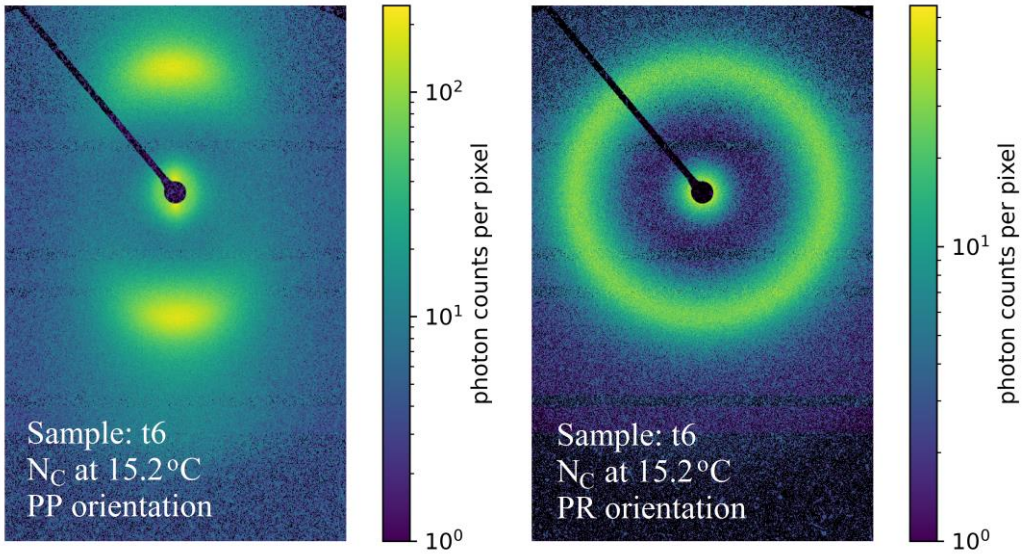

Figure 4.49. SAXS patterns of the N_C phase obtained from the sample with Tartrazine (t6) at 15.2°C for PP (left) and PR (right) orientations.

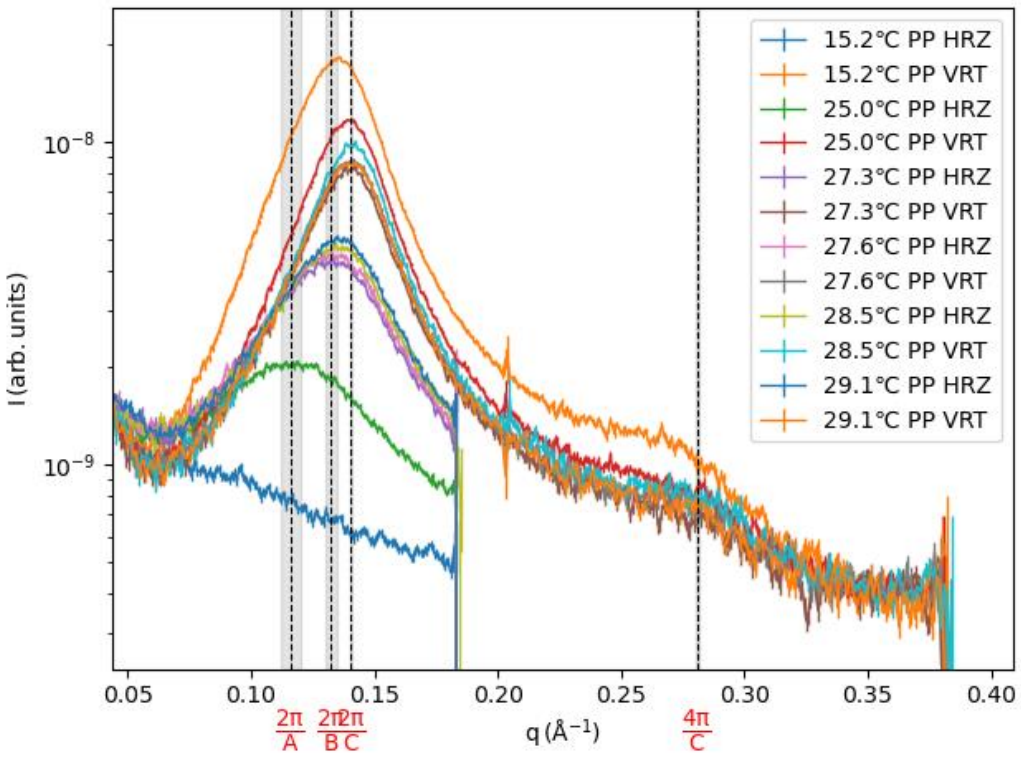

Figure 4.50. Scattering intensity vs scattering vector for the sample t6 at different temperatures to calculate the micellar structural parameters for the nematic phases.

The SAXS curves (Figures 4.21, 4.26, 4.32, 4.37, 4.43, and 4.50) for PP orientations were analyzed based on the analysis method proposed by Neto (120) and Galerne (94) by considerig that three nematic phases consist of similar orthorhombic micelles or micelles with biaxial symmetry, and these micelles are stacked in blocks of just a few units in the three directions. For the well-aligned N_D phases, the same SAXS patterns and curves are obtained in PP and PR orientations. However, the SAXS curves in N_B and N_C phases split into two different curves with almost the same change in the q values if N_D curves are chosen as the starting point. So, only PP orientations are used to analysis of the curves. Furthermore, it is only possible to calculate the micelle structural parameters of the samples studied in the N_D phases. The reasons for the last two situations are well-described in the references, (94,96,120) with the Supplementary Information. It is important to point out here that analysis of only the curves obtained from the N_D phases does not create any risk in the frame of this thesis because we aim to compare the relative effect of the dyes/drug molecules on the formation of different nematic phases.

Considering the biaxial symmetry of the micelles in the nematic phases, micelles have approximately a rectangular parallelepiped shape with the average available volume per micelle. In this volume, the micelle has the average dimensions A, B, and C, each of which can be evaluated from the SAXS intensity curves with $2\pi/q_X$, where q_X is the band positions of the SAXS intensity curves as a function of q in the Axis 1 or 2 directions for dimensions A and B, and in the Axis 3 direction for C (94). Because the calculation model assumes the existence of a uniform polar layer around the micelles and the uniform density of the micelle core composed of alkyl chains of the surfactant and cosurfactant molecules (96), the micelles core average dimensions A', B' and C' can be calculated by subtracting the thickness of the polar layer (w) from A, B, and C, respectively.

Furthermore, the calculation model is also available to calculate the average aggregation number (N_{agg}), the average area per polar head (a_0), and the shape anisotropy (SA). The last one can be obtained from the following equation:

$$SA = \frac{\left\{\left[\frac{A'+B'}{2}\right]-C'\right\}}{\left[\frac{A'+B'}{2}\right]} \qquad (4.1)$$

It sould be pointed out here that the SA enables us to compare the average thickness of the micelles core bilayer (C') relative to the average of the other two dimensions (A' and B') of the micelle core. It means that the SA gives information on the relative growth of the micelle core in the directions perpendicular to the amphiphiles bilayer direction. Tables 4.9. and 4.10. include N_{agg}, a_0, and SA values. Another important parameter is the average number of guest molecules (dyes/drug) per micelle, N_{guest}, which is calculated from the ratio of the N_{agg} to the molar ratio between the surfactants and the guest molecules.

For the samples s5, a11, t10, d6, a6, and t6, the results of the micelle structural parameters obtained from the SAXS analysis are given in Tables 4.7-4.10.

Table 4.7. Calculated some micelle structural parameters obtained from SAXS measurement results for s5, a11, t10 and d6.

Sample	A (Å)	B (Å)	C (Å)	A′ (Å)	B′ (Å)	C′ (Å)	w (Å)
s5	63.9±1.6	49.9±1.0	43.9±0.2	49.2±2.0	35.3±1.6	29.2±1.3	14.7±1.3
a11	65.1±2.4	49.5±1.1	43.7±0.2	50.3±3.0	34.7±2.2	28.9±1.9	14.8±1.9
t10	64.4±1.9	48.8±0.8	43.7±0.2	49.7±2.3	34.1±1.6	29.1±1.4	14.6±1.4
d6	72.3±3.2	49.0±0.8	43.7±0.2	57.2±3.8	33.9±2.3	28.6±2.1	15.1±2.1

Table 4.8. Calculated some micelle structural parameters obtained from SAXS measurement results for a6 and t6. The data for s5 given in Table 4.7 are repeated here for comparison.

Sample	A (Å)	B (Å)	C (Å)	A′ (Å)	B′ (Å)	C′ (Å)	w (Å)
s5	63.9±1.6	49.9±1.0	43.9±0.2	49.2±2.0	35.3±1.6	29.2±1.3	14.7±1.3
a6	70.8±2.6	47.8±0.9	44.1±0.2	56.0±3.1	32.9±2.0	29.3±1.8	14.9±1.8
t6	54.2±1.8	47.5±0.9	44.8±0.1	40.3±2.4	33.6±1.8	30.9±1.5	13.9±1.5

Laser conoscopy results exhibited that amaranth, tartrazine, and DSCG molecules bound to the micelles. The micelle bilayer thickness and the average polar layer thickness give us information about the location of the molecules on the micelle surfaces or the penetration to the micelle core. In a recent study (96), the SAXS analysis of DTMABr/DDeOH/water mixture doped with different SSY concentrations and some inorganic electrolytes, separately, showed that the micelle core bilayer thickness (C') and the polar layer thickness values were ~29-30 Å and ~14-15 Å, respectively, for SSY and electrolytes. It is well-known that electrolyte ions are present in the polar layer at the micelles' surfaces and cannot penetrate to the micelle core. Thus, obtaining similar C' and w values for electrolyte ions and SSY proved that the plank-like SSY molecules do not penetrate inside the core of the micelles. Instead, they localize on the micelles' surface or in the water layer region with their largest surface being parallel or at most inclined to the biaxial micelles surfaces (96). Remember that we used the same DTMABr/DDeOH/water host mixture with the same mole fractions of each component given in the reference (96). Because the similar C' and w values

(Tables 4.7 and 4.8) are obtained in the present study, the guest molecules amaranth, tartrazine, and DSCG have to localize on the micelle surfaces like SSY molecules, i.e., they do not penetrate inside the micelle core and localize on the micelle surfaces with their largest molecular surfaces.

Table 4.9. SA, N_{agg}, a_0 and N_{guest} values for s5, a11, t10 and d6 samples.

Sample	SA	N_{agg}	a_0 (Å)	N_{guest}	$N_D \rightarrow N_B$/°C
s5	0.31±0.04	158±5	53±3	3.1±0.1	21.2
a11	0.32±0.05	158±7	53±4	3.0±0.1	13.4
t10	0.31±0.04	154±5	54±3	3.0±0.1	19.2
d6	0.37±0.06	174±8	52±5	3.4±0.2	18.6

Table 4.10. SA, N_{agg}, a_0 and N_{guest} values for a6 and t6 samples. The data for s5 given in Table 4.9 are repeated here for comparison.

Sample	SA	N_{agg}	a_0 (Å)	N_{guest}	$N_D \rightarrow N_B$/°C
s5	0.31±0.04	158±5	53±3	3.1±0.1	21.2
a6	0.34±0.05	169±7	53±4	2.2±0.1	21.4
t6	0.16±0.05	130±5	56±4	1.7±0.1	27.6

The average area per polar head (a_0) gives information on the interactions between the ionic species at the micelle surfaces. If the ions interact strongly or weakly with the surfactant head groups, they screen the repulsions between the surfactant head groups and the a_0 values of the surfactants decrease. The strong (weak) interactions give rise to the formation of the close-contact (loosely bound) ion pairs. From the Hofmiester series point of view, while surfactant head groups and ions with similar chaotropic or kosmotropic character leads to formation of close-contact ion pairs, those with opposite character form loosely bound ones.

In Tables 4.9 and 4.10, the a_0 values are given. Considering the charges of both the head group of DTMABr and the ionic parts of each guest molecules, they behave as 1:1 electrolyte on the micelle surfaces and the head group of DTMABr interact with only one ionic part of each guest molecule. So, in our case, it can be

assumed that the a_0 is a measure of the strength of the interaction between surfactant head group and the guest molecule per its ionic part. SSY and amaranth have two and three same chaotropic ($–SO_3^-$) groups, and each $–SO_3^-$ group causes the same value of the a_0 for s5, a11 and a6 (53 Å). When one of the $–SO_3^-$ group in the structure of the amaranth is replaced by one kosmotropic $–COO^-$, i.e., tartrazine molecule, it is expected that the average chaotropy per ionic part slightly decreases with respect to the amaranth molecule, and the interactions between DTMABr head group and tartrazine is slightly weaker than DTMABr head group and amaranth. The last situation is confirmed with the a_0 values for t10 (54 Å) and t6 (56 Å). DSCG molecule has two kosmotropic$–COO^-$ groups. In the literature, there is no information about chaotropic or kosmotropic character of the additional ionic parts in the aromatic part of DSCG molecule (Figure 4.16). So, it is not easy to interpret its a_0 value if the X_{ion} (the total mole fraction values of the ions) values are not considered. However, as we discussed in the results of the laser conoscopy, the average degree of the kosmotropic/chaotropic character of DSCG as a molecule is between SSY and tartrazine if we take into account the transition from discotic nematic phase to the biaxial nematic phase. From this respect, it can be said that the SAXS results are in good agreement with both laser conoscopy and polarizing optical microscopy.

Amoung the micelle structural parameters obtained from the SAXS analysis, considering by the X_{ion} values, the N_{guest} values (Table 4.10), which was calculated from the ratio of the N_{agg} values to the molar ratio between the surfactants and the guest molecules, are more appropriate. By this way, all results obtained from laser conoscopy, polarizing optical microscopy and SAXS measurements are significant. As it can be seen in Table 4.10 (remember that s5, a6, t6 and d11 introduce same mole number of ionic parts to the mixtures with X_{ion}=0.26), as the kosmotropic character of the ionic parts of the guest molecules increases, the N_{guest} values decrease by favoring (unfavoring) the formation of N_C (N_D) phase. Although it cannot be possible to calculate the N_{guest} value for DSCG-included mixture (d11), because it gives only N_C phase, experimental results in the literature showed that the highest micelle surface curvature is observed in the N_C phase compared with the other nematic phases, which indicates the higher a_0 values. So, DSCG has to exhibit the highest (smallest) a_0 (N_{guest}) values with

respect to the other guest molecules. Consequently, the increasing order of chaotropic character of the guest molecules in the Hofmeister series by considering the ion numbers in the structure of dye/drug molecules is SSY>Amaranth>Tartrazine>DSCG. This order is in good agreement with the laser conoscopy results and the literature (96):

ClO_4^- > SCN^- > **Sunset Yellow** > **Amaranth** > I^- > ClO_3^- > **Tartrazine** > NO_3^- > Br^- > **DSCG**

As a result, the chaotropic degrees of the dyes and drug molecules were determined by considering the Hofmeister series of ions. It is also seen from the results of the present study that surfactant-based lyotropic nematic phases can be obtained by using dye molecules and/or drug molecules containing ionic groups in addition to traditional inorganic electrolyte ions. Another important point is that different types of nematic phases can be obtained by using less amount of dye molecules compared to electrolytes containing inorganic ions, and it is possible to control for obtaining a larger biaxial nematic phase region in partial phase diagrams. Because this is an active research field, the results obtained from the present study have contributed significantly to the studies in this field.

5. CONCLUSIONS AND RECOMMENDATIONS

In the present study, it was aimed to investigate the effects of interactions between ionic species on the micelle surfaces in the formation of lyotropic nematic phases by using cationic surfactant DTMABr and dye/drug guest molecules containing anionic groups in their molecular structures. The point of attention in these guest molecules is the number of ionic groups in their molecular structures and also the chaotropic and/or kosmotropic degrees of the ionic groups because these properties are an important parameter in the interactions of surfactant molecules and dye/drug molecules. The results indicate that those guest molecules have a greater effect on (a) the nematic-nematic phase transitions, (b) the biaxial nematic phase domain range in the partial phase diagrams, and (c), because higher birefringences mean higher micelle shape anisotropy, micelle shape anisotropy, than the conventional inorganic electrolyte ions. Furthermore, dye/drug molecules containing ionic parts in their structures may be sequenced in the Hofmeister series of ions. However, it would be pointed out that since the dye/drug molecules may have a resonance structure as a result of the existence of the aromatic parts in their structure, this resonance structure should be considered to investigate their effects on the formation of the lyotropic nematic phases. This may be also an important point for lyotropic chromonic liquid crystals (LCLCs) because the drug molecule DSCG has been widely investigated to form LCLCs.

6. REFERENCES

Vancouver citation system was used in this thesis.

1. Geelhaar T, Griesar K, Reckmann B. 125 years of liquid crystals--a scientific revolution in the home. Angew Chem Int Ed Engl. 2013;52(34):8798–809.

2. Mitov M. Liquid-crystal science from 1888 to 1922: Building a revolution. ChemPhysChem. 2014 May 19;15(7):1245–50.

3. Lehmann O. Über fliessende Krystalle.

4. Katariya Jain A, R. Deshmukh R. An overview of polymer-dispersed liquid crystals composite films and their applications. Liquid crystals and display technology. IntechOpen; 2020. 2 p.

5. Andrienko D. Introduction to liquid crystals. 2006.

6. Demus D, Goodby J, gray G, Spiess W, Vill V. Handbook of liquid crystals. Vol. 2A. VCH; 1996. 17 p.

7. https://uh.edu/~chembi/liquidcrystals.pdf.

8. Wang H, Xu T, Fu Y, Wang Z, Leeson MS, Jiang J, et al. Liquid crystal biosensors: Principles, structure, and applications. Biosensors (Basel). 2022 Aug 1;12(8):1–27.

9. Balasubramaniam VM, Sash-Y SK. Use of liquid crystals as temperature sensors in food processing research. J Food Eng. 1995;26:219–30.

10. Dierking I, Scalia G, Morales P. Liquid crystal–carbon nanotube dispersions. Journal of Applied Physics. 2005;97(4):044309. 2005 Feb 15;

11. Pauluth D, Tarumi K. Advanced liquid crystals for television. J Mater Chem. 2004 Apr 21;14(8):1219–27.

12. Woltman SJ, Jay GD, Crawford GP. Liquid-crystal materials find a new order in biomedical applications. In: Nature Publishing Group. 2007. p. 929–31.

13. Brook RJ, Cheetham A, Heuer A, Hirsch P, Marks TJ, Pettifor DG, et al. Monograps on the physics and chemistry of materials General Editors.

14. Burducea G. Lyotropic liquid crystals I. specific structures. Rom Rep Phys. 2004;56(1):66–86.

15. Birdi K. Surface Chemistry Essentials. 2014.

16. Chandrasekhar S, Sadashiva BK, Suresh KA. Liquid crystals of disc-like molecules. 1977;9(5):471–80.

17. Osman MA. Molecular structure and mesomorphic properties of thermotropic liquid crystals. III. Lateral substituents. Molecular Crystals and Liquid Crystals. 1985 Jun;128(1–2):45–63.

18. https://ukessays.com/essays/chemistry/classifications-liquid-crystals-7625.php.

19. Rapalli VK, Waghule T, Hans N, Mahmood A, Gorantla S, Dubey SK, et al. Insights of lyotropic liquid crystals in topical drug delivery for targeting various skin disorders. J Mol Liq. 2020 Oct 1;315.

20. Mezzenga R, Seddon JM, Drummond CJ, Boyd BJ, Schröder-Turk GE, Sagalowicz L. Nature-inspired design, and application of lipidic lyotropic liquid crystals. Advanced Materials. 2019 Aug 1;31(35):1–19.

21. Saklani R, Yadav PK, Nengroo MA, Gawali SL, Hassan PA, Datta D, et al. An injectable in situ depot-forming lipidic lyotropic liquid crystal system for localized intratumoral drug delivery. Mol Pharm. 2022 Mar 7;19(3):831–42.

22. Almeida MR, Stephani R, Dos Santos HF, De Oliveira LFC. Spectroscopic and theoretical study of the "Azo"-Dye e124 in condensate phase: evidence of a dominant hydrazo form. Journal of Physical Chemistry A. 2010 Jan 14;114(1):526–34.

23. Engels T, Von Rybinski W. Liquid crystalline surfactant phases in chemical applications. J Mater Chem. 1998;8(6):1313–20.

24. Hara M. Mesostructure and orientation control of lyotropic liquid crystals in a polysiloxane matrix. Polym J. 2019 Oct 1;51(10):989–96.

25. Lydon J. Chromonic liquid crystal phases. Curr Opin Colloid Interface Sci. 1998;3(5):458–66.

26. theecowell. https://theecowell.com/blog/surfactant-basics.

27. Fairhurst CE, Fuller S, Gray J, Holmes MC. Lyotropic surfactant liquid crystals. In: Handbook of liquid crystals. 1998. p. 341–55.

28. Nakama Y. Surfactants. In: Surfactants in cosmetic science and technology: Theoretical principles and applications. 2017. p. 231–44.

29. Duncke A, Valeska A, Da Silva B, Nele M. Influence of cation volume on liquid crystals of emulsified crude oil systems. In: 9º Congresso Brasileiro De Pesquisa E Desenvolvimento Em Pretroleo E Gas. 2017. p. 1–8.

30. Shiri MSZ, Henderson W, Mucalo MR. A review of the lesser-studied microemulsion-based synthesis methodologies used for preparing nanoparticle systems of the noble metals, Os, Re, Ir and Rh. Materials. 2019 Jun 1;12(12):1–26.

31. Lee KS, Lee JH. Hybrid chemical EOR using low-salinity and smart waterflood. In: Hybrid enhanced oil recovery using smart waterflooding. Elsevier; 2019. p. 65–110.

32. Israelachvili JN. Intermolecular and surface forces. 3rd ed. London; San Diego: Academic Press; 2011.

33. Holmberg K. Surfactants and polymers in aqueous solution. 2nd ed. John Wiley & Sons; 2003. 545 p.

34. Dawin UC, Lagerwall JPF, Giesselmann F. Electrolyte effects on the stability of nematic and lamellar lyotropic liquid crystal phases: Colligative and ion-specific aspects. Journal of Physical Chemistry B. 2009;113(33):11414–20.

35. Kale KM, Zana R. Effect of the nature of the counterion on the volume change upon micellization of ionic detergents in aqueous solutions. J Colloid Interface Sci. 1977;67(2):312–22.

36. J. Lenglet, A. Bourdon, J. C. Bacri, and G. Demouchy (2002). Phys. Rev. E 65, 031408-1-14. Phys Rev E 65.

37. Antônio M. Figueiredo Neto, Silvio R. A. Salinas. The physics of lyotropic liquid crystals_phase transitions and structural properties . 2005;9.

38. Manojlović JŽ. The krafft temperature of surfactant solutions. Thermal Science. 2012;16(2):631–40.

39. Dierking I, Martins Figueiredo Neto A. Novel trends in lyotropic liquid crystals. Crystals. 2020;10(7):604. Vol. 10. 2020. p. 604.

40. Barim G. Investigation of lithium salt-nonionic surfactant mesophases and their applications in solar cells as gel electrolyte. [MSc Thesis]. 2013.

41. Singh S. Liquid crystals: Fundamentals. Phys Today. 2003;56(11):69–70.

42. Collings P, Hird M. Introduction to liquid crystals chemistry and physics. Taylor & Francis Ltd.; 1997. 154–156 p.

43. Allain V, Bourgaux C, Couvreur P. Self-assembled nucleolipids: From supramolecular structure to soft nucleic acid and drug delivery devices. Nucleic Acids Res. 2012 Mar;40(5):1891–903.

44. Alfutimie A, Curtis R, Tiddy GJT. Gel phase (Lβ) formation by mixed saturated and unsaturated monoglycerides. Colloids Surf A Physicochem Eng Asp. 2014 Aug 20;456(1):286–95.

45. Brusselle D, Bauduin P, Girard L, Zaulet A, Viñas C, Teixidor F, et al. Lyotropic lamellar phase formed from monolayered θ-shaped carborane-cage amphiphiles. Angewandte Chemie - International Edition. 2013 Nov 11;52(46):12114–8.

46. Rizwan SB, Boyd BJ, Rades T, Hook S. Bicontinuous cubic liquid crystals as sustained delivery systems for peptides and proteins. Expert Opin Drug Deliv. 2010 Oct;7(10):1133–44.

47. Albayrak C. New solvents for surfactants self-assembly: molten hydrated salts and concentrated aqueous electrolyte solutions. [PHd Thesis]. 2013.

48. Lombardo D, Kiselev MA, Magazù S, Calandra P. Amphiphiles self-assembly: Basic concepts and future perspectives of supramolecular approaches. Advances in Condensed Matter Physics. 2015;2015(151683):1–22.

49. Lee H, Labes MM. Lyotropic cholesteric and nematic phases of disodium cromoglycate in magnetic fields. Molecular crystals and liquid crystals. 1982;84(1–4):137–57.

50. Forrest BJ, Reeves LW. New lyotropic liquid crystals composed of finite nonspherical micelles. Chem Rev. 1981;81(1):1–14.

51. Cimis MA, Leonard W A. A type II aqueous cholesteric lyomesophase. Can J Chem. 1980;58(1538):1533–41.

52. Figueiredo Neto AM. Micellar cholesteric lyotropic liquid crystals. Liq Cryst Rev. 2014 Jan 1;2(1):47–59.

53. Topçu G. Investigation of uniaxial and biaxial nematic phase properties of dye-doped lyotropic liquid crystals. [MSc Thesis]. [Bolu]; 2020.

54. Kroin T, Figueiredo Neto AM. Bend periodic distortion of the texture in nematic lyotropic liquid crystals with and without ferrofluid. Physical Review. 1987;36(6):1–5.

55. Fortinini S, Barbero G, Figueiredo Neto AM. Determination of the effective splay-bend elastic constant of a lyotropic nematic liquid crystals. Physical Rewiev E. 1995;53(3):1–7.

56. Cevc G, Richardsen H, Richardsen R. Lipid vesicles and membrane fusion. Adv Drug Deliv Rev. 1999;38:207–32.

57. Gu-Yuan Li, Jia-Jia Yu, Dong-Ming Mo, Maitiniyazi Bake, Ling-Feng Chen, You-Rong Li. Electro-optical properties of nematic lyotropic chromonic liquid crystals. 2022 Feb 15;348(5).

58. Flautt J, Lawson K, Cohen M. Molecular structure, and the properties of liquid crystals. J Am Chem Soc. 1967;6(4):503.

59. Akpinar E, Neto AMF. Experimental conditions for the stabilization of the lyotropic biaxial nematic mesophase. Crystals. 2019;9(3):158.

60. Boden N, Corne SA, Jolleyt KW. Lyotropic mesomorphism of the cesium pentadecafluorooctanoate/water system: high-resolution phase diagram. J Phys Chem. 1987;91(15):4092–105.

61. Akpinar E, Otluoglu K, Turkmen M, Canioz C, Reis D, Figueiredo Neto AM. Effect of the presence of strong and weak electrolytes on the existence of uniaxial and biaxial nematic phases in lyotropic mixtures. Liq Cryst. 2016 Sep 1;43(11):1693–708.

62. Akpinar E, Reis D, Neto AMF. Effect of alkyl chain length of alcohols on nematic uniaxial-to-biaxial phase transitions in a potassium laurate/alcohol/K 2SO 4/water lyotropic mixture. Liq Cryst. 2012 Jul;39(7):881–8.

63. Braga WS, Kimura NM, Luders DD, Sampaio AR, Santoro PA, Palangana AJ. Reentrant isotropic-calamitic nematic phase transition in potassium laurate-decanol- D2O mixtures. European Physical Journal E. 2007 Nov;24(3):247–50.

64. Nasrin L, Kabir E, Rahman M. External magnetic field-dependent tricritical points of uniaxial-to-biaxial nematic transition. Phase Transitions. 2016 Feb 1;89(2):193–201.

65. Kim YK, Senyuk B, Shin ST, Kohlmeier A, Mehl GH, Lavrentovich OD. Surface alignment, anchoring transitions, optical properties, and topological defects in the thermotropic nematic phase of organo-siloxane tetrapodes. Soft Matter. 2014 Jan 21;10(3):500–9.

66. Matthias Lehmann. The dawn in the area of thermotropic biaxial nematics Symposium on Biaxial Liquid Crystals. Liquid Crystals Today. 2009 Jun;18(1).

67. ander J. Tans, Alwin R. M. Verschueren & Cees Dekker. Room-temperature transistor based on a single carbon nanotube. letters to nature. 1998 May 7;393.

68. Ray H. Baughman. Carbon Nanotubes--the Route Toward Applications. sciencemag. 2002;297.

69. de Heer WA, Chatelain A., Ugarte D. A carbon nanotube field-emission electron source. science. 1995;1179(80).

70. Collins PG, Avouris P. Nanotubes for Electronics. 2000;283(6):62–9.

71. Thostenson ET, Ren Z, Chou TW. Advances in the science and technology of carbon nanotubes and their composites: a review [Internet]. Available from: www.elsevier.com/locate/compscitech

72. Weiss V, Thiruvengadathan R, Regev O. Preparation and characterization of a carbon nanotube - Lyotropic liquid crystal composite. Langmuir. 2006 Jan 31;22(3):854–6.

73. C. N. Rao, B. C. Satishkumar, A. Govindaraj, and M. Nath. Nanotubes. ChemPhysChem. 2001;2(2):79–105.

74. Baughman RH, Cui C, Zakhidov AA, Iqbal Z, Barisci JN, Spinks GM, et al. Carbon nanotube actuators. Science (1979). 1999 May 21;284(5418):1340–4.

75. Kong W, Pei L, Zhang J. Linear dichroism spectroscopy of gas phase biological molecules embedded in superfluid helium droplets. Int Rev Phys Chem. 2009 Jan;28(1):33–52.

76. Dierking I, Scalia G, Morales P, LeClere D. Aligning and reorienting carbon nanotubes with nematic liquid crystals. Advanced Materials. 2004 Jun 4;16(11):865–9.

77. Popa-Nita V, Barna V, Repnik R, Kralj S. Mixtures Composed of Liquid Crystals and Nanoparticles. In: Syntheses and Applications of Carbon Nanotubes and Their Composites. InTech; 2013.

78. P. G. de Gennes and J. Prost. "The Physics of Liquid Crystals," Oxford University Press, UK,. 1993;

79. Lynch MD, Patrick DL. Organizing Carbon Nanotubes with Liquid Crystals. Nano Lett. 2002 Nov;2(11):1197–201.

80. Jan Lagerwall, Giusy Scalia, Miroslav Haluska, Ursula Dettlaff-Weglikowska, Siegmar Roth, Frank Giesselmann. Nanotube alignment using lyotropic liquid crystals. Advanced Materials. Advenced materials. 2007;

81. Lebovka N, Dadakova T, Lysetskiy L, Melezhyk O, Puchkovska G, Gavrilko T, et al. Phase transitions, intermolecular interactions and electrical conductivity behavior in carbon multiwalled nanotubes/nematic liquid crystal composites. J Mol Struct. 2008 Sep 17;887(1–3):135–43.

82. Okano K, Noguchi I, Yamashita T. Anisotropic carbon nanotube films fabricated from a lyotropic liquid-crystalline polymer. Macromolecules. 2010;43(13):5496–9.

83. Song Z, Yang Y, Xin X. Lyotropic Liquid Crystals Incorporated with Different Kinds of Carbon Nanomaterials or Biomolecules. In: Liquid Crystals - Recent Advancements in Fundamental and Device Technologies. InTech; 2018.

84. Yu LJ, Saupe A. Liquid crystalline phases of the sodium decyl sulfate/decanol/water system. Nematic-nematic and cholesteric-cholesteric phase transitions. Journal of the American Chemistry Society. 1980;102(15):4879–83.

85. Yu L.J., Saupe A. Observation of a Biaxial Nematic Phase in Potassium Laurate-1-Decanol-Water Mixtures. Phys Rev . 1980;(45):1000–3.

86. Akpinar E, Canioz C, Turkmen M, Reis D, Figueiredo Neto AM. Effect of the surfactant alkyl chain length on the stabilisation of lyotropic nematic phases. Liq Cryst. 2018 Jan 26;45(2):219–29.

87. Hendrikx Y, Charvolin J, Rawiso M. Uniaxial-biaxial phase transition in lyotropic nematic solutions: local biaxiality in the uniaxial phase. Phys Rev B. 1986;33(5):3534–6.

88. Bartolino R, Chiaranza T, Meuti M, Compagnoni R. Uniaxial and biaxial lyotropic nematic liquid crystals. The American Physical Society. 1982;26(2):1116.

89. Santos OR, Braga WS, Luders DD, Sampaio AR, Kimura NM, Simoes M, et al. Optical characterization of a biaxial nematic between uniaxial nematic lyotropic phases. Phase Transitions. 2021;94(6–8):546–55.

90. Alben R. Phase transitions in a fluid of biaxial particles. Physical Review Letter. 1972;30(17):778–81.

91. Stroobants A, Lekkerkerker WNH. Liquid crystals phase transitions in a solution of rodlike and disklike particles. J Phys Chem. 1984;88(16):3669–74.

92. Palffy-Muhoray P, De Bruyn JR, Dunmur DA. Phase behavior of binary nematic liquid crystal mixtures. J Chem Phys. 1985;82(11):5294–5.

93. Geoffrey R. Luckhurst, Timothy J. Sluckin. Biaxial Nematic Liquid Crystals: Theory, Simulation and Experiment. 2015.

94. Galerne Y, Figueiredo Neto AM, Liebert L. Microscopical structure of the uniaxial and biaxial lyotropic nematics. J Chem Phys. 1987;87(3):1851–6.

95. Toda M, Toda M. Physical review letters in nearly linear lattice dynamics. "H. Beck, in dynamical propeyties of solids, edited observation of a biaxial nematic phase in potassium laurate-1-decanol-water mixtures. Prog Theor Phys Suppl. 1967;45(E):205.

96. Akpinar E, Topcu G, Reis D, Neto AMF. Effect of the anionic azo dye Sunset Yellow in lyotropic mixtures with uniaxial and biaxial nematic phases. J Mol Liq. 2020 Nov 15;318.

97. https://commons.wikimedia.org/wiki/File:Ordinay_extraordinary_ray_in_birefringence.png).

98. P. Pincus. Magnetic Properties of Liquid Crystal. J Appl Phys. 2003 Dec;974–979(41).

99. Mingsheng Wang, Le He, Serkan Zorba, Yadong Yin. Magnetically Actuated Liquid Crystals. Nano Lett. 2014 Jun;3966–3971(14).

100. Neto AMF, Salinas SRA. The physics of lyotropic liquid crystals: phase transitions and structural properties. Vol. 62. Oxford University Press on Demand; 2005.

101. Oliveira EA, Liebert L, Figueiredo Neto AM. A new soap/detergent/water lyotropic liquid crystal with a biaxial nematic phase. Liq Cryst. 1989;5(6):1669–75.

102. Akpinar E, Reis D, Figueiredo Neto AM. Lyotropic mixture made of potassium laurate/1-undecanol/K2SO4/water presenting high birefringences and large biaxial nematic phase domain: A laser conoscopy study. European Physical Journal E. 2012 Jun;35(6).

103. Gökce H, Bahçeli S. The molecular structures, vibrational spectroscopies (FT-IR and Raman) and quantum chemical calculations of n-alkyltrimethylammonium bromides. Opt Spectrosc. 2013 Nov;115(5):632–44.

104. Horowitz VR, Janowitz LA, Modic AL, Heiney PA, Collings PJ. Aggregation behavior and chromonic liquid crystal properties of an anionic monoazo dye. Phys Rev E Stat Nonlin Soft Matter Phys. 2005 Oct;72(4):1–10.

105. Park HS, Kang SW, Tortora L, Nastishin Y, Finotello D, Kumar S, et al. Self-assembly of lyotropic chromonic liquid crystal sunset yellow and effects of ionic additives. Journal of Physical Chemistry B. 2008 Dec 25;112(51):16307–19.

106. Akpinar E, Reis D, Yildirim M, Neto AMF. New lyotropic mixtures with non-chiral N-acylamino acid surfactants presenting the biaxial nematic phase investigated by laser conoscopy, polarized optical microscopy and X-ray diffraction. Materials. 2014;7(6):4132–47.

107. Akpinar E, Uygur N, Ordu OD, Reis D, Neto AMF. Effect of the surfactant head-group size dependence of the dye-surfactant interactions on the lyotropic uniaxial to biaxial nematic phase transitions. J Mol Liq. 2021 Jun 15;332.

108. Khatory A, Lequeux F, Kern F, Candau SJ. Linear and Nonlinear Viscoelasticity of Semidilute Solutions of Wormlike Micelles at High Salt Content. Vol. 9, Langmuir. 1993.

109. Mu, J.-H.; Li, G.-Z.; Jia, X.-L.; Wang, H.-X.; Zhang, G.-Y. J. Phys. Chem. B 2002, 106, 11685–11693. (106).

110. Yu D, Huang X, Deng M, Lin Y, Jiang L, Huang J, et al. Effects of Inorganic and Organic Salts on Aggregation Behavior of Cationic Gemini Surfactants". J Phys Chem B, . 2010;(114):14955–64.

111. Erol Akpinar, Meric Turkmen, Cihan Canioz, Antônio Martins Figueiredo Neto. Role of kosmotrope-chaotrope interactions at micelle surfaces on the stabilization of lyotropic nematic phases. The European Physical Journal E volume . 2016 Nov 16;107(39).

112. Collins KD. Charge density-dependent strength of hydration and biological structure. Biophys J. 1997;72(1):65–76.

113. Marcus Y,. Chem. Rev. . 2009;1346(109).

114. Phillips AJ, Henderson JA, Jackson KL. "Pyrans and their Benzo Derivatives: Structure and Reactivity" in "Comprehensive Heterocyclic Chemistry III." 2008;7(7):337–418.

115. Hepworth, John D., Christopher D. Gabbutt and B. Mark Heron. "Pyrans and their Benzo Derivatives: Structure" in Comprehensive Heterocyclic Chemistry II, chapter 5.07. Pergamon, Elsevier SciLtd. 1996;301–50.

116. Ibanez, A. C. S., Marji E,, Luk YY,. RSC Adv., . 2018;(8):29598–606.

117. Leontidis E. Hofmeister anion effects on surfactant self-assembly and the formation of mesoporous solids. Vol. 7, Current Opinion in Colloid & Interface Science. 2002.

118. Wen J, Shen X, Shen H,, Zhang FS. "Hofmeister series and ionic effects of alkali metal ions on DNA conformation transition in normal and less polarised water solvent." Molecular Physics, . 2014;112:2707-2719.

119. Umapathi R, Reddy PM, Rani A,, Venkatesu P. "Influence of additives on thermoresponsive polymers in aqueous media: a case study of poly(Nisopropylacrylamide)." Physical Chemistry Chemical Physics. 2018;(20):9717–44.

120. Neto AMF, Galerne Y, Levelut AM,, Liébert L. Pseudo-lamellar ordering in uniaxial and biaxial lyotropic nematics: a synchrotron X-ray diffraction experiment. Journal de Physique Lettres. 1985;(46):499-505.